UNIVERSITY OF OKLAHOMA

GRADUATE COLLEGE

FABRICATING HIGH-QUALITY STRUCTURAL COMPOSITE LAMINATES AND TAILORING THEIR SURFACE MICROSTRUCTURE BY APPLYING MAGNETIC PRESSURE AND MAGNETIC FIELD

A DISSERTATION

SUBMITTED TO THE GRADUATE FACULTY

in partial fulfillment of the requirements for the

Degree of

DOCTOR OF PHILOSOPHY

By

MAYA PISHVAR
Norman, Oklahoma
2019

FABRICATING HIGH-QUALITY STRUCTURAL COMPOSITE LAMINATES AND TAILORING THEIR SURFACE MICROSTRUCTURE BY APPLYING MAGNETIC PRESSURE AND MAGNETIC FIELD

A DISSERTATION APPROVED FOR THE
SCHOOL OF AEROSPACE AND MECHANICAL ENGINEERING

BY

Dr. M. Cengiz Altan, Chair

Dr. Zahed Siddique

Dr. Mrinal C. Saha

Dr. Yingtao Liu

Dr. Shivakumar Raman

© Copyright by MAYA PISHVAR 2019
All Rights Reserved.

Dedicated to

My beloved and fabulous husband, Mehrad

My wonderful parents, Hossein and Shahdokht

Acknowledgments

I sincerely thank Prof. M. Cengiz Altan, my advisor, for his kind and consistent academic and mental support throughout my studies at the University of Oklahoma (OU). I am very grateful to my committee members, Prof. Shivakumar Raman, Prof. Zahed Siddique, Prof. Mrinal C. Saha, and Prof. Yingtao Liu for their continuous encouragement and invaluable feedbacks.

I am extremely lucky to have enthusiastic and talented collaborators: Drs. Mehrad Amirkhosravi, M Akif Yalcinkaya, Youssef K. Hamidi, and Gorkem E. Guloglu. Special thanks to them for helpful discussions, and mostly for their friendships. I truly appreciate every single member and alumni of the Composite Manufacturing Research Laboratory at OU for being such wonderful labmates and friends. I thank the AME Machine Shop at OU for their helpful assistance in facilitating this research.

I am of course very grateful to the funding support of Graduate Research and Teaching Assistant, Jim and Bee Close scholarship, and Gallogly College of Engineering Dissertation Excellence Award.

I am grateful to my friends all over the world. I also thank my dear parents, Kobra (Shahdokht) Ghamkhari Tarigheh and Hossein Pishvar, my brother, Maysam (Omid) Pishvar who have always offered unbounded love and support and encouraged me to pursue my dreams. I also appreciate my mother-in-law, Nazanin Akhavan Deilami, along with the rest of my family for their immense love and kindness.

Finally, and most importantly, I thank my husband, my best friend, and the love of my life, Mehrad Amirkhosravi, who has been present in all steps of this long

academic journey. You have always helped me keep moving toward success and happiness with your unwavering love, patience, and support. I look forward to spending the rest of my life with you.

Table of Contents

List of Tables

List of Figures

Abstract

Advanced fiber reinforced polymer (FRP) composites are widely used in structural applications due to their high specific strength and stiffness. Generally, high-quality, advanced FRP composites are produced using an autoclave. However, the disadvantages associated with autoclave curing include high initial capital investment and operating costs. As a result, there is an increasing interest in the development of out-of-autoclave (OOA) techniques to produce composite parts with comparable properties to those obtained in an autoclave, but at a lower cost. In the first part of this dissertation, a novel technique, magnet assisted composite manufacturing (MACM), is developed to produce high-quality FRP composite laminates out of an autoclave. In this technique, high-temperature permanent magnets are utilized to apply sufficiently high consolidation pressure during cure of laminates. To establish MACM as a viable OOA method for producing structural composite laminates, the microstructure and properties of laminates fabricated by MACM are compared with those cured in an autoclave. The high flexural properties, fiber volume fraction of over 60% with less than 1% voids of the laminates fabricated by MACM revealed the potential of this process to be used as a lower-cost alternative to autoclave cure, without diminishing the quality of the part.

Despite the favorable mechanical properties of FRP composite materials, their non-mechanical properties, e.g., thermal or electrical conductivities still is a major concern, limiting their application. It is well-known that incorporation of a third phase into structural composite laminates is quite effective in improving multiple non-mechanical properties. The second part of the dissertation involves the development of a novel cascaded suspension deposition method to introduce well-dispersed short fibers

into the molded laminates, allowing the control of the surface properties of the resulting laminates. Towards this goal, the three-phase composite laminates are fabricated first by depositing short nickel coated carbon (NiC) fibers on a glass fabric surface by the proposed method and then followed by vacuum infusion. To demonstrate the effectiveness of this technique, the microstructure morphology of the deposited fabric and the resulting composite is quantitatively characterized. The findings suggest that with this technique, short fibers are distributed on the laminate surface with a uniform fiber volume fraction and excellent dispersion with random orientation.

Controlling the orientation and alignment of the third phase in three-phase composite laminates is an effective approach for tailoring the anisotropy, and thus improving the functionalities of structural composites. The third part of the dissertation introduces a new magnetic-field assisted composite processing method to induce alignment of short fibers on the surface of three-phase composite laminates. For this purpose, magnetic field generated by permanent magnets are utilized to align NiC fibers in three ways: (i) during deposition of fibers by cascaded suspension deposition, (ii) on the deposited fabric after mold filling in VARTM, and (iii) on the deposited fabric during deposition, mold filling, and after mold filling. The degree of alignment and the required field strength are evaluated as a function of NiC fiber length and nickel coating thickness. The results suggest that with the proposed method, it is possible to obtain an anisotropic distribution of fibers while maintaining the uniform fiber volume fraction and good dispersion throughout the surface of the laminate. Thus, the proposed method allows tailoring surface anisotropy, thus improving the required properties in the desired direction for high-performance and other applications of FRP composites.

Chapter 1. Introduction

The objective of the current dissertation is threefold. First, this research is concerned with developing a novel fabrication method to produce high-quality composite laminates out of an autoclave. Second, a novel deposition technique is developed to introduce well-dispersed short fibers into the molded laminates, allowing the control of the surface properties of the resulting composite. Third, a new magnetic-field assisted composite processing method is proposed to control the orientation of conductive short fibers in structural laminates for tailoring the anisotropy, and thus improving their functionalities.

1.1. Out-of-autoclave processing of composite laminates

Fiber reinforced polymer (FRP) composites have been widely used in several industrial applications due to their unique advantages including high strength-to-weight ratio and excellent corrosion and fatigue resistance [1-3]. For structural applications, FRP composites are in the form of a laminate, typically composed of multiple plies of prepregs (i.e. fabrics pre-impregnated with polymeric matrix). Autoclave curing is currently the standard technique for producing high-quality FRP composite parts, especially in the aerospace industry [4]. In autoclaves, high compaction pressure and elevated temperature are applied using a pre-determined curing cycle to ensures full consolidation of the laminate, leading to a high fiber fraction (≈60%) and low void content (<2%) [5, 6].

Despite the great advantages of autoclaves, high capital investment for the equipment as well as high operational costs and part size constraints have motivated researchers to find alternative lower-cost out-of-autoclave (OOA) methods [4, 7].

Among them, liquid composite molding (LCM) techniques such as resin transfer molding (RTM) or vacuum assisted resin transfer molding (VARTM) are of interest as they produce good-quality composite parts and offer attractive features such as reasonable cost and flexibility [8-10]. In the RTM process, multiple plies of fabric (or preform) are placed into a two-piece matched rigid mold and the resin is injected into the preform in the closed mold under pressure [8]. In VARTM, however, a flexible sheet is used as the upper mold which is sealed to the rigid mold using a sealant tape, and the resin is infused into the preform under vacuum [11]. A key issue in the infusion processes is the gel time of the resin system, which may not be enough to completely wet the fabric with resin and premature gelation may occur during infusion [12]. In addition, the high impregnation rate of fibrous reinforcement increases the risk of entrapping voids in the final part, which may adversely affect the performance and long-term durability of composites [13, 14]. Accordingly, several variants of VARTM have been developed such as Seeman composites resin infusion molding process (SCRIMP) [15], controlled atmospheric resin infusion process (CAPRI) [16], pressurized infusion (PI) [17], compaction of dry fiber preforms with stationary and moving magnets [13], and applying magnetic consolidation pressure in VARTM [14].

Vacuum bag only (VBO) prepreg processing is another approach in OOA techniques [18]. In VBO, partially impregnated prepregs are used with new resin formulations that allow removal of entrapped air during a lengthy vacuum hold before elevated temperature curing in a standard oven [19]. Since the applied consolidation pressure is limited to 0.1 MPa, the high levels of absorbed moisture by the prepreg and

insufficient air evacuation time may lead to process-induced defects such as voids in the VBO part [18, 20, 21].

Quickstep process is, one of the OOA technologies, developed by an Australian company (Quickstep Technologies Pty Ltd.) [22]. In Quickstep, two floating rigid or semi-rigid molds are used to sandwich the composite laminate in-between [22-24]. In this process, heat is quickly applied to the composite laminate by circulating a heat transfer fluid (HTF) in both the top and bottom sides. A flexible, thermally conductive, membrane or bladder separates the laminate and the mold from HTF. Using flow of HTF makes it possible to achieve a very high ramp rate of 10–15 K min^{-1}, much faster than 2–3 K min^{-1} ramp rate generally used in an autoclave. The higher ramp rate results in a lower minimum viscosity of the resin and better fiber wetting, leading to a better fiber-matrix adhesion in Quickstep manufactured composite parts [25]. Accordingly, the interlaminar fracture toughness under Mode I and Mode II for carbon epoxy composites made by Quickstep are comparable to those made in an autoclave [25]. In addition, the rapid heating and cooling process in Quickstep may save the processing time by 67% compared to autoclave [25]. It is also observed that faster heating rates do not necessarily lead to higher void contents compared to slower heating rates, a positive aspect of an OOA process [24]. In addition, a higher ramp rate affects the chemorheology of the epoxy-based thermoset resin system, where higher glass transition temperature with similar molecular network structure is reported in Quickstep processed samples compared to the autoclave cured ones [26]. However, panels made by Quickstep absorb slightly higher moisture content, probably because of their higher resin content and cross-link density [27]. It is well-established that the absorbed may

adversely affect mechanical properties and durability of polymeric composites [27]. To improve the quality of Quickstep laminates by reducing their void content to below 1%, Muric-Nesic et al. [28] subjected the laminates during cure to vibrations with the low frequency of around 10 Hz.

Another alternative approach to autoclave curing is prepreg compression molding (PCM), also known as hot press molding. In the PCM process, an uncured laminate made of prepregs is pressed and cured between the heated molds [29, 30]. The PCM process is well-known for its high productivity, low equipment cost, and simplicity. However, the cost of PCM molds is typically high because of the required structural rigidity to apply high pressures (≈10 MPa) and tight tolerances to avoid leakage [31]. Recently, Lee et al. [29] found that with applying vacuum pressure in the PCM process, the common PCM-process induced defects such as micro grooves and voids can be reduced in the composite products.

Although OOA techniques are more cost-efficient than autoclave curing, the composite parts produced via these processes may not achieve the same levels of mechanical properties as those obtained in an autoclave. One of the objectives of the current work, therefore, is to develop a novel technique, magnet assisted composite manufacturing (MACM) to produce high-quality composite laminates out of an autoclave. In this technique high-temperature permanent magnets are utilized to generate sufficiently high consolidation pressure during cure of prepregs, thus eliminating the necessity of using an autoclave.

1.2. Controlling surface microstructure of structural laminates

The FRP composites are very attractive material for structural applications, especially in the aerospace industry due to their high strength and stiffness to weight ratio and low sensitivity to fatigue and corrosion [32, 33]. This outstanding combination of properties has promoted the replacement of traditional metals by FRP composites. For instance, Boeing 777 uses 12% composites and 50% aluminum while in Boeing 787, aluminum usage dropped to 20% and composites usage increased to 50%. However, the low conductivity of composites compared to metals currently limit their applications [34].

To tailor mechanical and functional properties of composites such as thermal and electrical conductivities, most research so far has focused on the incorporation of micro- or nano-sized reinforcements into traditional FRP composites [35-41]. Typically, for fabrication of three-phase (consisting of particle reinforcements, fabric, and resin) composites, the resin is first modified by adding particles and then the particle/resin suspension is infused into the fabric by VARTM [37, 40, 42, 43]. However, a uniform and stable dispersion of particles within the polymer matrix, as well as unavoidable dramatic increase in viscosity of the resin due to the addition of particles and filtration of particles during infusion are critical issues in the processing of these three-phase composites [39, 40, 44, 45].

One alternative approach to manufacture three-phase composite laminates is to first, deposit the short fibers or other nanoscale reinforcements onto the fabric surface and then, infuse resin into the deposited fabric by VARTM. With this approach, resin viscosity does not increase and the challenges with the conventional VARTM process

are overcome. Several techniques have been introduced to deposit short fibers on the fabric surface, such as chemical vapor deposition (CVD) [46, 47], electrophoretic deposition (EPD) [48, 49], spraying processing [50-53], and aqueous suspension deposition [54].

To achieve a very high reinforcement content and preferred in-plane orientation in the three-phase composites, the reinforcements are grown onto the fabric surface by the CVD process [55]. In addition, the CVD process is applicable for a variety of reinforcements and fabric substrates. For instance, He et al. [56] reported that homogeneously aligned carbon nanotubes-glass/epoxy composites can be fabricated with CVD process, showing significantly improved electrical conductivity and thermo-mechanical and flexural properties compared to glass/epoxy composites. However, the use of high temperatures and predeposited catalysts along with the difficulties in the processing of large parts are the limitations of CVD method [48]. Furthermore, Sager et al. [46] reported that with the growth of carbon nanotubes on the surface of carbon fibers using the CVD process, the tensile strength of the fiber reduces at least by 30%, possibly due to thermal degradation and surface oxidation of fibers.

Alternatively, the EPD process has been applied successfully to fabricate three-phase composites because of its simplicity, scalability, and cost-effectiveness [57]. In EPD, charged particles, dispersed in a suitable solvent, migrate towards an electrode under an applied electric field, resulting in the accumulation and homogeneous deposition of particles at the relevant electrode [58]. In this regard, Rodriguez et al. [59] demonstrated that with EPD process amine-functionalized carbon nanofibers can be uniformly deposited on the surface of a layer of carbon fabric using water as a solvent.

However, a uniform deposition of particles with this method depends on several processing parameters including the PH level of suspension, applied voltage, deposition time, and isolation process of electrodes [60].

In spraying processing, the dispersed reinforcements in a solvent are sprayed onto the fabric surface using an airbrush, and then the solvent on the fabric is removed, remaining the reinforcements-deposited fabric [52]. This process can be modified by spraying a kind of epoxy resin with high viscosity on the deposited fabric to anchor the reinforcements, thus preventing their flushing during infusion [53]. Shan et al. [53] reported that the modified spraying technique can produce composites with enhanced interlaminar fracture toughness while preserving their in-plane mechanical properties. This method is simple and scalable; however, it may be difficult to control the dispersion and distribution of reinforcements throughout the resultant composite.

To directly deposit reinforcements on the fabric surface, aqueous suspension deposition can be used [54, 61, 62]. In this process, the reinforcements are first dispersed in deionized water by ultrasonication and then, the fabric is immersed in a bath containing the reinforcement/water suspension, followed by drying the deposited fabric [54]. Li et. al [54] demonstrated that with the deposition of hydroxyl-functionalized carbon nanotubes, the interfacial shear strength of the carbon fiber/epoxy composites increases up to 43% compared those made without deposition. However, during the immersion process, the reinforcements are deposited on both sides of the fabric surface, which may not be preferred for some applications.

To assess the effectiveness of the deposition techniques for the fabrication of multifunctional materials, previous studies have focused on measuring mechanical,

thermal, electrical, and/or magnetic properties of the resultant three-phase composite. However, a detailed quantitative microstructural analysis of the deposition morphology in terms of: (i) spatial uniformity of fiber volume fraction; (ii) degree of dispersion; and (iii) orientation and degree of alignment on the fabric surface and on the fabricated laminates has never been conducted.

In the present work, a novel and simple method, allowing uniform and isotropic deposition of micron-sized fibers on the fabric surface, is introduced for fabrication of three-phase composites with controlled surface microstructure. This method, cascaded suspension deposition, is based on slowly cascading the fibers/water suspension on the fabric surface immersed in water followed by the sedimentation of fibers under gravity. The effectiveness of the proposed technique to uniformly distribute fibers on the surface of the fabric and the resulting structural laminates are investigated through comprehensive microstructural analysis. For this purpose, the uniformity of fiber volume fraction, as well as, degree of dispersion and alignment of the fibers are assessed. Also, the effects of the concentration of deposited fibers, fabric architecture, and resin flow on the process-induced microstructure are investigated.

1.3. Tailoring anisotropy in structural laminates

The fundamental limitations of FRP composites are the poor conductivities, which hinders FRP applications in thermal management systems and electronic packing. To address the poor conductivity properties of FRPs, integration of conductive short fibers into traditional FRP composites is a promising technique. Typical conductive reinforcements used to manufacture conductive polymer composites include metal powders and carbon-based materials such as carbon fibers, graphene nanoplatelets, and

carbon nanotubes [63-67]. However, at low volume fractions of reinforcements, the conductivity of the composite is low, similar to that of the pure polymer. To considerably improve the conductivity, a high loading (i.e. volume fraction of ≈ 50%) of randomly distributed reinforcements is required, thus forming some conductive pathways in composites [68-71]. For example, Mazov et. al reported that the thermal conductivity of polypropylene-based composites with 16 wt.% multiwall carbon nanotubes is only around 0.56 W/m × K [72]. However, the processing of composite at high reinforcements loading is difficult and the formation of aggregates of reinforcements may adversely affect the mechanical properties of the composite [72-74]. Therefore, it is desirable to increase the conductivity of the composite without having high reinforcements content.

Controlling the orientation and alignment of short fibers is a promising method for significantly improving the conductivity of the composite in the direction of fibers orientation [75-77] compared to composites with randomly-oriented fibers. For instance, Khan et al. demonstrated a very low percolation threshold of about 0.0031 vol% in multi-walled carbon nanotubes (MWCNTs) epoxy composites along the direction of MWCNT alignment, significantly lower than 0.034 vol% for randomly-oriented MWCNT epoxy composites [75]. In addition, with inducing alignment of short fibers, it is possible to introduce anisotropy in the composite, thus tailoring direction-dependent properties.

For inducing alignment of short fibers in three-phase composites, currently, a popular method is to align reinforcements by deposition methods on the fabric surface prior to fabrication of three-phase laminate by VARTM [78, 79]. For instance, Wicks et

al. [78] implemented aligned carbon nanotubes (CNTs) in the alumina-fiber epoxy composite by growing vertically-aligned CNTs by chemical vapor deposition directly on the surface of individual fibers. Stahl et al. [80] shear pressed the vertically aligned CNT arrays to change vertical alignment to a nearly horizontal plane of thin solid sheet. Then, they integrated the dry or resin infused sheet between prepreg plies prior to the laminate cure.

An alternative approach for inducing alignment of short fibers in three-phase composites is by using external fields during composite fabrication, which has the advantages of scalability and precise control of the alignment. Reinforcements orientation and alignment can be induced in composites by applying magnetic field [81-83], electric field [84-86], acoustic field [87], and shear flow [88] during composite fabrication. Regarding inducing alignment with the shear flow, it is difficult to obtain continuous conductive pathways or end-to-end contacts, leading to low anisotropy [89]. Comparing magnetic field with electric field, magnetic field does not have the limitations of dielectric breakdown or electrode polarization using electric fields [90]. Compared to the acoustic field, magnetic field can be generated without the use of a complex set-up [87], e.g. using permanent magnets. Thus, among these feasible approaches, magnetic field is chosen in this work because of its attractive capabilities.

Thermodynamically, a combination of parameters such as fiber size, field strength, and magnetic susceptibility anisotropy leads to magnetic field induced alignment [91]. For example, Camponeschi et al. [92] applied a magnetic field of up to 25 T to orient and align CNTs in polymer composite, which is quite high. Therefore, short fibers are coated with magnetic nanoparticles, especially nickel-based

nanoparticles, to align them in a polymer resin without the need to apply high magnetic fields [83, 93]. Controlling the orientation of nickel coated carbon (NiC) fibers in a polymer resin using magnetic field has been previously demonstrated in Ref. [81, 94]. They reported that NiC fibers with an average aspect ratio of 45 possess an anisotropic diamagnetic susceptibility of 2.5×10^{-2}, and can be aligned under a low intensity magnetic field (<0.2 T). Most of the reported research efforts in this area have been focused on inducing alignment of short fibers in polymer resin using an external field. However, controlling the orientation of short fibers in three-phase composites by using external field has not been elucidated.

In the present work, a new magnetic-field assisted composite processing is proposed for inducing alignment of short fibers in molded laminates, thus tailoring their surface anisotropy. In the proposed technique, magnetic field generated by a set of permanent magnets is used for controlling the orientation of NiC fibers on the surface of three-phase NiC/glass/epoxy laminates. Different degrees of alignment of fibers are induced by applying magnetic field: (i) on the fabric substrate during deposition of fibers, (ii) on the deposited fabric after mold filling by VARTM, and (iii) on the fabric substrate during deposition, mold filling, and after mold filling. Since a good dispersion and uniform distribution of fibers on the fabric surface is necessary for achieving improved properties of composites, cascaded suspension deposition is adopted.

1.4. Dissertation outline

Chapter 2 presents the development of a new feasible technique, MACM, for fabricating structural composite laminates out-of-autoclave. The ability of MACM to fabricate high-performance laminates with fiber and void volume fractions and

mechanical properties comparable to those made by autoclave curing is also demonstrated.

A novel method, cascaded suspension deposition, to introduce well-dispersed short fibers into the molded laminates, allowing the control of the surface properties of the resulting composite is proposed in chapter 3. Comprehensive analysis of the process-induced microstructure morphology on the fabrics and on the fabricated laminates are carried out by assessing: (i) spatial uniformity of fiber volume fraction; (ii) degree of dispersion; and (iii) process-induced orientation and degree of alignment. To demonstrate the flexibility of the proposed method, the effects of fiber concentration, fabric architecture, and resin flow are studied.

Chapter 4 includes two parts. The first part of chapter 4 investigates the alignment of nickel coated carbon (NiC) fibers by magnetic field during cure of polymer composites. The appropriate level of magnetic field for achieving a high degree of alignment of fibers is identified. In the second part of chapter 4, a new magnetic-field assisted composite processing method is proposed to align NiC fibers on the surface of three-phase composite laminates. Given the results of the first part of chapter 4, an appropriate level of magnetic field generated by a set of permanent magnets is applied for inducing alignment of NiC fibers without disturbing the uniformity of microstructure in the composite. This chapter investigated the effects of varying physical properties of fibers (i.e. fibers aspect ratio and nickel coating) on the microstructure morphology of composites.

Chapter 5 states the conclusions and contributions of this work, as well as recommendations for future work.

Chapter 2. Magnet Assisted Composite Manufacturing: A Novel Fabrication Technique for High-Quality Composite Laminates

A novel fabrication method, magnet assisted composite manufacturing (MACM), is developed to produce high-quality composite laminates out of an autoclave. This technique involves the placement of high-temperature Neodymium permanent magnets on a vacuum bag to generate sufficiently high consolidation pressure during cure, thus eliminating the necessity of using an autoclave. The objective of this chapter is to demonstrate the ability of MACM to fabricate high-performance laminates which have comparable mechanical properties, fiber volume fraction, and void content to those achieved by autoclave curing. Towards this goal, eight-ply, woven carbon/epoxy laminates are fabricated in an oven by MACM and also in an autoclave using the same thermal cycle. The thickness of the laminates cured by MACM indicates that an effective consolidation pressure of 0.29 MPa (42 psi) can be generated by the magnets during cure at 177°C (350°F). The high flexural properties, high fiber volume fraction, and the low void content of the laminates fabricated by MACM validate the feasibility of this process as a lower-cost alternative to autoclave cure, without compromising the part quality. Considerable reduction of void content to under 1% is also achieved by applying magnets during cure when the resin viscosity is at a minimum.

2.1. Introduction

Various processing techniques are developed to fabricate high-performance composite laminates to meet functional design requirements at a reasonable cost. Manufacturing techniques such as autoclave curing, hot-press molding [95], vacuum-

bag-only (VBO) curing [96, 97], and Quickstep [25] have been broadly used for fabricating high-quality composite laminates from prepregs. Among these methods, autoclave curing is primarily utilized for the fabrication of structural composites in the aerospace industry, where the prepreg lay-up is placed in a vacuum bag and subjected to high consolidation pressure and temperature during a cure cycle. The benefits of using an autoclave include the ability to achieve fiber volume fractions above 60% [98] for improved mechanical properties as a result of applying sufficiently high consolidation pressure [99, 100]. The consolidation pressure, which is often applied throughout the cure cycle, helps reduce the formation of voids and enables removal of volatiles, trapped air, and excess resin out of the composite laminate. If the consolidation pressure is not adequate, elimination of the voids will be incomplete, thus yielding a composite laminate with relatively poor mechanical properties [101-104]. In addition to the level of consolidation pressure, the time when it is applied was shown to have a significant effect on the resulting void content [105, 106]. It should be noted that along with overall void content, spatial distribution and geometrical features of voids such as size and shape morphology could have noticeable adverse effects [107-110]. For example, microcracks may grow from high-aspect-ratio elliptical voids located at the fiber-matrix interface that could lead to premature fracture of the laminates [111, 112]. Consequently, overall void content, as well as process-induced void morphology throughout the laminate, should be investigated for evaluating the effectiveness of a manufacturing process.

Although the benefits of using an autoclave are well established, they are expensive, labor-intensive to operate, and consume excessive energy [113], thus leading

to a higher cost per cured part. As a result, development of more cost-effective out-of-autoclave (OOA) technologies such as hot-press molding, VBO cure processing, and Quickstep is highly desirable for the fabrication of high-performance composite laminates.

The hot press molding involves pressing the laminate into the heated rigid mold so that parts with two good surfaces, high fiber volume fraction (56%) and low void content (<2%) can be manufactured using high enough pressure [30, 114]. However, the sensitivity of matched-die to material variation and the dependency of this technique on thermal conductivity of the mold are some of the common drawbacks [115].

Vacuum-bag-only (VBO) cure involves fabricating parts in an oven with only vacuum-bag consolidation pressure up to 101 kPa. However, this level of pressure may not be sufficient to suppress void growth and remove entrapped air. Thus, the composite laminates fabricated using this method can be prone to voids [116], especially when the prepreg contains a reactive resin matrix [117]. Also, during VBO cure processing, the presence of moisture in a humid environment can significantly affect the quality of composites [18]. In VBO curing, a vacuum hold before initiating the cure cycle and heat transfer rates lower than an autoclave are necessary to minimize void content. Therefore, typically longer cure cycles are used in VBO compared to autoclaves [118].

Quickstep is a rapid OOA technology which uses as high as 40ºC/min ramp rates and shorter cure cycles compared to autoclaves [119, 120]. The rapid heating/cooling of the laminate is achieved by utilizing a Heat Transfer Fluid (HTF) due to the higher heat capacity of fluids. The higher ramp rates lead to the lower minimum viscosity of the resin and possibly improved fiber-matrix adhesion due to better fiber

wetting [25]. In addition to the vacuum pressure, the weight of the HTF provides a modest consolidation pressure of 10 to 30 kPa in Quickstep process where high-quality laminates with 61% fiber volume fraction and 2-5% void content can be manufactured [119, 121]. Khan et al. [27, 122] reported that 977-2A carbon/epoxy laminates manufactured by Quickstep absorb a high amount of moisture because of higher resin content and increased crosslink density compared to laminates cured in an autoclave. Despite the reduction in cycle time and energy consumption, Quickstep requires relatively expensive equipment (approximately two-thirds of an equivalent autoclave) [123], periodic replacement of the flexible membrane, and transferring HTF to control the heat rate [118].

Although OOA technologies are more cost-efficient than autoclave curing, mechanical properties of composites manufactured by autoclaves are typically higher due to the higher fiber volume fraction and lower void levels [95]. Therefore, developing new OOA processes that can produce laminates matching or exceeding the mechanical properties of the autoclave-cured laminates without increasing the production cost, process time, and energy consumption would be highly desirable. Towards this goal, curing composite parts under sufficiently high pressure (i.e., comparable to autoclave pressure) generated by magnetic force may offer an attractive alternative solution.

The utilization of an electromagnetic clamping device to consolidate the composite laminates is recently proposed by Ziegenbein and Colton [124]. In this device, the clamping pressure is generated between a rubber membrane containing iron particles and an array of electromagnets. If the actively cooled electromagnets are

utilized, the maximum possible clamping pressure is estimated to be 0.1 MPa which is far below the required processing pressure for prepregs. Also, the effectiveness of the electromagnetic clamping device is not demonstrated by fabricating composite laminates.

A more robust and feasible approach to generate sufficient consolidation pressure is to utilize high-power permanent magnets. For this case, the vacuum bag containing the composite laminate can be sandwiched between the magnets and a magnetic tool material, possibly a thin steel sheet. For fabricating geometrically complex shapes, the thin steel sheet can be easily formed to the desired shape and placed over the underlying tool, which is often made of a lighter metal such as aluminum or a durable composite. A variety of permanent magnetic materials that can generate considerable compressive pressure over small gaps exists. Among these, Neodymium Iron Boron, SmCo, Alnico, Ceramic (Ferrite), and Flexible (Rubber) magnets are utilized for numerous industrial applications and, depending on their grade, may be used up to 840°C without losing much of their magnetic strength. Pallapa and Yeow [125] reported that Neodymium Iron Boron, NdFeB, magnets have the highest energy products (160-400 kJ/m^3) compared to other materials and can generate up to 0.8 MPa compressive magnetic pressure. The compressive force can be maintained for long-term use, where the total irreversible loss in magnetic properties is expected to be only up to 2% after ten years of operation [126].

In this chapter, a new and innovative out-of-autoclave manufacturing technique for producing high-quality, structural composite laminates is presented. This technique referred to as “Magnet Assisted Composite Manufacturing” (MACM), involves

utilizing the compressive force of high-power, high-temperature permanent magnets as the consolidation pressure while the laminate is placed in a vacuum bag and going through the conventional cure cycle in an oven. The MACM technique is highly promising because it does not require special tooling or expensive equipment, and thus could produce structural composites at a much lower cost compared to those made by autoclave cure. Improving fiber volume fraction and overall quality of the laminate at critical, high-stress locations would be possible by applying the magnetic pressure only on these critical areas of the laminate. Although it is beyond the scope of this work, MACM may be effectively used for manufacturing large structural composites. For such applications, one can slide an array of magnets covering a small area over the vacuum bag, instead of covering the entire part surface with magnets.

The potential of the MACM process is demonstrated by curing eight-ply carbon fiber/epoxy laminates in a variety of manufacturing scenarios. Experimental results including void and fiber volume fraction, microstructural analysis, and flexural properties of the laminates manufactured by MACM are presented and compared with those obtained from laminates cured in an autoclave. Furthermore, the proper time of applying the consolidation pressure based on temporal changes in resin viscosity is investigated.

2.2. Materials and methods

2.2.1. Materials

The composite material used in this work is TENCATE IM7/EX-1522, which is a plain weave carbon/epoxy prepreg system. The uncured resin content is 45±3% by weight. IM7 is a PAN-based carbon fiber with a relatively high performance and

intermediate modulus that has been primarily used in the aerospace composites. EX-1522 is a toughened, high-performance epoxy resin with a glass transition temperature of 180ºC. A 2.2-2.8°C/min ramp rate with a 180 min hold at 177°C (350°F) and 0.27-0.69 MPa (40-100 psi) autoclave pressure is the recommended cure cycle.

2.2.2. High-temperature permanent neodymium magnets

Sixteen through-the-thickness magnetized N38EH neodymium magnets (K&J Magnetics) of dimensions 2.54 cm in length, 2.54 cm in width, and 5.08 cm in thickness are used to provide compressive pressure on the lay-up which is placed on a magnetic tool plate (see Fig. 1.). The highest operating temperature of each magnet is 200°C with a maximum energy product of 302.4 kJ/m^3 (38 MGOe). A compressive pressure of 0.55 MPa can be generated when the magnets are sandwiched without a gap between two steel plates at room temperature. The actual magnetic pressure applied on the lay-up will be less than 0.55 MPa due to: (a) increased temperature during cure and (b) the small gap between the magnets and the bottom tool plate (i.e. lay-up thickness).

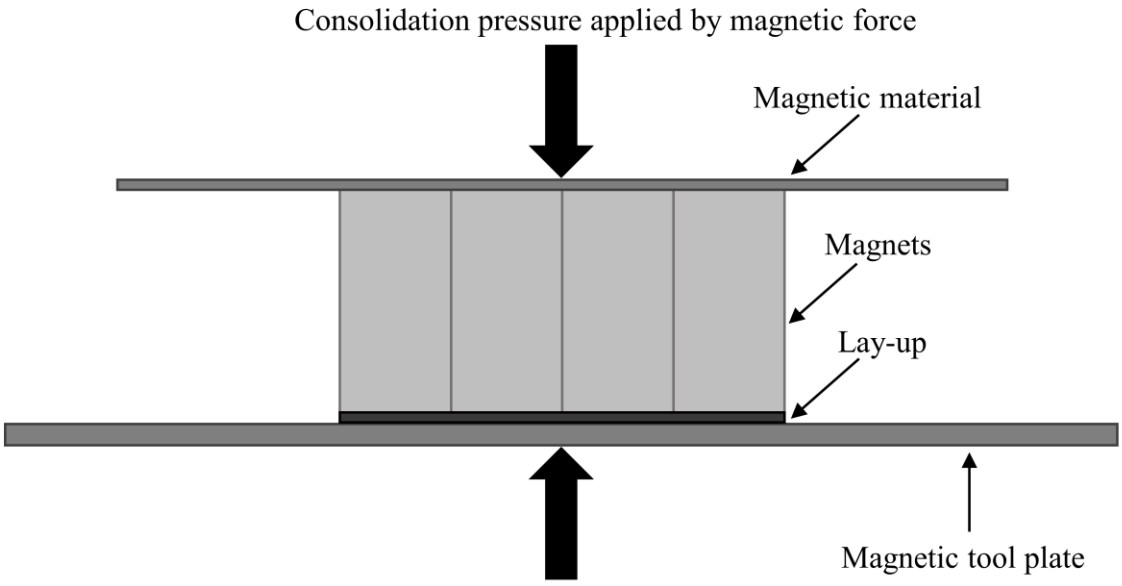

Figure 1. Consolidation pressure applied by magnetic force.

2.2.2.1. Effect of elevated temperature on magnetic compression during cure

The compressive pressure, *P*, exerted by a permanent magnet at the lay-up surface is given by [124]

$$P = \frac{B^2}{2\mu_0} \quad (1)$$

where *B* is the magnetic field flux density and μ_0 is the permeability of the lay-up. In deriving equation (1), the following assumptions have been made: 1) The flux density, *B*, on the surface does not vary; 2) The magnet completely covers the underlying lay-up, leading to a uniform compressive pressure on the lay-up surface.

The magnetic flux density, *B*, for N38EH magnets used in this work is given as 1.093 T at room temperature. Considering the decrease in *B* at elevated temperatures and assuming the lay-up permeability remains constant, one can estimate the reduction in compressive pressure applied by the magnets during cure. Fig. 2 illustrates the linear reduction in magnetic compressive pressure as a function of temperature which is reversible up to the maximum operating temperature of the magnets (200ºC). At cure temperature of 177ºC, the pressure will be reduced approximately by 35%.

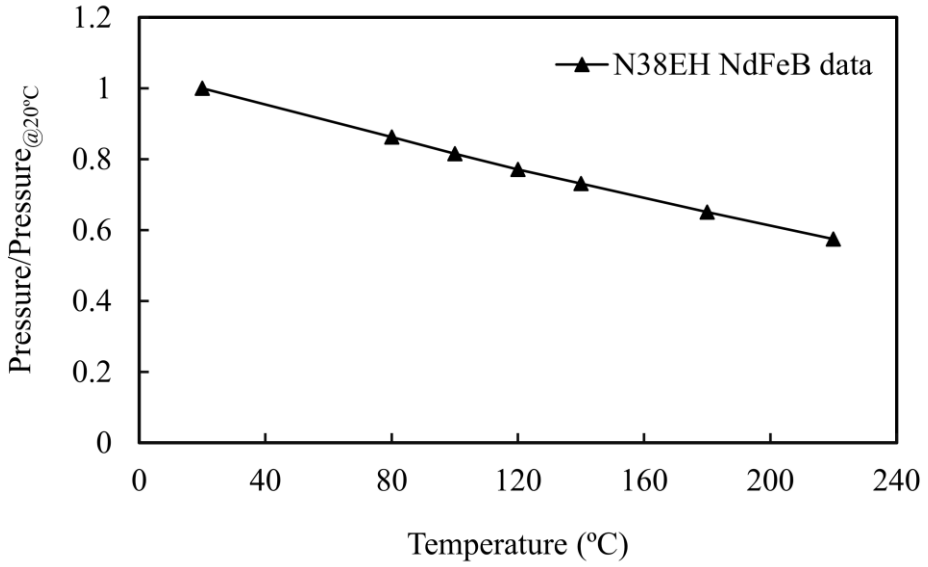

Figure 2. Normalized compressive pressure exerted by a N38EH neodymium magnet versus temperature.

2.2.2.2. Effect of lay-up thickness on magnetic compression during cure

The maximum compressive pressure is achieved when the magnets are touching the steel tool plate. However, the magnetic pressure depends on the thickness of the lay-up. The thickness of the lay-up decreases during cure, so the magnetic pressure will increase gradually. According to the previously published literature, the thicknesses of the fabricated carbon fiber–epoxy prepreg laminates for 8, 16, and 20 plies are approximately 2.1 to 4.3 mm [127-129]. Considering these thicknesses, the N38EH is capable of generating the maximum pressure of 0.3 MPa (44.76 psi), 0.22 MPa (31.70 psi), and 0.2 MPa (30.18 psi) for 8,16, and 20 plies respectively. Fig. 3 presents the effect of lay-up thickness on magnetic compressive pressure. It is seen that magnetic consolidation pressure will decrease in an approximately exponential manner with increasing the lay-up thickness. For the current lay-up (8-ply prepreg) with the initial

and final thicknesses of 2.5 and 2.0 mm, the consolidation pressure gradually changes from 0.28 MPa (41 psi) to 0.31 MPa (46 psi) during cure. As a result, the sufficient magnetic pressure (~30 psi) can be generated by N38EH for consolidating the laminate up to 20 plies inside the oven.

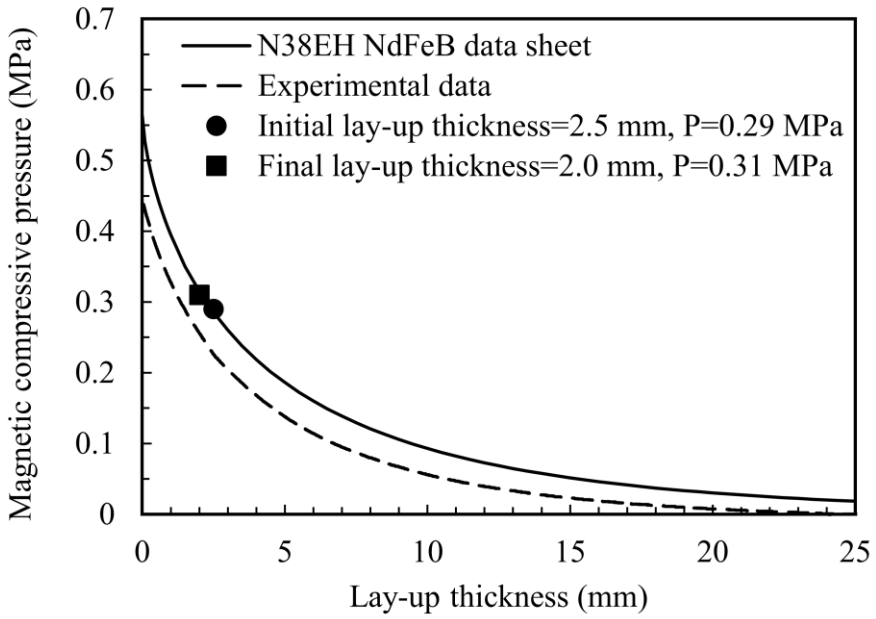

Figure 3. Compressive pressure exerted by a N38EH neodymium magnet versus gap distance.

2.2.3. Rheological measurements

Applying magnetic compressive pressure at a different time during cure cycle may facilitate improved resin flow and reduction in void content. Therefore, characterization of the minimum viscosity and gel point could be helpful in selecting when the magnets should be applied on the lay-up during the cure cycle.

Toward this goal, the rheological characterization of IM7/EX-1522 prepreg is performed by an Alpha Technologies APA rheometer with a disc radius of 19 mm and a gap size of 2.8 mm. The experiment is conducted at a frequency of 1 Hz under a

constant strain of 0.5%. The autoclave/oven cure profile (i.e. initial ramp of 2.2ºC/min followed by 177ºC hold for 180 min) is utilized for rheological characterization to determine when the minimum viscosity and gel point are reached for this prepreg. Fig. 4 depicts the change of complex dynamic viscosity over time during cure. It is seen that the minimum viscosity of the resin referred to as point **A** occurs at 55 min and 145ºC. The variation of tan delta and elastic shear modulus during cure is shown in Fig. 5. Point **B**, the gel point, takes place at 62 min and 161ºC. The gel point is determined according to ASTM D7750-12 as the time when the value of tan delta drops rapidly and simultaneously the value of elastic shear modulus (G') increases very promptly.

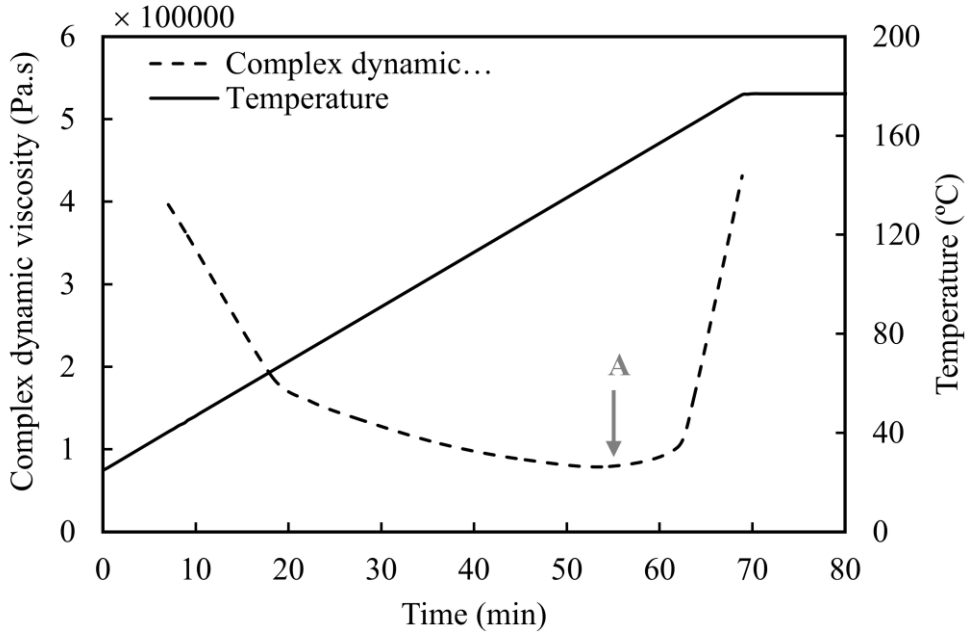

Figure 4. Complex dynamic viscosity as a function of time subjected to cure schedule during the rheological test (Point A is the minimum viscosity).

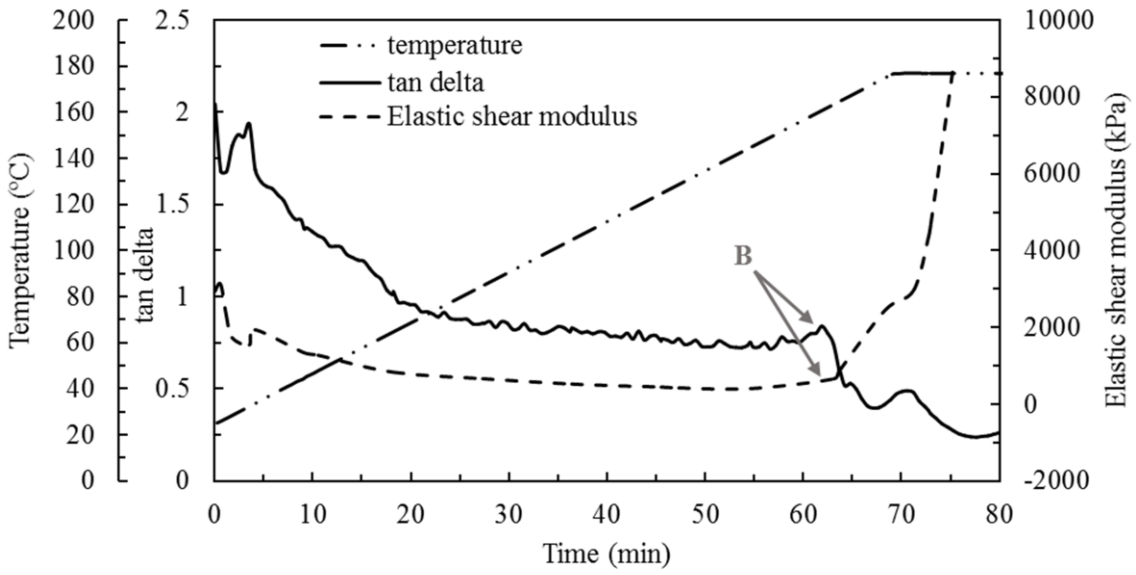

Figure 5. Tan delta, and elastic shear modulus as a function of time subjected to cure schedule during the rheological test (Point B is the gel point).

2.2.4. Magnet assisted composite manufacturing (MACM)

The new manufacturing technique, magnet assisted composite manufacturing (MACM), to fabricate composite parts is schematically illustrated in Fig. 6. This technique uses the compressive force of high-temperature permanent magnets as the consolidation pressure on the laminate. Briefly, the lay-up assembly consists of the vacuum bag, caul plate, bleeder/breather plies, porous teflon, and prepreg which is surrounded by an edge dam placed on the bottom steel tool plate. After the vacuum is applied, sixteen N38EH NdFeB magnets (25.4 × 25.4 × 50.8 mm), which are placed together in a 4x4 configuration on a 2.4 mm-thick top steel plate, compress the lay-up, as shown in Fig. 7. Then, the whole cure assembly (i.e. bottom steel tool plate, lay-up, magnets, and top steel plate) is placed in an oven. The cure cycle consists of a heat ramp of 2.2ºC/min to 177ºC followed by an 180 min isothermal hold and cooling to room

temperature at 3.5ºC/min. A vacuum pressure of 88 kPa (i.e., 13 kPa absolute pressure) is applied throughout the cure cycle.

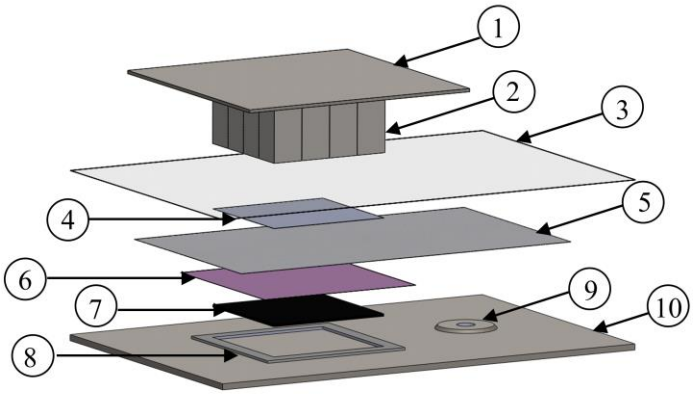

1. 2.4-mm thick magnetic material
2. Magnets
3. Vacuum bag
4. Caul plate
5. Bleeder/Breather
6. Porous teflon
7. Prepregs
8. Dam
9. Vacuum port
10. 4.7-mm thick magnetic mold material

Figure 6. Schematic illustration of the new manufacturing technique used to fabricate composite parts.

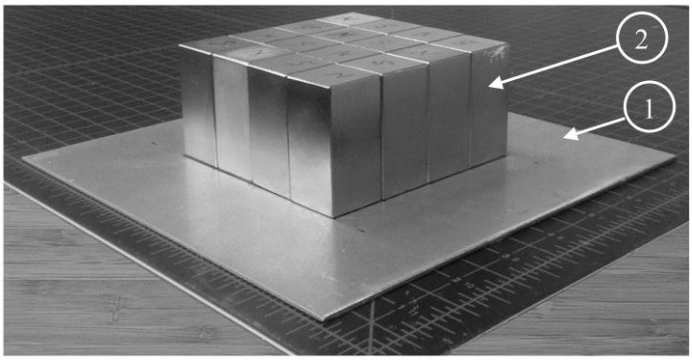

1. Magnetic material top plate with dimensions (length × width × thickness) of 203 × 203 × 2.4 mm
2. Sixteen N38EH NdFeB Magnets

Figure 7. Photograph of the arrangement of magnets that are employed in the proposed manufacturing technique.

In this work, 8-ply IM7/EX-1522 laminates (102 mm × 102 mm) are fabricated under seven scenarios in the oven and autoclave, as listed in Table 1. Two laminates for each fabrication scenario are produced to determine repeatability. In the first scenario (Oven-0MPa), the laminates are manufactured in the oven without magnets. Scenario 2 (Oven-Mag) is considered to investigate the effectiveness of the MACM process, where

magnets are applied throughout the cure cycle in the oven. Since applying pressure at different times during cure has been reported to improve laminate quality [12, 36], scenario 3 (Oven-Mag-μ_{min}), and 4 (Oven-Mag-Gel) are investigated, where the magnets are applied at minimum viscosity (point A) and gel point (point B) respectively, until the end of the cure cycle. Applying magnets at the point of minimum viscosity is expected to further enhance resin flow and help reduce the void content throughout the laminate. To establish the MACM process as a viable method, the mechanical properties, fiber volume fraction and void content of the composites manufactured in the oven with or without using MACM are compared to those manufactured in the autoclave under identical cure cycle. Hence, three additional scenarios are considered: scenario 5 (Autocl-0MPa), autoclave curing without any pressure, scenario 6 (Autocl-0.2MPa), autoclave curing with 0.2 MPa pressure, and scenario 7 (Autocl-0.4MPa), autoclave curing with 0.4 MPa pressure.

Table 1. Seven fabrication scenarios used in manufacturing of IM7/EX-1522 composite laminates.

Fabrication scenario		Manufacturing process
1	Oven-0MPa	Oven curing using vacuum bag only, without pressure
2	Oven-Mag	Magnet assisted composite manufacturing (MACM) in oven
3	Oven-Mag-μ_{min}	MACM applied at minimum viscosity in oven
4	Oven-Mag-Gel	MACM applied at gel point in oven
5	Autocl-0MPa	Autoclave curing using vacuum bag only, without pressure
6	Autocl-0.2MPa	Autoclave curing with 0.2 MPa pressure
7	Autocl-0.4MPa	Autoclave curing with 0.4 MPa pressure

2.2.5. Void and fiber volume fraction measurement

The density of each composite specimen is identified by the suspension technique. In this method, the Cargill Labs 2.49 g/cm^3 heavy liquid is diluted with water until the specimen is suspended in the mixture. Fiber and matrix weight content are determined using a hot sulfuric acid-hydrogen peroxide digestion method as described in ASTM D3171 Procedure B. The density of cured resin is also measured by the suspension method and found to be 1.46 g/cm^3. The density of fiber reinforcement is obtained to be 1.79 g/cm^3 using a nitrogen pycnometer. Fiber volume fraction (V_f) and void volume fraction (V_v) are calculated according to the following equations as recommended by ASTM D3171.

$$\text{Fiber volume fraction (\%)} = \left[\frac{\rho_c W_f}{\rho_f}\right] \quad (2)$$

$$\text{Void volume fraction (\%)} = 100 - \rho_c \left[\frac{W_f}{\rho_f} + \frac{W_m}{\rho_m}\right] \quad (3)$$

where W_f is the fiber weight fraction in the composite, ρ_f is the density of the fiber, ρ_c is the density of the the composite specimen, W_m is the matrix weight fraction in the composite, and ρ_m is the density of the matrix.

2.2.6. Image analysis

A detailed image analysis is one of the most accurate methods for the characterization of microvoid morphology. SEM is used for imaging of 3 mm x 2 mm through-the-thickness cross-sectional area from all samples. The composite specimens are mounted in acrylic resin, polished, and coated with gold/palladium to obtain SEM images at both the 50X and 200X magnifications. Four different cross-sections locations are analyzed for each processing scenario to reduce experimental uncertainty

due to spatial variation of voids. Image analysis software is used to determine the location, size, and shape of all visually identified voids.

Equivalent diameter, D_{eq}, is obtained from the void area and can be used to determine the void size distribution for each specimen,

$$D_{eq} = \sqrt{\frac{4A}{\pi}} \tag{4}$$

where A is the void area. Small voids are defined as voids with an equivalent diameter lower than 20 μm. Voids with the equivalent diameter between 20 μm and 100 μm are classified as medium voids. Voids with an equivalent diameter above 100 μm are regarded as large voids.

To classify void shapes with respect to their circularity according to ASTM F1877-05, roundness, R, is defined,

$$R = \frac{4A}{\pi d_{max}^2} \tag{5}$$

where d_{max} is the maximum diameter within the void. Roundness equals unity for a perfectly circular void and goes to zero for a highly elongated void. A lower roundness value (R<0.5) represents elongated to very elongated voids. Voids with roundness in the range (0.5<R<0.9) are considered slightly elongated. Roundness greater than (0.9<R) is observed in mostly circular voids.

2.2.7. Flexural test

Three-point bending tests are conducted using a Com-Ten 705TN system as per ASTM D790. A total of 12 specimens (length= 76.2 mm and width=12.7 mm, six from each laminate) are used to determine flexural properties. The support span for all

specimens is controlled so that a support span-to-depth ratio of 32:1 is achieved. The specimens are tested at a crosshead rate of 2 mm per minute.

2.3. Results and discussion

2.3.1. Fiber volume fraction and void content

The fiber volume fraction, void volume fraction, and average thickness of the composite laminates cured under different fabrication scenarios are shown in Table 2. It is seen that the fiber volume fraction and void content of the composites manufactured in the oven and autoclave using the same thermal profiles without applying external pressure are similar. The fiber volume fraction of 51-52% and a void volume fraction of 4.8-5.0% obtained without applying any pressure during cure establish the baseline values that can be improved by either applying magnets or autoclave pressure.

Table 2 shows that other five fabrication scenarios significantly change fiber volume fraction and void content. In fact, all five scenarios Oven-Mag, Oven-Mag-μ_{min}, Oven-Mag-Gel, Autocl-0.2MPa, and Autocl-0.4MPa record substantial enhancements in fiber volume fraction as well as a reduction in microvoids. Table 2 further confirms that fabricating carbon epoxy composites with high fiber volume fraction (~60%) and low void volume fraction (<3%) is possible when magnets are placed on the vacuum bag throughout the cure cycle (Oven-Mag). Application of magnets at minimum viscosity (Oven-Mag-μ_{min}) has an additional advantage in reducing the void volume fraction to 0.9% while maintaining 60% fiber volume fraction. Thus, use of the sufficient consolidation pressure as well as applying this pressure at the proper time helps to fabricate high-quality composite parts, which has been reported earlier [107, 130, 131]. Table 2 also confirms that higher consolidation pressure results in higher

fiber volume fraction and lower laminate thickness. Thus, the highest fiber volume fraction (≈ 63%) and the lowest thickness (1.63 mm) are attained at 0.4 MPa autoclave pressure (i.e., by scenario referred to as Autocl-0.4MPa). Obviously, in MACM, the magnetic pressure increases while the thickness of the laminate decreases during the consolidation of the laminate. This is in contrast with the autoclave curing where it is common practice to apply a uniform pressure during cure. One can estimate that the laminate thickness of 1.68 mm, which is obtained by applying the magnets either at the minimum viscosity point or throughout the cure, would have been produced by applying 0.29 MPa (42 psi) constant pressure in an autoclave. This high level of equivalent pressure level further validates the possibility of using magnets during cure of commercial prepregs in lieu of autoclaves, even at the elevated cure temperature of 177°C (350°F).

Table 2. The fiber volume fraction, void content, and average thickness for laminates fabricated by different fabrication scenarios (*n*=6 for fiber and void volume fraction and *n*=18 for average thickness, 95% confidence intervals).

Fabrication scenario		Fiber volume fraction (%)	Void volume fraction (%)	Average thickness (mm)
1	Oven-0MPa	51.2 ± 0.7	4.8 ± 0.5	1.96 ± 0.01
2	Oven-Mag	59.6 ± 0.3	2.5 ± 0.2	1.68 ± 0.01
3	Oven-Mag-μ_{min}	60.4 ± 0.7	0.9 ± 0.2	1.68 ± 0.03
4	Oven-Mag-Gel	55.0 ± 1.1	1.5 ± 0.9	1.85 ± 0.03
5	Autocl-0MPa	51.9 ± 0.7	5.0 ± 0.4	1.90 ± 0.01
6	Autocl-0.2MPa	57.6 ± 0.9	1.7 ± 0.6	1.72 ± 0.02
7	Autocl-0.4MPa	62.9 ± 0.4	1.7 ± 0.5	1.63 ± 0.01

2.3.2. Void shape and location

To investigate the quality of the laminates and identify the salient features of the process-induced microstructure, SEM micrographs of the composite laminates manufactured under different processing scenarios are shown in Figs. 8-11 at 50X and 200X magnifications.

Figs. 8(a) and (b) exhibit the micrographs of the typical laminate fabricated in oven and autoclave, respectively in the absence of cure pressure at 50X magnification. As expected, similar voids in terms of size and shape are distributed throughout the laminates manufactured by the scenarios 1 (Oven-0MPa) and 5 (Autocl-0MPa). In Figs. 8(a) and (b), a number of voids located inside the fiber tows, in the matrix region, and between the plies can be observed. Most of these voids would form due to entrapment of air between the layers, absorbed moisture by the prepreg, and volatiles expelled during the cure reaction [132]. In fact, the location of the voids primarily dictates their size and shape such that the vast majority of large and medium size voids are located in the matrix region and between the plies. The shape of voids varies from near-spherical in resin rich areas to irregular, asymmetric voids within fiber tows. The presence of ellipsoidal voids found along the fiber direction suggests that voids are trapped and elongated due to consolidation during cure. Formation of the elongated and high-aspect ratio void morphology during processing has been discussed in detail by Lundstrom [133]. It is also expected that, unless the resin flow or compaction pressure governs the void shape, the viscosity of the resin becomes low enough during cure to maintain the circularity of voids, which is the lowest surface energy shape and thus is the most stable form.

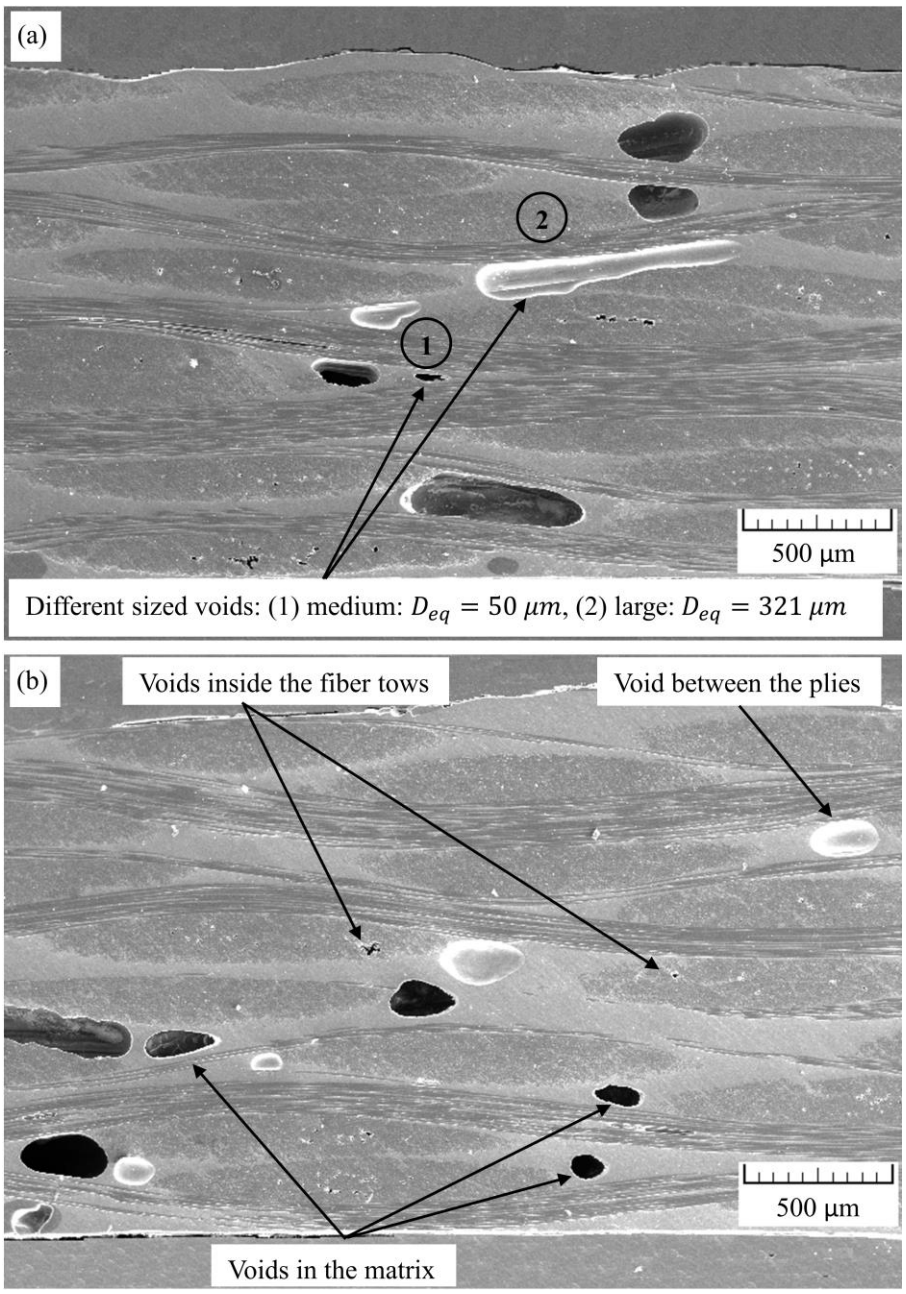

Figure 8. Micrographs of the laminates (50×) manufactured without cure pressure in different scenarios: (a) Oven-0MPa and (b) Autocl-0MPa.

The micrograph of laminates from scenarios 2 (Oven-Mag), 6 (Autocl-0.2MPa), 7 (Autocl-0.4MPa) are presented in Figs. 9 (a), (b), and (c), where similar voids are observed. From these figures, it is seen that most voids are elongated and located between the plies, extending along the fiber-matrix interface which are often observed

in unidirectional composite laminates cured in an autoclave at moderate to high consolidation pressures [134]. It is evident that as a result of consolidation pressure the thickness of resin-rich regions is decreased compared to the scenarios without the curing pressure shown in Figs. 8(a) and (b). Consolidation pressure also has a significant effect on the shape and amount of voids. Due to more lateral resin flow during consolidation, lower void content and generally, a smaller void size is obtained. Figs. 9 (a-c) show that applying consolidation pressure formed highly elongated voids with sharper edges, i.e. with lower roundness, *R*, value. These voids are situated at the fiber/matrix interface and compressed between the stiffer fiber tows. Applying higher pressure certainly is necessary for the reduction of void content, but in the meantime, high pressure may entrap voids at the fiber-matrix interface, making them more detrimental than the voids located within the matrix or the fiber tows. For example, Fig. 9 (c) depicts a highly elongated, 1272 μm-long (a relatively big void compared to the other scenarios) void is trapped between plies when the autoclave pressure is 0.4 MPa (Scenario 7).

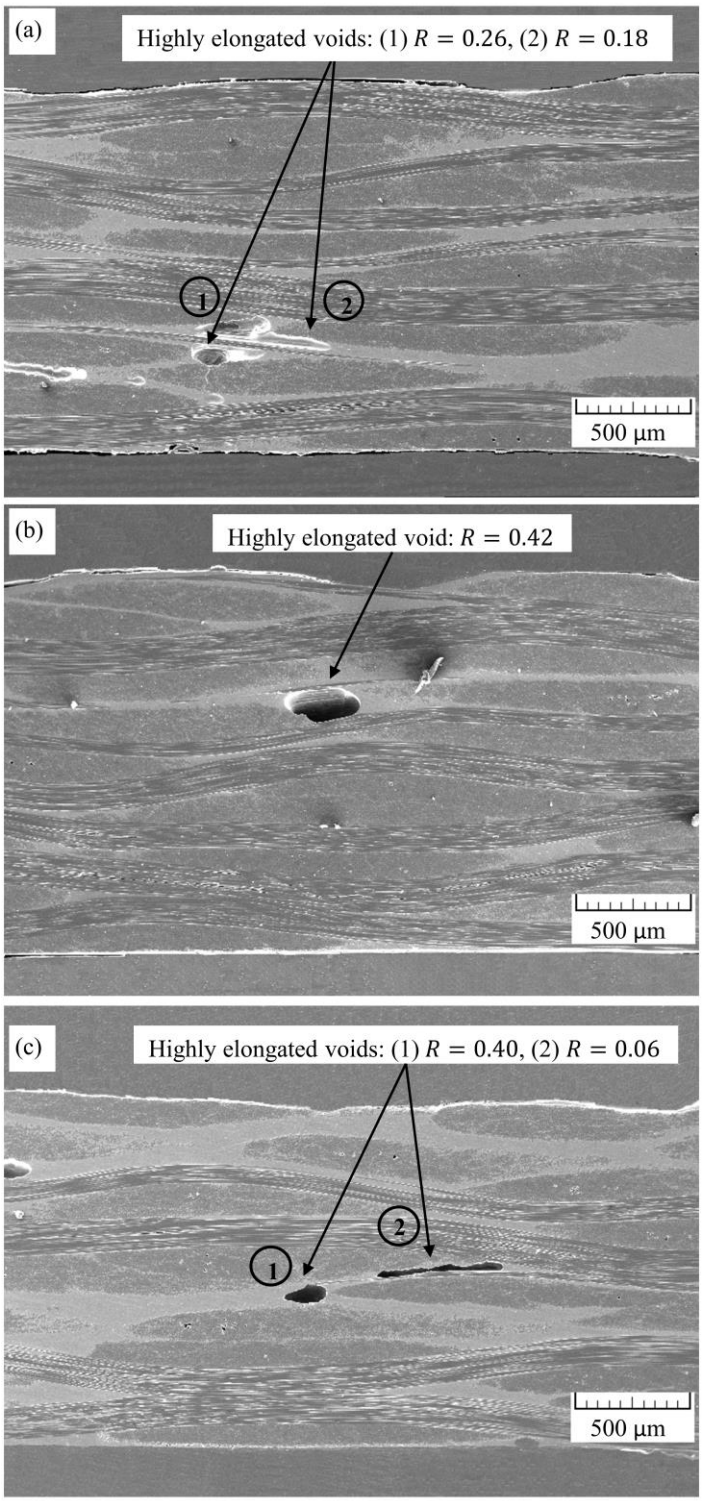

Figure 9. Micrographs of laminates (50×) manufactured under consolidation pressure in different scenarios: (a) Oven-Mag, (b) Autocl-0.2 MPa, and (c) Autocl-0.4 MPa.

Fig. 10 illustrates micrographs of laminates manufactured in the fabrication scenarios 3 (Oven-Mag-μ_{min}) and 4 (Oven-Mag-Gel). It can be clearly seen that applying magnets at minimum viscosity helps achieve improved resin flow, facilitates void migration, and thus reduces the number as well as the size of voids (Fig. 10 (a)). Also, the sample manufactured in scenario 3 (Oven-Mag-μ_{min}) has smaller resin rich areas than those fabricated in scenario 4 (Oven-Mag-Gel).

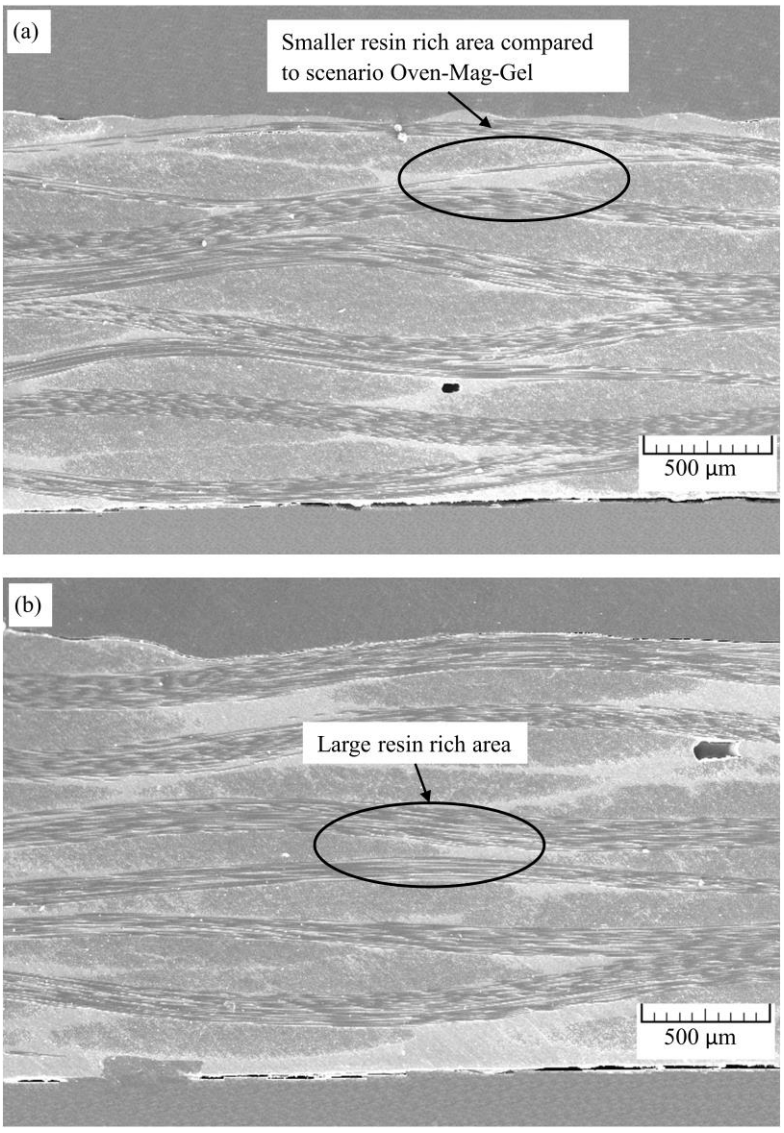

Figure 10. Micrographs of laminates (50×) manufactured under consolidation pressure by magnets applied in different scenarios: (a) Oven-Mag-μ_{min} and (b) Oven-Mag-Gel.

Figs. 11 (a-c) show the voids in the laminates from scenarios 1 (Oven-0MPa), 2 (Oven-Mag), and 3 (Oven-Mag-μ_{min}) at 200X magnification. In scenarios 1 (Oven-0MPa), due to the absence of consolidation pressure, smaller voids within fiber tows (i.e., intratow voids) may coalesce and form an extended porosity network. The magnetic compressive pressure in scenarios 2 (Oven-Mag) has significantly reduced the amount of small, mostly isolated voids inside the tows. A further reduction of voids inside fiber tows is achieved in scenario 3 (Oven-Mag-μ_{min}) such that, as fiber tows became highly compacted, intratow voids seem to be almost eliminated as shown in Fig. 11 (c).

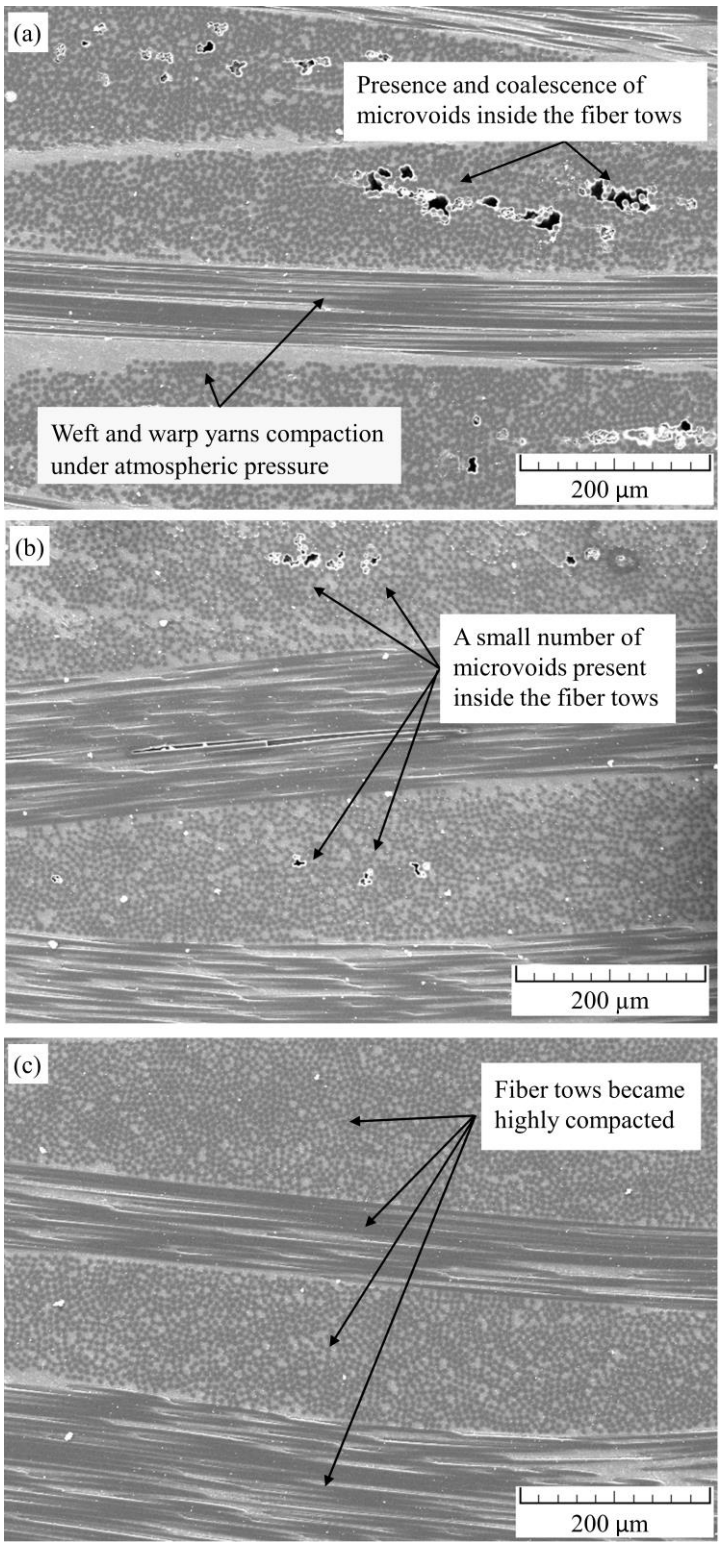

Figure 11. SEM micrograph of the voids (200×) observed in the composite laminates manufactured in different scenarios: (a) Oven-0MPa, (b) Oven-Mag, and (c) Oven-Mag-μ_{min}.

2.3.3. Size and shape distribution of voids

Fig. 12 represents void size distribution as estimated from the equivalent diameter. Using magnets in scenario 2 (Oven-Mag), the relative percentage of smaller voids (~84%) is slightly increased while the void content reduced approximately by 50% compared to scenario 1 (Oven-0MPa). A similar void size and content are observed in the laminates manufactured in an autoclave under 0.2 and 0.4 MPa pressure, which show above 92 percent of voids are smaller than 20 μm (i.e., small voids). It is noticed that if the magnetic pressure is applied at the minimum viscosity, in addition to the overall void volume fraction, the relative percentage of small voids is reduced to 77%, suggesting that mobilizing or coalescing small voids at the lowest resin viscosity becomes easier.

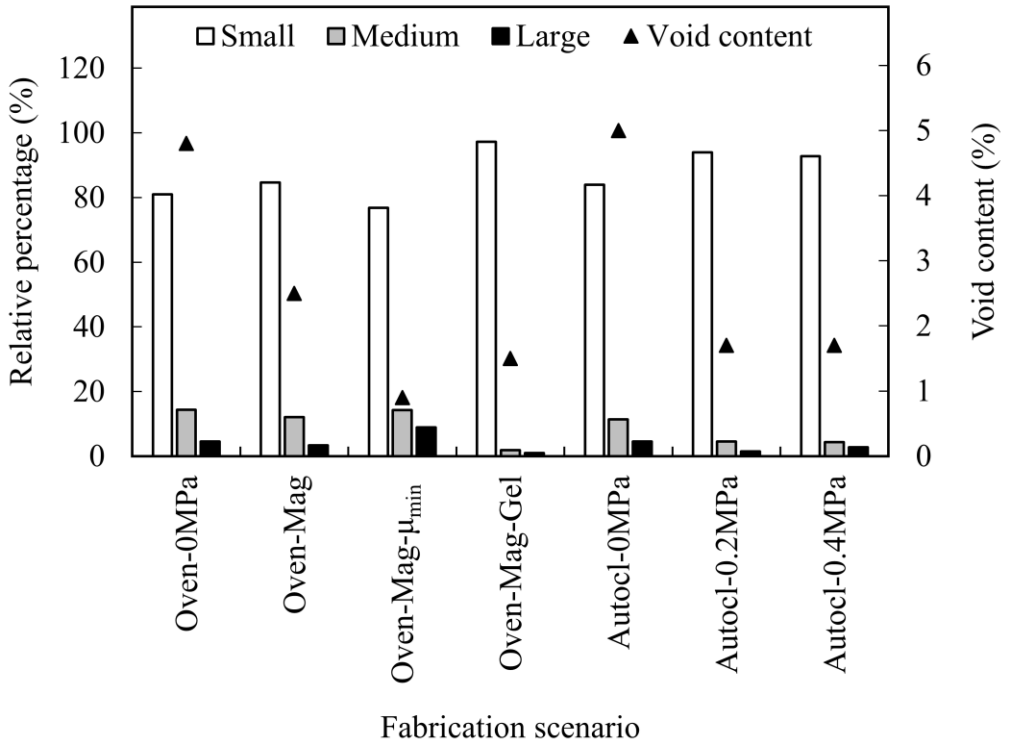

Figure 12. Size distribution of voids based on the equivalent diameter under different fabrication scenarios.

The void shape morphology given by roundness values is presented in Fig. 13. The shapes of the voids primarily depend upon the applied pressure, and in this regard, the roundness of voids in processing scenarios 1 (Oven-0MPa) and 5 (Autocl-0MPa) are quite similar. It is seen that while the void volume fraction remained at around 5% in both cases, approximately 68% and 27% of the voids are slightly elongated or elongated, respectively. Applying magnets in scenario 2 (Oven-Mag) resulted in a modest increase in elongated voids to 36% of the total void fraction of 2.5%. However, for this case, weekly elongated voids still remain dominant at nearly 60% of the total void fraction. Thus, the shape morphology and the location of these voids suggest that their source could be trapped air during the lay-up or volatiles expelled during cure.

When magnets are applied at a minimum viscosity in scenario 3 (Oven-Mag-μ_{min}), a more slender void morphology (~43% elongated and 57% slightly elongated) is observed. It is also seen that changing autoclave pressure from 0.2 MPa to 0.4MPa, reduced the mostly circular voids and slightly increased void elongation while maintaining the same void content of 1.7%. When magnets are applied at gel point in scenario 4 (Oven-Mag-Gel), 75% of voids are slightly elongated, and 20% are elongated with a lower total void content of 1.5% compared to oven or autoclave cure. Nevertheless, when the magnets are applied at the lowest resin viscosity, the lowest total void fraction of 0.9% is obtained which, unlike other laminates, is made of only elongated voids. The void volume fraction, morphology, and size coupled with the laminate fiber volume fraction given in Table 2 govern the quality and mechanical properties of the laminates.

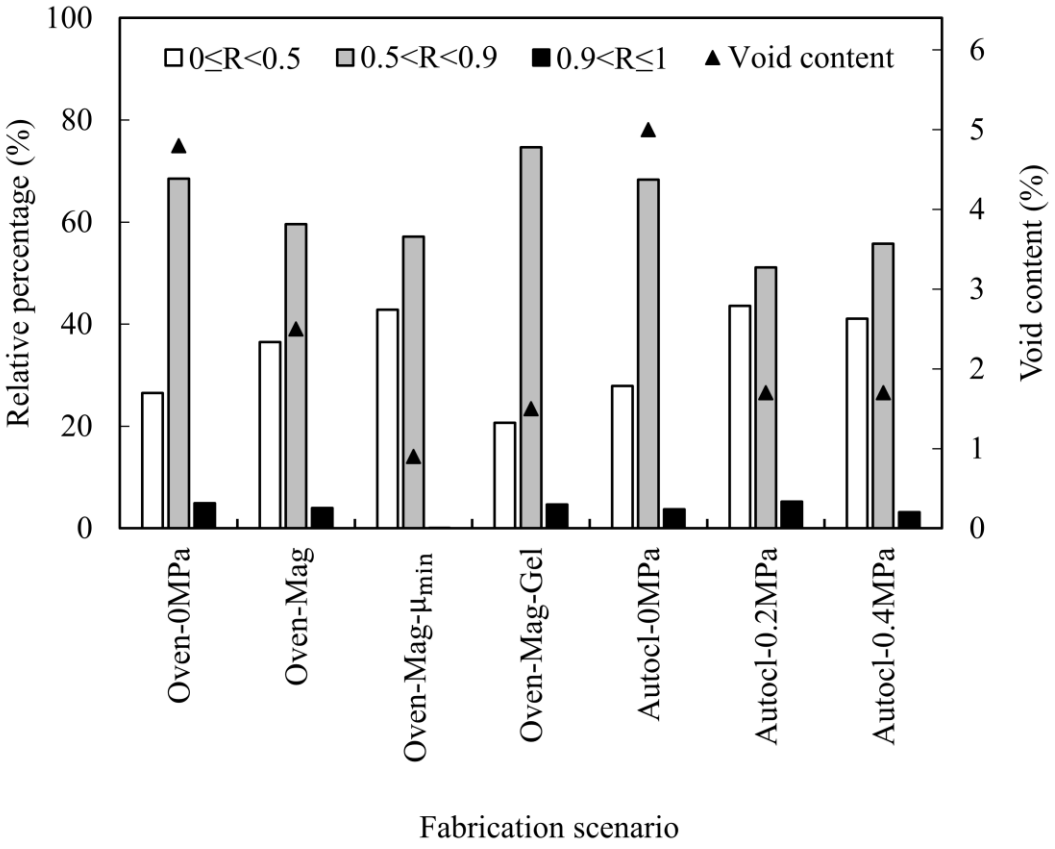

Figure 13. Voids shape morphology given by roundness, R, under different fabrication scenarios.

2.3.4. Flexural properties of composite laminates fabricated by MACM and conventional cure

The flexural strength of the laminates fabricated by different scenarios is displayed in Fig. 14. The fiber volume fraction is also included in Fig. 14 for reference and also to establish the expected positive effect of increased fiber content on the flexural strength. The error bars indicate 95% confidence interval. Fig. 14 confirms that the flexural strength of composites cured under magnets and higher autoclave pressure is greater than those manufactured without any external pressure. The composites manufactured in scenario 2 (Oven-Mag) shows a significant, 17-21%, improvement in

flexural strength compared to scenarios 1 (Oven-0MPa) and 5 (Autocl-0MPa). Also, scenario 2 (Oven-Mag) yielded a relatively high 60% fiber volume fraction and showed 8% to 11% improvement in flexural strength compared to scenario 6 (Autocl-0.2MPa) and 7 (Autocl-0.4MPa). The effectiveness of the MACM method is confirmed by the higher flexural strength of the Oven-Mag samples compared to those fabricated in an autoclave. Despite a marked increase in fiber volume fraction from 57.6% to 62.9%, the flexural strength of samples fabricated at 0.4 MPa showed a slight decrease in strength compared to the laminate fabricated at 0.2 MPa. This reduction, although within experimental uncertainty, may be an indication of the increased importance of void shape and location, particularly for laminates with very low void content.

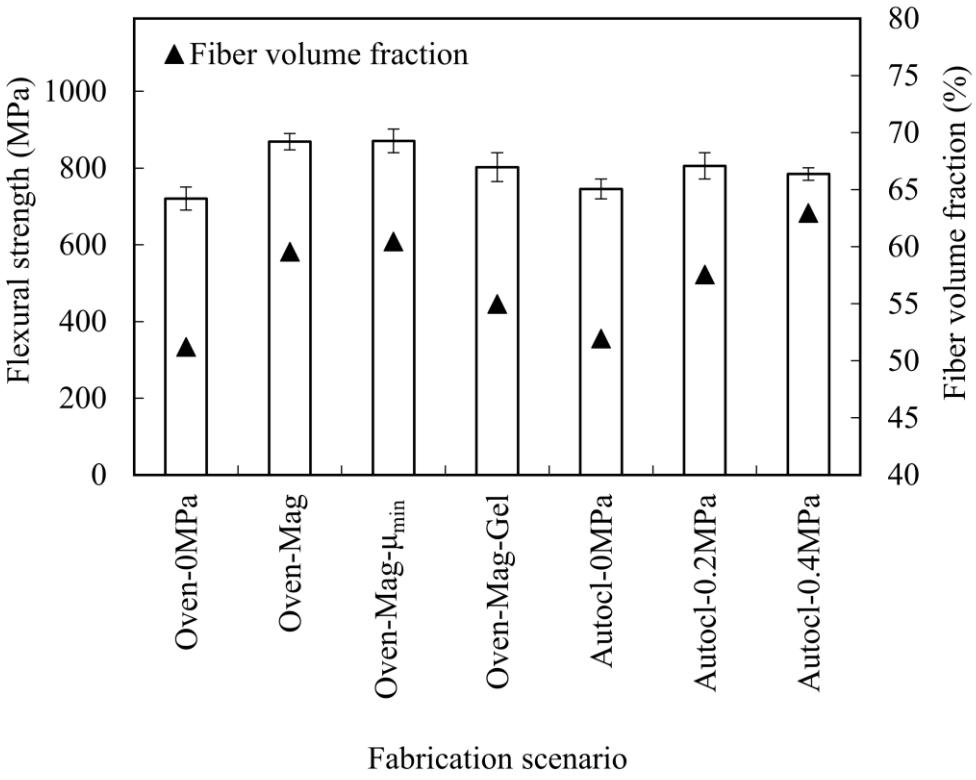

Figure 14. Flexural strength of composites fabricated by different scenarios. Fiber volume fraction for each scenario is also shown for reference. (*n*=12, 95% confidence interval error bars).

It needs to be emphasized that the composites manufactured by applying magnets at the minimum resin viscosity showed the highest flexural strength (17-21% increase in strength compared to scenarios 1 and 5) and also the lowest void content (0.9%). In scenario 4 (Oven-Mag-Gel), the flexural strength is nearly the same as those obtained in scenario 6 (Autocl-0.2MPa), despite a lower fiber volume fraction in scenario 4. This result corroborates the benefits of applying magnets even late in the cure cycle. The application of magnetic pressure at gel point, where most of the resin flow has taken place, had succeeded in removing most of the voids, and therefore increased the flexural strength of the laminate.

The flexural modulus of the laminates fabricated by different scenarios along with their fiber volume fraction are plotted in Fig. 15. As expected, the effect of the fiber volume fraction is more dominant in the flexural modulus. An improvement of about 20-22%, 12-14%, and 5-6% in flexural modulus is observed in scenarios 2 (Oven-Mag), 3 (Oven-Mag-μ_{min}), and 4 (Oven-Mag-Gel) respectively, compared to those fabricated in scenarios 1 (Oven-0MPa) and 5 (Autocl-0MPa). Applying higher consolidation pressure in autoclave led to higher fiber volume fraction and flexural modulus. Thus, compared to those made by scenario 5 (Autocl-0MPa), the laminates fabricated by scenarios 7 (Autocl-0.4MPa) and 6 (Autocl-0.2MPa) showed 19% and 11% enhancement in flexural modulus. The fiber volume fraction is also increased to 63% and 58%, respectively, from the baseline value of 51-52% when the pressure is not applied. The results show that the flexural modulus of composites fabricated in scenario 2 (Oven-Mag) and 7 (Autocl-0.4MPa) are the highest. The slightly lower flexural

modulus of the composites fabricated in scenario 4 (Oven-Mag-Gel) compared to scenario 6 (Autocl-0.2MPa) is due to the lower fiber volume fraction.

Since the prepregs are cured using the same thermal cycle both in oven and autoclave, the fact that oven-cured composites with the application of magnetic pressure exhibited considerably better properties than composites manufactured in autoclaves with 0.2 and 0.4 MPa pressure confirms the ability of the MACM method in producing autoclave quality laminates.

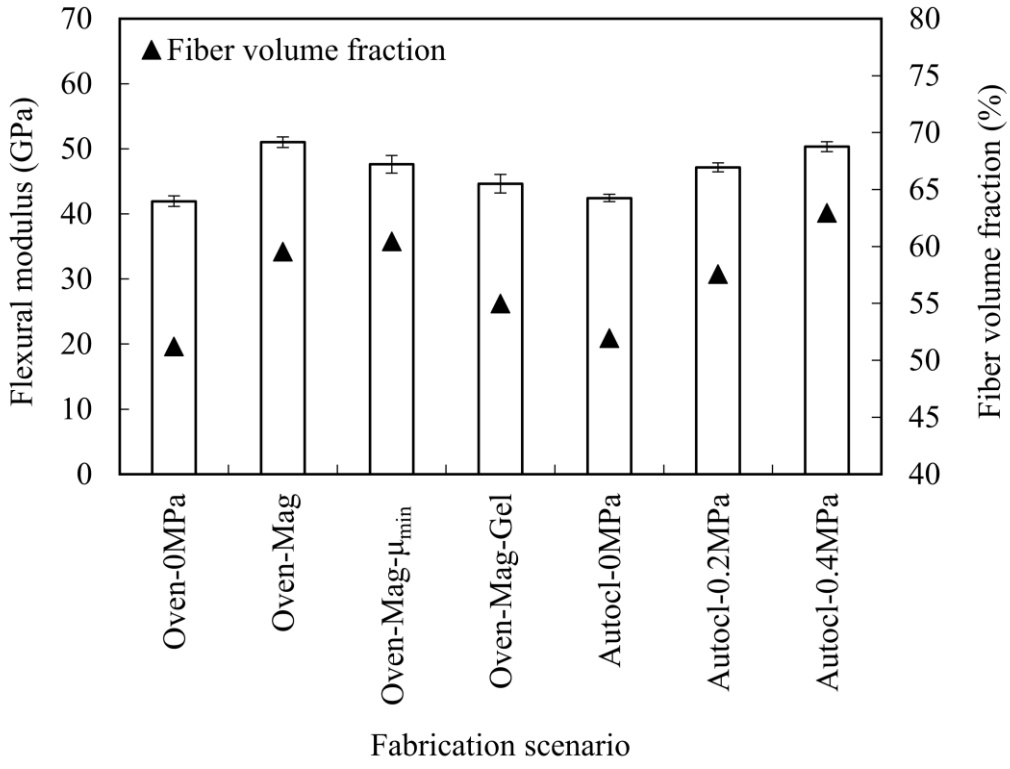

Figure 15. Flexural modulus of composites fabricated by different scenarios. Fiber volume fraction for each scenario is also shown for reference. (*n*=12, 95% confidence interval error bars).

2.4. Concluding remarks

The primary purpose of this chapter is to introduce the magnet assisted composite manufacturing (MACM) process and establish it as a viable out-of-autoclave

manufacturing method for structural composite laminates by experimentally comparing the performance of laminates fabricated by MACM with the laminates cured in an autoclave. The MACM process uses permanent magnets to apply a consolidation pressure on a vacuum bag during cure in an oven, thus eliminates the need to use an autoclave to achieve high fiber volume fraction and low void content. Application of magnets when the resin viscosity is at a minimum provided additional benefits of higher fiber volume fraction and lower void content, thus leading to higher flexural properties and enhanced structural integrity. The following observations can be highlighted as the salient features of MACM:

(a) The results suggest that magnetic compressive pressure is high enough for fabricating 8-ply laminates with sufficiently high fiber volume fraction (60%) and low void volume fraction (<3%). If the magnets are applied when the viscosity is at a minimum, even lower void volume fraction under 1% is achievable.

(b) Applying magnets during cure in an oven caused a substantial improvement in flexural properties, matching or exceeding the properties obtained in an autoclave. Improvements in both strength and modulus of about 21% are achieved in laminates manufactured by MACM.

(c) Applying magnets even late in the cure cycle when the resin is at gel point is shown to be beneficial. For this case, MACM is successful in decreasing the void content to 1.5% so that the flexural strength of the laminates are nearly the same as those cured in an autoclave under 0.2 MPa pressure.

It is possible to fabricate aerospace quality composite structures using MACM method without having to apply consolidation pressure in an autoclave. Conclusive results obtained so far suggests that, in some cases, the proposed technique can be utilized as a substitute for autoclave curing. Future improvements in the proposed method are possible by sliding the magnets over larger areas of the composite during cure for manufacturing large, high-quality parts.

Chapter 3. Fabrication of Three-Phase NiC/Glass/Epoxy Composites with Controlled Surface Microstructure Using a Cascaded Suspension Deposition Method

Fabrication of multifunctional materials via incorporation of a third phase into structural composite laminates is of great interest, especially for manipulating surface properties. However, achieving a uniform, well-dispersed surface microstructure in three-phase composites is quite challenging by using the traditional fabrication processes. In this chapter, a novel cascaded suspension deposition method is presented to introduce well-dispersed short fibers into the molded laminates, allowing the control of the surface properties of the resulting three-phase composite. Towards this goal, the micron-sized, nickel coated carbon (NiC) fibers are uniformly deposited on a glass fabric surface by the proposed method. The deposited fabric is then used to fabricate NiC/glass/epoxy composite laminates by vacuum assisted resin transfer molding (VARTM). The deposition morphology on the glass fabrics and on the fabricated laminates are investigated by assessing: (i) spatial uniformity of fiber volume fraction; (ii) degree of dispersion; and (iii) process-induced orientation and degree of alignment. To demonstrate the flexibility of the proposed method, the effects of fiber concentration, fabric architecture, and resin flow are studied. The experimental results reveal that, in all fabrication cases, the cascaded suspension deposition technique is capable of depositing short fibers on the fabric surface with a uniform fiber volume fraction and excellent dispersion with random orientation. Additionally, it is observed that the resin flow during VARTM does not considerably disturb the deposition-induced

microstructure of the NiC fibers, which allows the successful fabrication of three-phase laminates by VARTM.

3.1. Introduction

Advanced fiber reinforced polymer (FRP) composites have been widely used in aerospace, automotive, and marine industries owing to their high specific strength, excellent corrosion resistance, and favorable fatigue tolerance. In recent years, multifunctional polymer composites that possess high thermal stability, high electrical and thermal conductivity, and novel optical properties, besides high load-bearing capacity have attracted growing interest [75, 94, 135-138]. Several studies during the last decade have revealed that incorporation of micro- or nano-sized reinforcements into traditional composites is quite effective in enhancing multiple thermo-mechanical properties simultaneously [35, 39, 41, 139]. The common practice in fabricating multifunctional, three-phase composites is to: (i) modify the resin by adding particle reinforcement using high shear mixing and/or sonication and (ii) infuse the particle/resin suspension into the fabric using liquid composite molding (LCM) techniques such as vacuum assisted resin transfer molding (VARTM) [37, 40-42].

There are major challenges involved in infusing particle/resin suspension into the fabric during liquid composite molding processes. One challenge is the difficulty in obtaining a homogenous dispersion of nanotubes or larger short fibers throughout the resin. Especially at high volume fractions, fiber aggregation and filtration may take place, resulting in local defects and nonuniform properties [140]. The micro or nano-scale aggregates often create stress concentration zones, leading to premature failure and reduction in composite performance [141, 142]. For instance, Manchado et al. [141]

found that increasing nanotube concentration in the polymer matrix from 0.75 to 1% decreased the tensile modulus of the fabricated composite by more than 8%. Another challenge is the significant increase in viscosity of the resin due to the incorporation of short fibers or smaller nano-scale additives, which often results in processing difficulties in VARTM [143, 144]. Increased viscosity slows down the impregnation and may result in filtration of fibers [40]. Additionally, as the filling rate decreases, resin gelation may occur before the part is completely filled [13, 145]. Accordingly, the addition of nanoparticles at concentrations above 0.5% has been reported to cause blockage of resin flow in VARTM and incomplete fabric wetting [39]. Thus, mixing much larger short fibers with the resin and infusion of this mixture into a preform may not be a feasible option in making composite products.

The above drawbacks to fabricate three-phase composite laminates by VARTM can be overcome by depositing short fibers or other nanoscale reinforcements onto the fabric surface prior to fabrication. Hence, various techniques have been developed in the literature including chemical vapor deposition (CVD) [46, 47], electrophoretic deposition (EPD) [48, 49], spraying method [50, 51], and aqueous suspension deposition [54]. The CVD process, widely used for nanoparticle growth on fiber substrates, requires a catalyst for the decomposition of hydrocarbon gases at temperatures ranging from 700 to 1000 °C [146, 147]. This process provides a strong bond between fibers and substrates and allows control of nanoparticle location and alignment [46]. However, the high temperature and chemical atmosphere used in this process may degrade the fiber properties [46]. An attractive alternative to overcome some of the limitations of the CVD process is the use of solution-based processes such

as EPD process. In EPD, charged reinforcements in a liquid medium are attracted and deposited onto the electrode surface of opposite charge under an applied DC electric field. The benefits offered by EPD is the ability to uniformly deposit micro- and nano-sized particles and control the deposition thickness [148]. However, the uniformity of particle distribution by this method depends on several factors such as the PH level of suspension, applied voltage, deposition time, and isolation of the electrodes [60]. In spraying method, the reinforcements, mainly carbon nanotubes, are dispersed in an organic ethanol solvent and the solution is then sprayed evenly onto one or both sides of the fabric using a mist spray gun. Spraying fiber-containing solution is especially beneficial for selective placement of reinforcements but may cause problems such as particles agglomeration [52].

A relatively new and promising technique to introduce nanoparticles on a variety of substrates is aqueous suspension deposition [54, 61, 62]. In this process, the nanoparticles are dispersed in the deionized water by ultrasonication to obtain a stable suspension at the desired concentration and then, the fabric is immersed in the suspension. The nanotubes are deposited on both sides of the fabric surface during immersion. After deposition, the fabric is removed from the aqueous suspension bath, dried, and the resin is infused into the deposited fabric using VARTM. Compared to other methods, this method has the advantages of being simple, scalable, low temperature, and inexpensive because of the use of the aqueous medium for deposition. However, immersing the fabric in a particle suspension may lead to variations in the spatial distribution of particles throughout the preform surface, resulting in nonuniform properties of the fabricated composite. In addition, with this method, controlling the

concentration of particles on the fabric surface may be difficult. The existing literature on this method or other deposition techniques is mainly focused on evaluating the properties of the resultant composite. A detailed quantitative analysis of the process-induced microstructure morphology in terms of: (i) spatial uniformity of fiber volume fraction; (ii) degree of dispersion; and (iii) process-induced preferred orientation and degree of alignment, have not been performed either on the deposited fabric or on the fabricated composite laminates.

In this chapter, a novel method, cascaded suspension deposition, is introduced to incorporate micron-sized fibers into the molded laminates. This technique is scalable because of using an aqueous medium, and thus can be used to tailor the surface properties of large structural composites. First, the cascaded suspension deposition for the fabrication of a three-phase composite is demonstrated by the deposition of micron-sized fibers on the fabric surface. Then, composite laminates are fabricated using the deposited fabric by VARTM. Spatial uniformity of fiber volume fraction, as well as the degree of dispersion and alignment of short fibers are quantitatively assessed both on the deposited fabric surface before impregnation and on the laminate surface after fabrication. In addition, a detailed analysis of microstructural changes caused by resin flow during impregnation is presented. The effects of different short fiber concentrations and fabric architecture (random mat or plain weave) are also investigated to demonstrate the flexibility of the proposed technique.

3.2. Experimental

3.2.1. Materials

Nickel coated carbon (NiC) fibers are considered as a popular conductive reinforcement option in a polymer matrix, because of the high specific strength and semiconductivity of carbon fibers, as well as high electrical conductivity of nickel [81, 94, 149, 150]. Therefore, in this work, NiC fibers with a density of 2.14 g/cm^3 (Conductive Composites Co.) are used as the third phase. The nominal length and average diameter of the fibers are reported by the supplier to be 250 and 7 μm, respectively. However, a detailed microscopy analysis of several sample fibers shows a nonuniform fiber length distribution (see Fig. 16). The actual average fiber length is measured to be 169.6 ± 61.2 μm. Also, no significant variation is observed in the diameter of the fibers. Two types of glass fabrics with different architectures are chosen in this work: chopped strand random mat (Fiberglast, part#250) and plain weave (Hexcel, HexForce 3733). The areal density of random mat and plain weave fabrics are, respectively, 0.458 kg/m^2 and 0.197 kg/m^2. The INF-114 epoxy resin and INF-211 curing agent (Pro-Set Inc.), mixed at 100/27.4 weight ratio, is selected as the resin system because of its low viscosity of ~300 mPa s at 22 °C.

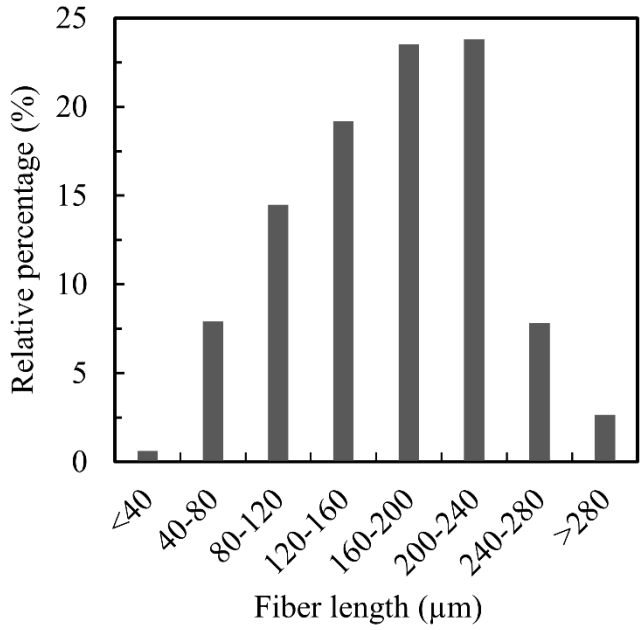

Figure 16. NiC fiber length distribution analysis using ≈2000 fibers. The corresponding mean value is 170 μm.

3.2.2. Cascaded suspension deposition: Deposition of micron-sized NiC fibers on a fabric surface

In this chapter, a novel cascaded suspension deposition technique is developed to achieve a uniform and isotropic deposition of micron-sized fibers on the fabric surface. Fig. 17 displays the schematic of this technique in detail, illustrating multiple steps involved in the homogeneous deposition of NiC fibers on the glass fabric surface. In this technique, two cascaded trays (i.e., upper suspension tray and lower deposition tray) are used. The suspension tray contains the short fibers/water suspension and the deposition tray contains water with the fabric placed at the bottom. The suspension tray is positioned at a short distance above the deposition tray for slowly cascading the fibers/water suspension into the deposition tray. The deposition process is completed by the sedimentation of fibers on the fabric surface under gravity, followed by draining the

water from the deposition tray and drying the fabric. To achieve a uniform deposition of fibers on the fabric surface, the processing details are as follows (see Fig. 17): (i) the perforated bottom surface of the suspension tray is covered prior to cascading so that the fibers can be well dispersed in water by sonication; (ii) the suspension tray perforations are small enough to generate a continuous cascading flow and large enough to allow micron-sized fibers easily flow through; (iii) the fabric in the deposition tray is immersed in a few centimeters deep water to prevent forming artificial cascading lines on the fabric, thus eliminating the possibility of nonhomogeneous fiber deposition; and (iv) after sedimentation of fibers, the water in the deposition tray should be slowly drained, avoiding any disturbance in deposition-induced microstructure or fiber wash out.

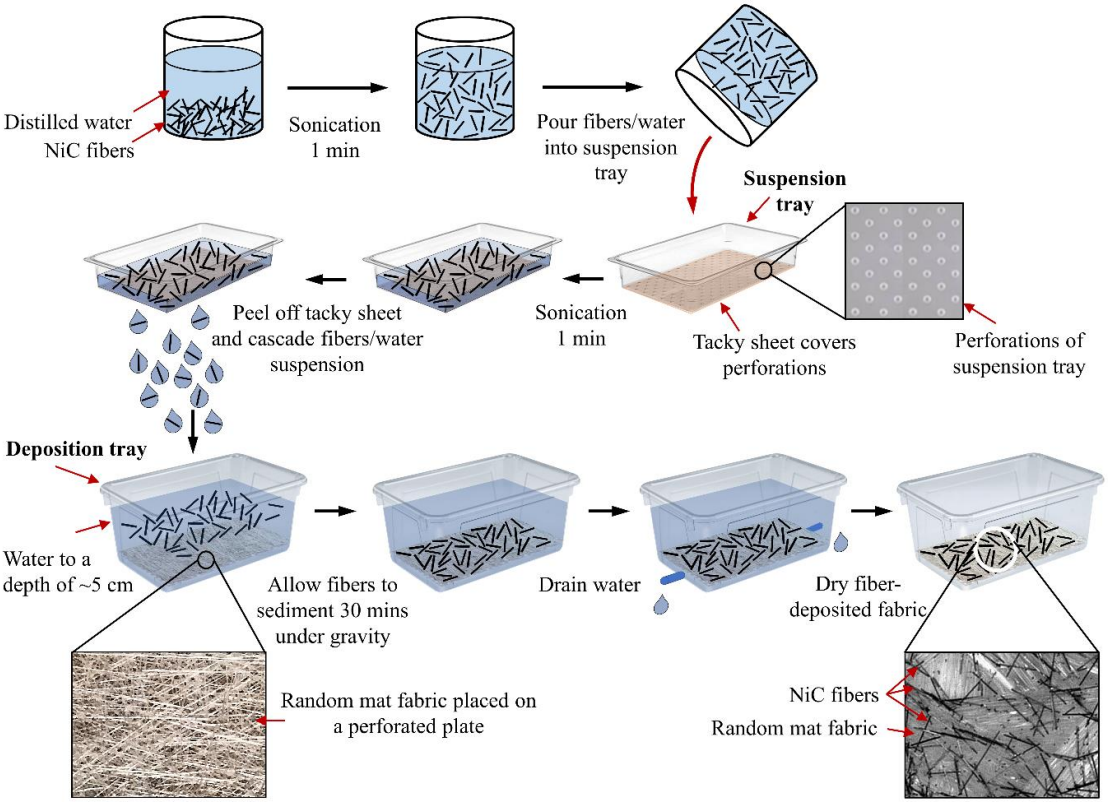

Figure 17. Schematic of the cascaded suspension deposition for depositing NiC fibers on the glass fabric surface. The NiC short fibers, initially dispersed at the top suspension tray, are deposited by sedimentation on the glass fabric placed at the bottom of the deposition tray.

To investigate the flexibility of the proposed technique and its ability to uniformly deposit short fibers on different fabric substrates, two types of fabric with random and plain weave architectures are considered. Furthermore, depositing different concentrations of NiC fibers and the resulting process-induced microstructure is studied. For this purpose, 0.05, 0.1, and 0.2 g NiC fibers are deposited on a 12.7 × 12.7 cm^2 random mat fabric, respectively.

3.2.3. Fabrication of composite laminates

Three-phase composite laminates containing NiC fibers on the surface of glass/epoxy laminate are fabricated using VARTM, as illustrated in Fig. 18. After the

deposition of NiC fibers on the fabric surface using the cascaded suspension, the dried fabric is laid-up on the tool plate as seen in Fig. 18. The lay-up assembly is covered with a vacuum bag and sealed. Finally, the resin is infused under vacuum pressure. After completion of the filling, the inlet is clamped while the outlet line is kept open for an additional 5 min to remove excess resin. The laminate is then cured in an oven for 8 h at 60 °C, thirty minutes after the start of resin infusion.

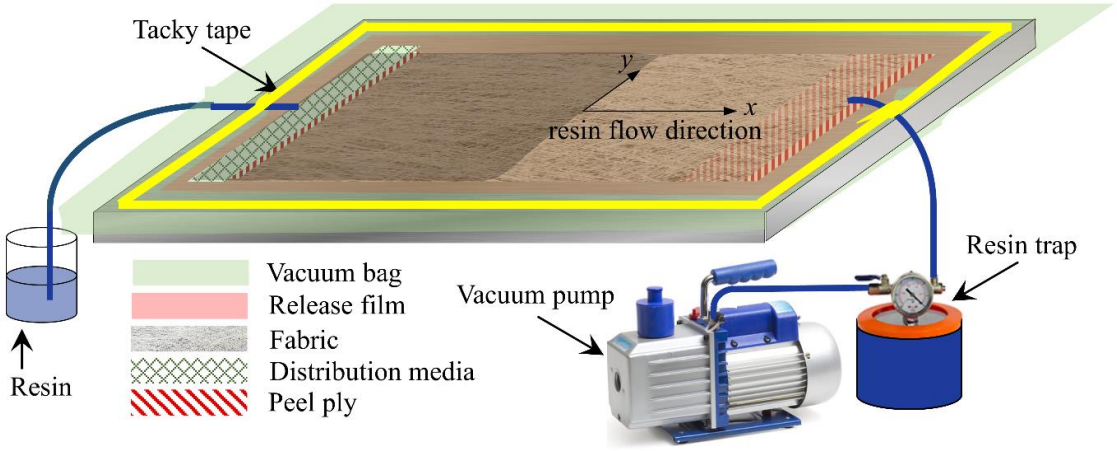

Figure 18. Schematic of the VARTM experimental setup.

Apart from the method described above, a conventional fabrication method for three-phase composites is the addition of fibers into the resin and then infusing the resin/fiber mixture into the fabric. This approach, although has been the subject of considerable research, often leads to processing problems such as increased resin viscosity and filtration of fibers. In this work, both conventional infusion and the proposed cascaded suspension deposition approaches are employed to demonstrate the difference in the dispersion quality and uniformity of the microstructure of the fabricated laminates.

Table 3 presents the five different scenarios performed in this work to fabricate 12.7 × 12.7 cm^2 three-phase NiC/glass/epoxy composite laminates. These scenarios are labeled in the following order: fabrication method, glass fabric type, and NiC/resin weight fraction. For the fabrication methods, “M” stands for “Mix NiC fibers with resin + VARTM” and “CD” is for “Cascaded suspension deposition + VARTM”. For the glass fabric type, “R” is for random mat and “P” stands for plain weave. Finally, “NiC#%” represents the NiC fibers/resin weight fraction (i.e. #% is 0.5, 1, or 2%). In the first scenario, M-R-1%NiC, the conventional approach is considered where NiC fibers are first mixed with epoxy resin, and then the mixture is sonicated. Subsequently, the curing agent is added such that the fibers/resin weight fraction becomes 1%. Then, the mixture is degassed in a sonication bath and subsequently, infused into random mat fabric. The second scenario, CD-R-0.5%NiC, however, uses the cascaded suspension deposition approach, where 0.05 g fibers are first deposited on a single layer of 12.7 × 12.7 cm^2 random mat fabric and then the neat epoxy resin is introduced into the deposited fabric. The difference between scenarios CD-R-0.5%NiC, CD-R-1%NiC, and CD-R-2%NiC is that the concentration of NiC fibers increases from 0.5% to 1% and 2% wt. of resin, respectively. These scenarios are performed to investigate the effect of different fiber concentration on the process-induced microstructure. To investigate the effect of fabric architecture, the last scenario, CD-P-1%NiC, is used, where NiC fibers (at 1% wt. of resin) are deposited on plain (P) weave fabric.

Table 3. Five fabrication scenarios for the three-phase NiC fibers/glass fabric/epoxy composite laminates.

Fabrication method-glass fabric type-NiC/resin (wt. %)	Fabrication method	Glass fabric type	NiC/resin (wt. %)
M-R-1%NiC	Mix NiC fibers with resin + VARTM (M)	Random Mat (R)	1
CD-R-0.5%NiC	Cascaded Suspension Deposition + VARTM (CD)	Random Mat (R)	0.5
CD-R-1%NiC		Random Mat (R)	1
CD-R-2%NiC		Random Mat (R)	2
CD-P-1%NiC		Plain Weave (P)	1

3.2.4. Comprehensive analysis of process-induced microstructure

Quantitative and comparative analyses of the microstructure of the deposited fabrics and composite laminates are carried out to assess the following three important parameters: (i) spatial uniformity of fiber volume fraction, (ii) degree of dispersion, and (iii) preferred orientation and degree of alignment of NiC fibers. Fig. 19 illustrates four distinct microstructural patterns with different levels of spatial uniformity of fiber content, dispersion, and isotropy. These images schematically demonstrate how the three microstructural parameters can convey independent yet complementary information about the laminate morphology. For example, Figs. 19(a) and (b) both exhibit well-dispersed and randomly oriented short fibers. However, unlike the uniform fiber volume fraction in Fig. 19(a), Fig. 19 (b) shows a low fiber volume fraction region in the middle, which would most likely translate into a higher variation in its properties. Similarly, Figs. 19(a) and (c) illustrate well-dispersed fibers with uniform fiber volume

fraction, while Fig. 19(c) depicts the preferred orientations at 0° and 90°, unlike the perfect isotropy in Fig. 19(a). Fig. 19(d) is an example of poorly-dispersed fibers with non-uniform volume fraction distribution and random orientation. The detailed quantitative assessment of each one of these parameters is described in the following sections.

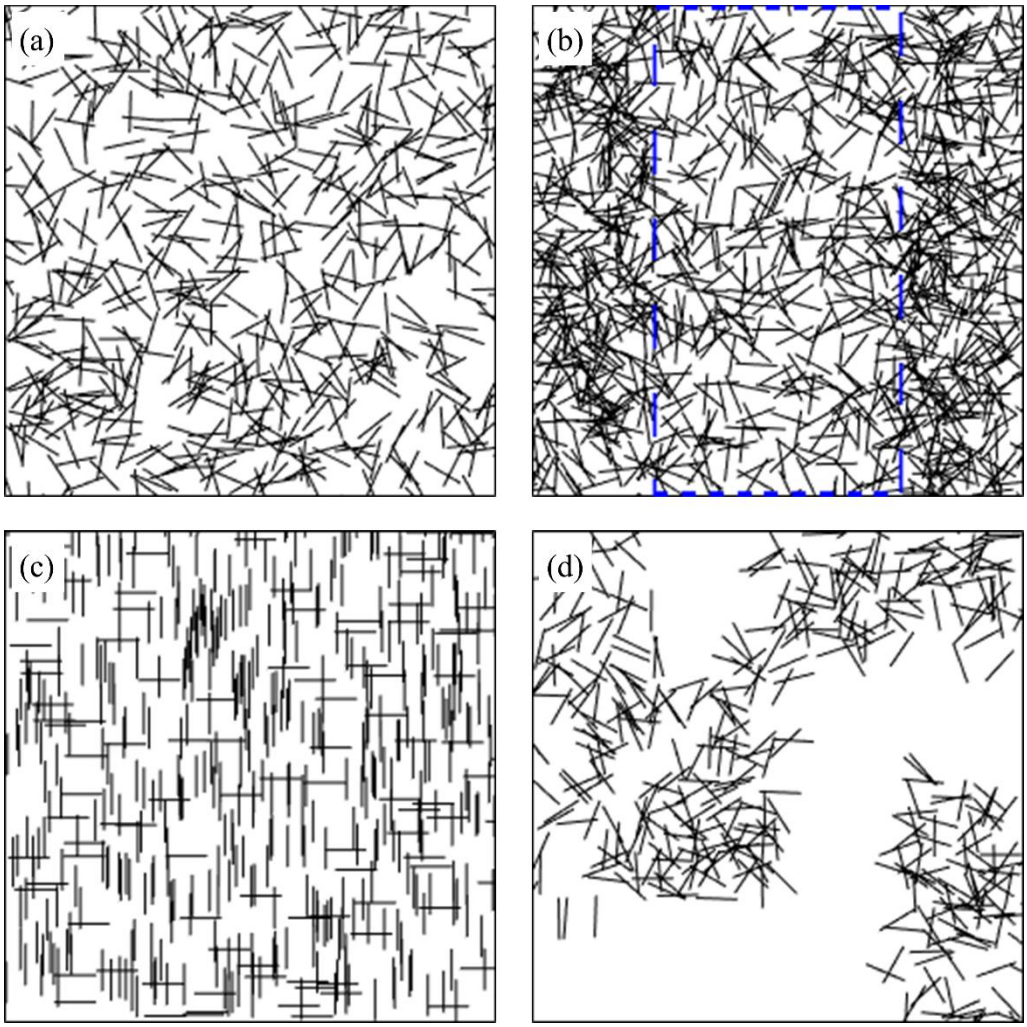

Figure 19. Representative demonstrations of discontinuous fibers forming different microstructural patterns: (a) uniform fiber volume fraction/well-dispersed/no preferred angle; (b) non-uniform fiber volume fraction/well-dispersed/no preferred angle; (c) uniform fiber volume fraction/well-dispersed/preferred angles at 0° and 90°; and (d) non-uniform fiber volume fraction/poorly-dispersed/no preferred angle.

3.2.4.1. Spatial uniformity of fiber volume fraction

A uniform fiber volume fraction throughout the laminate is essential to obtain a homogeneous part with uniform properties. To quantify the spatial uniformity of fiber volume fraction, high-resolution optical scanning is carried out covering the entire surface of the fabricated composite (127×127 mm^2). For this purpose, a commercial flatbed scanner (Epson Perfection V550) is used for obtaining images at a high resolution of 4800 dpi, where the pixel size is 5.3 μm. Thus, at this resolution, a few hundred micron-long individual fibers with 7 μm diameter can be clearly identified. To the best of our knowledge, this is the first application of these scanners to capture individual micron-sized fibers. For analysis of fiber volume fraction uniformity, a 100×100 mm^2 area is extracted from the center of each scanned image to eliminate the possible edge effects. Then, the light scattering effects due to surface roughness of the laminate are filtered from each extracted image using ImageJ software. To separate the background (i.e. resin and glass fabric) from the deposited NiC fibers, the preprocessed images are binarized and inverted so that the white (gray value of 255) and black (gray value of 0) pixels correspond to NiC fibers and background, respectively. Fig. 20 shows a scanned image of CD-R-1%NiC laminate after: (a) removing light scattering and (c) binarizing and inverting the image. The zoomed areas in the red square boxes of the left images are shown in Figs. 20(b) and (d). Fig. 20(b) clearly illustrates the spatial distribution of fibers on the surface of the laminate. As Fig. 20(d) demonstrates, the images are inverted to visualize NiC fibers better, where fibers are shown in white.

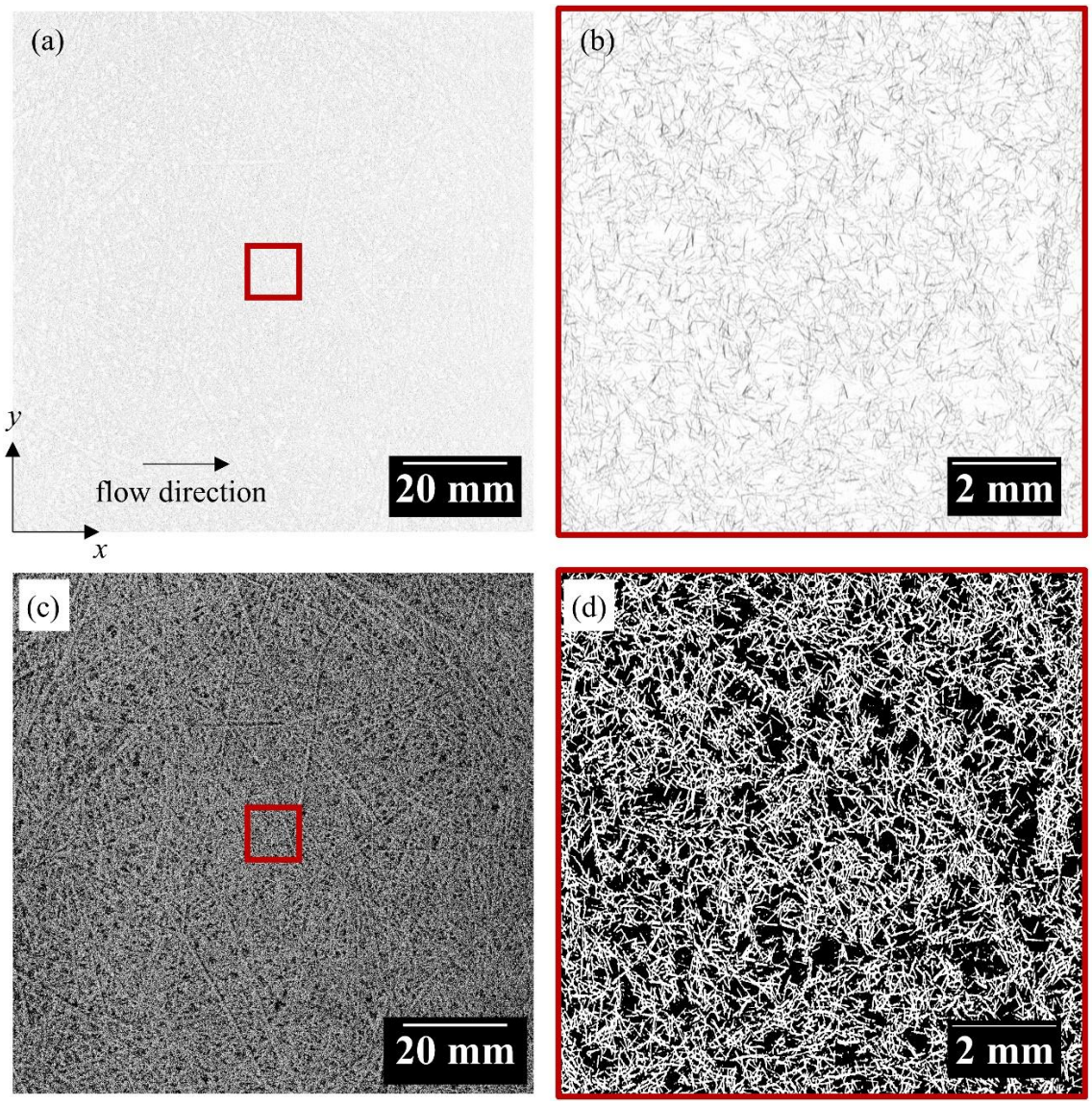

Figure 20. Example of a scanned image of CD-R-1%NiC laminate: (a) grayscale image after removing light scattering, (b) zoomed area of the box shown on the upper left image where the deposited NiC fibers are identified individually, and (c) binarized and inverted image, and (d) zoomed area of the box shown on the lower left image. The ability to identify each NiC fiber deposited on the laminate surface is clearly enhanced by image processing.

Considering that the gray value of each pixel of the binary image is correlated with the presence of fiber at that location, it is possible to quantify the amount of fiber deposition on the laminate surface. For convenience, this information is averaged along

(i.e., longitudinal) and transverse to the flow direction and later given as the level of fiber deposition plotted against the *x*- or *y*-axis of the laminate, normalized with respect to the laminate length *L*. This quantitative analysis is performed by first dividing the 100 × 100 mm^2 binary laminate image into 18700 equal-sized (i.e., ≈1 mm × 100 mm), partially overlapping areas along the *x*-direction. Each area covers almost 1 mm (200 pixels) along the laminate length, whereas the area height is the same as the entire image height of 100 mm (18900 pixels). It should be noted that these areas partially overlap, where each new analysis area adds a new pixel line of 5.3 μm × 100 mm further along the flow direction, while removing a similar one-pixel line from closer to the inlet gate. The choice of size of these areas is a trade-off between two considerations: smoothing noisy grayscale data and determination of actual variations in deposited fibers (i.e., surface fiber volume fraction). The average gray value of pixels within each 1 × 100 mm^2 window is obtained and assigned as the amount of fiber deposition in that window centered at (*x*). Then, the obtained average gray values of all windows are plotted along the *x*-direction, indicating the variation in fiber deposition on the laminate surface. The lower variation of these fiber deposition values along (*x*) or transverse (*y*) to the flow direction implies uniformity of the fiber deposition on the composite surface (i.e., uniformity of the fiber volume fraction).

3.2.4.2. Degree of dispersion of fibers

A number of studies have shown the importance of achieving a good dispersion level to obtain the optimum properties of composites [151-153]. Typically, the literature reports the uniformity of dispersion of fibers based on the uniformity of properties in composite parts as opposed to directly analyzing the dispersion level using the

microstructural information. In this work, however, a quantitative assessment of fiber dispersion is performed using an area disorder parameter. For this purpose, optical images of NiC fibers-deposited fabric and three-phase composite laminates are captured, covering five equidistant regions of 2×2 mm^2 areas near the inlet, between inlet and center, at the center, between center and outlet, and close to outlet. Fig. 21 shows steps of image processing for the quantitative assessment of dispersion of NiC fibers. Fig. 21 (a) presents an example of an optical image of deposited fabric on a 2×2 mm^2 area. Individual NiC fibers within the image, in Fig. 21(a), are selected and the positions (x, y) of the center of the fibers are determined, as depicted in Fig. 21(b) and (c), respectively. For an accurate determination of fiber dispersion, periodic boundary conditions are implemented at the left, right, top, and bottom of the image (see Fig. 21(d)). The red line in Fig. 21(d) passes through the boundary points of Fig. 21(c). The points outside red line region in Fig. 21(d) are generated by applying periodic boundary condition, i.e. shifting the boundary points located at the red line. A Delaunay network of triangular cells is constructed such that the positions of the center of the fibers are located at the vertex of the triangles, as presented in Fig. 21(e). It should be noted that the triplet of fibers is selected such that for each vertex of a triangle, the other two are the nearest neighbors (i.e., locations of the two closest fibers). The solid black rectangle in Fig. 21(e) shows the 2×2 mm^2 area of the original image. As Fig. 21(e) depicts, applying periodic boundary condition caused the Delaney network to expand to the entire region of the image (i.e. solid black rectangle), in which the degree of dispersion of fibers can be accurately calculated over the entire image area. Otherwise, the Delaney network only covers a smaller sub-region of image where fibers are located, and the

calculated degree of dispersion does not fully represent the state of dispersion in the entire image. Once the network is constructed, the mean ($\overline{A}$) and standard deviation (σ_A) of the area of Delaunay triangles (A) are calculated. It is important to note that only the area of triangles that their centers (shown by red dots in Fig. 21(e)) are located inside the solid black rectangle are considered for analysis of area disorder.

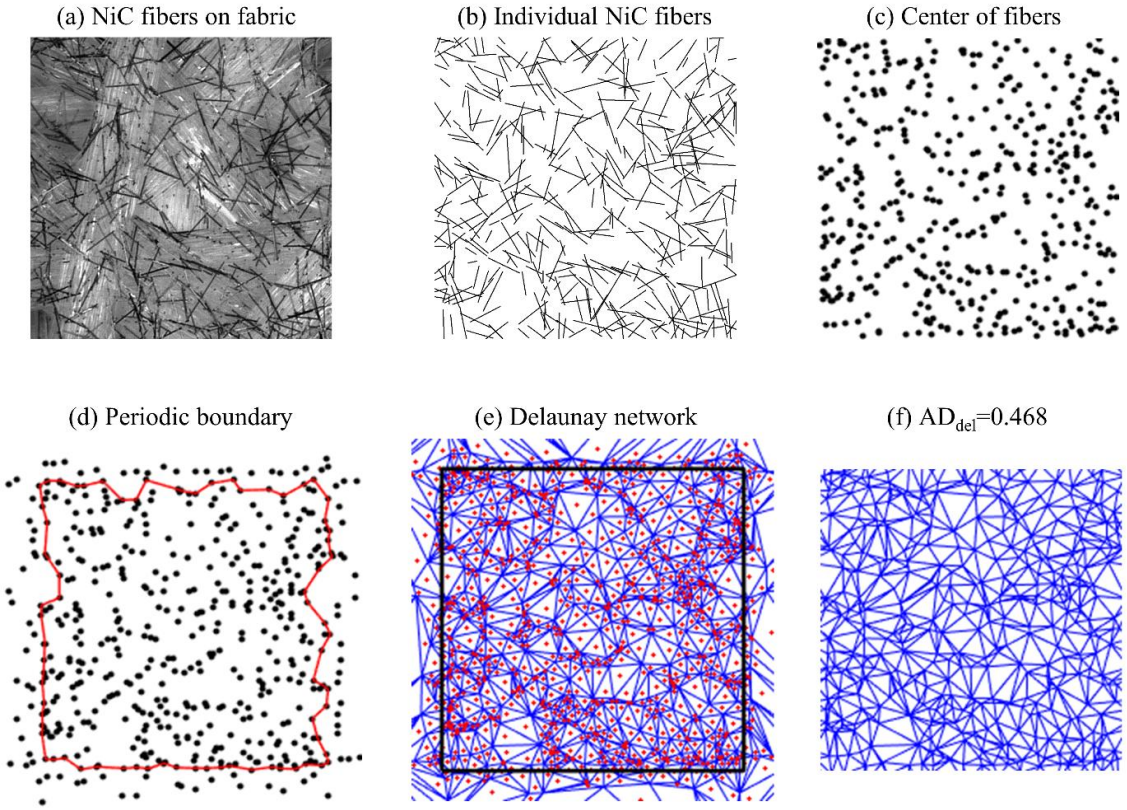

Figure 21. Steps of image processing for the quantitative assessment of dispersion: (a) optical image of NiC fibers-deposited fabric on a 2×2 mm^2 area, (b) identification of individual fibers, (c) determination of the center of each fiber, (d) applying periodic boundary condition, (e) construction of Delaunay network, determination of center of triangles, and identifying triangles whose centers lie inside the image (i.e. solid black rectangle), and (f) determination of area disorder, AD$_{del}$, from finalized Delaunay network.

The area disorder (AD_{del}), which is a dimensionless quantity for the robust characterization of dispersion quality, is determined as [154],

$$AD_{del}=1-(1+\sigma_A/\bar{A})^{-1} \quad (6)$$

The AD_{del} is between 0 and 1 since standard deviation (σ_A) can change between 0 and ∞. The AD_{del} closer to zero refers to a more regular array of particles while the AD_{del} closer to 1 corresponds to a highly clustered system.

For analysis of AD_{del}, approximately, 300, 600, and 850 fibers depending on the concentration of fibers (i.e. 0.5, 1 and 2% wt. of resin) from each image are selected. To have a reference value for well-dispersed, randomly-distributed fibers, the same number of fibers (i.e. 300, 600, and 850 fibers) are generated with a random position in a 2×2 mm^2 area. Accordingly, the reference area disorder value, AD_{del}(ref.), is determined to be 0.466 for an ideal microstructure of random distribution of fibers, regardless of the number of fibers. Thus, the AD_{del} equal or close to the AD_{del}(ref.) corresponds to well-dispersed, randomly-distributed fibers. The larger the value of AD_{del} from the AD_{del}(ref.) correlates to a more clustered, aggregated distribution.

3.2.4.3. Degree of alignment of fibers

The process-induced fiber orientation plays an important role in the anisotropy of the composite properties. To obtain isotropic material properties, the orientation of short fibers should have a random orientation distribution. In addition to the fact that the substrate fabric architecture may affect fiber orientation during deposition, the resin flow can also induce alignment of fibers during infusion. Thus, for the first time, the effects of fabric architecture, as well as resin flow on in-plane orientation of fibers, is demonstrated and quantified. For alignment analysis, optical images of NiC fibers-

deposited fabric and three-phase composite laminates are taken, covering five regions of the 2×2 mm^2 area, as similarly conducted in the dispersion analysis. To obtain the orientation angle of each fiber, a line is drawn along the fiber's axis. Then, the angle between this line and the horizontal line (i.e. parallel to the direction of resin flow) is calculated and placed into a data bin of 20°. Thus, the planar orientation domain between -90° to 90° is divided into 9 bins, where 0° orientation refers to being aligned in the resin flow direction. After identifying the orientation of all fibers in each optical image, a normalized histogram of the frequencies of the orientation angles is generated. The probability density function of the orientation angles is also estimated using a kernel distribution. The kernel distribution is a nonparametric approach to estimate the probability of a random variable. The kernel density estimator is given by,

$$f_h(u) = \frac{1}{nh}\sum_{i=1}^{n} K\left(\frac{u-u_i}{h}\right) \tag{7}$$

where n is the total number of fibers and u_1, u_2,…, u_n are the individual orientation data. $K(u)$ is a kernel probability density function and h is the bandwidth, also called the smoothing parameter, which controls the smoothness of the kernel estimator. Here, a Gaussian or a normal estimator is used.

$$K(u) = \frac{1}{\sqrt{2\pi}} e^{-\frac{1}{2}u^2} \tag{8}$$

For all cases, the smoothing parameter, h, is estimated by minimizing the asymptotic mean squared error [155].

3.3. Results and discussion

Representative optical images of NiC fibers at three different concentrations, i.e. 0.05, 0.1, and 0.2 g, deposited on the 12.7 × 12.7 cm^2 random mat fabric are shown in

Figs. 22(a)-(c). Fig. 22 shows that the concentration of NiC fibers affects the deposition microstructure on the fabric surface. Furthermore, the images of fibers deposited on the random mat and plain weave fabrics are given in Figs. 22 (a) and (b), respectively. As can be seen in Fig. 23, the fabric architecture, size of inter tow gaps, and gap locations are also affecting the microstructure morphology. In addition to these two factors, the resin flow during laminate fabrication may induce microstructural changes that could possibly alter the state of NiC fibers dispersion, orientation, and volume fraction distribution. Therefore, to validate the performance of the cascaded suspension deposition method, a detailed analysis of microstructure formed by the NiC fibers on deposited fabrics, as well as the final microstructure formed after the fabrication of laminates are reported in the following sections.

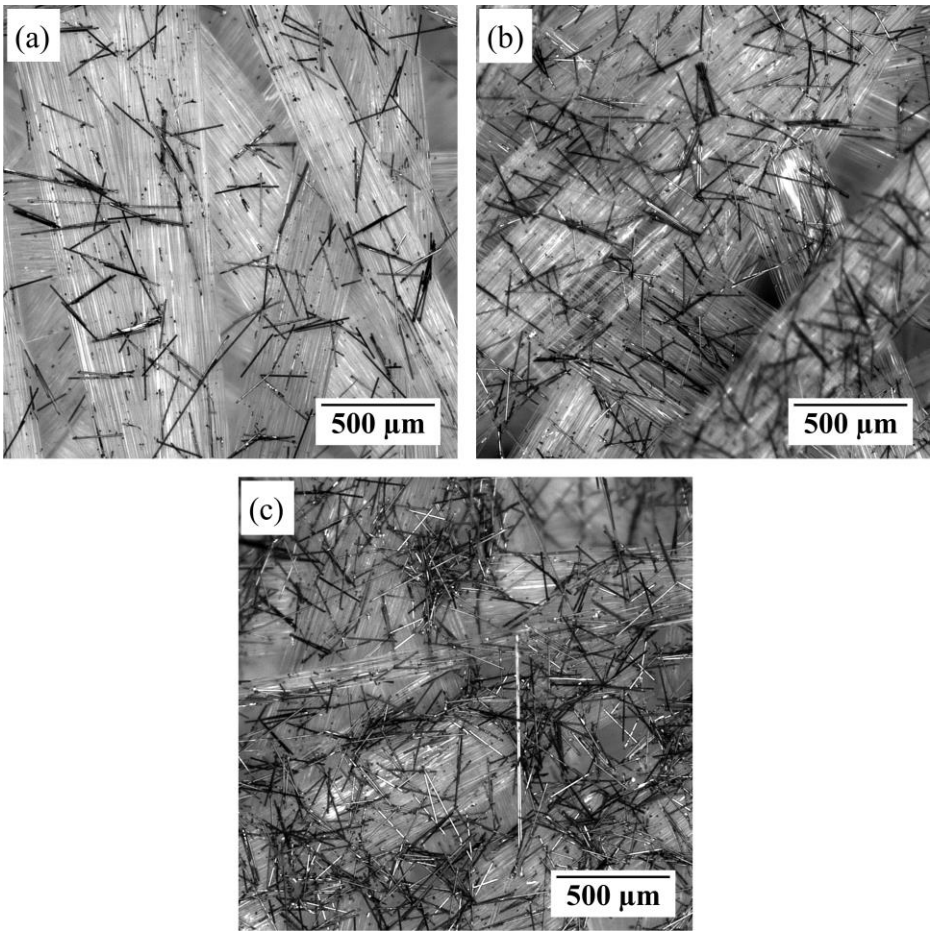

Figure 22. Representative optical images of NiC fibers-deposited random mat glass fabric at three different concentrations, where 0.05, 0.1, and 0.2 g NiC fibers are deposited on 12.7 × 12.7 cm^2 fabric surface, respectively.

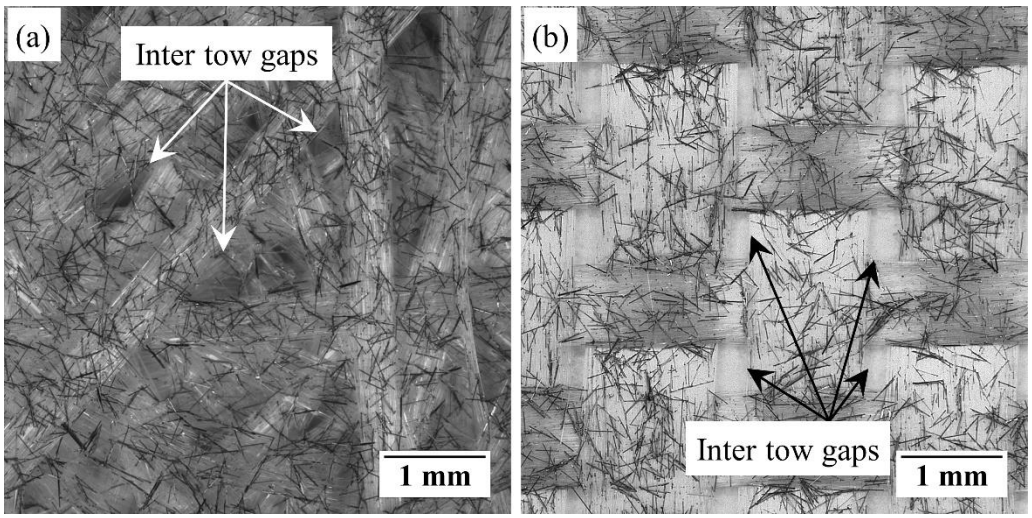

Figure 23. Microscopy images of NiC fibers deposited on (a) random mat and (b) plain weave glass fabric surfaces, showing that the fabric architecture, size of inter tow gaps, and gap location affect the microstructure morphology.

3.3.1. Comparison of the conventional approach of mixing fibers with resin and cascaded suspension deposition

An image of the top surface of the composite laminate produced by the common practice of mixing of NiC fibers with resin and then infusing the mixture into the fabric, M-R-1%NiC, is shown in Fig. 24(a). Although the fibers were well-dispersed in resin prior to infusion, the black region at the inlet in Fig. 24(a) indicates that the random glass mat filtered most of the NiC fibers very near the inlet. Hence, the filtration caused the NiC fibers to accumulate at the inlet and sharply decreased their concentration away from the inlet, seen by the light-gray region adjacent to the black area. In addition, a significant increase in resin viscosity is observed with the addition of short fibers. This factor, along with the increased resistance to flow due to the accumulation of fibers, increased the filling time from 3 min to 11 min. For a visual comparison, Fig. 24(b) shows a photograph of the top surface of the composite laminate produced with cascaded suspension deposition technique (CD-R-1%NiC), at the same fiber

concentration. Unlike Fig. 24(a), a mostly uniform gray color is observed throughout the entire surface of laminate, indicating an even distribution of NiC fibers. At a higher magnification, some small, lighter colored areas can be detected on the laminate surface that correspond to the gaps in the fabric architecture, where short fibers cannot be deposited. Fig. 24(b) also illustrates that no significant accumulation or movement of NiC fibers occurred during infusion of resin into the deposited fabric in VARTM. Comparison between Figs. 24(a) and (b) suggests that fabrication of three-phase composites with micron-sized fibers is in fact not feasible with conventional mixing approach of using VARTM process. A similar observation was reported for nano-sized fibers at concentrations above 1.5 wt.% [156]. As an alternative, the proposed cascaded deposition technique followed by the VARTM process can be easily incorporated to manufacture three-phase composites. However, the influences of the fiber concentration, fabric architecture, as well as resin flow on the spatial distribution, dispersion, and orientation of fibers need to be understood.

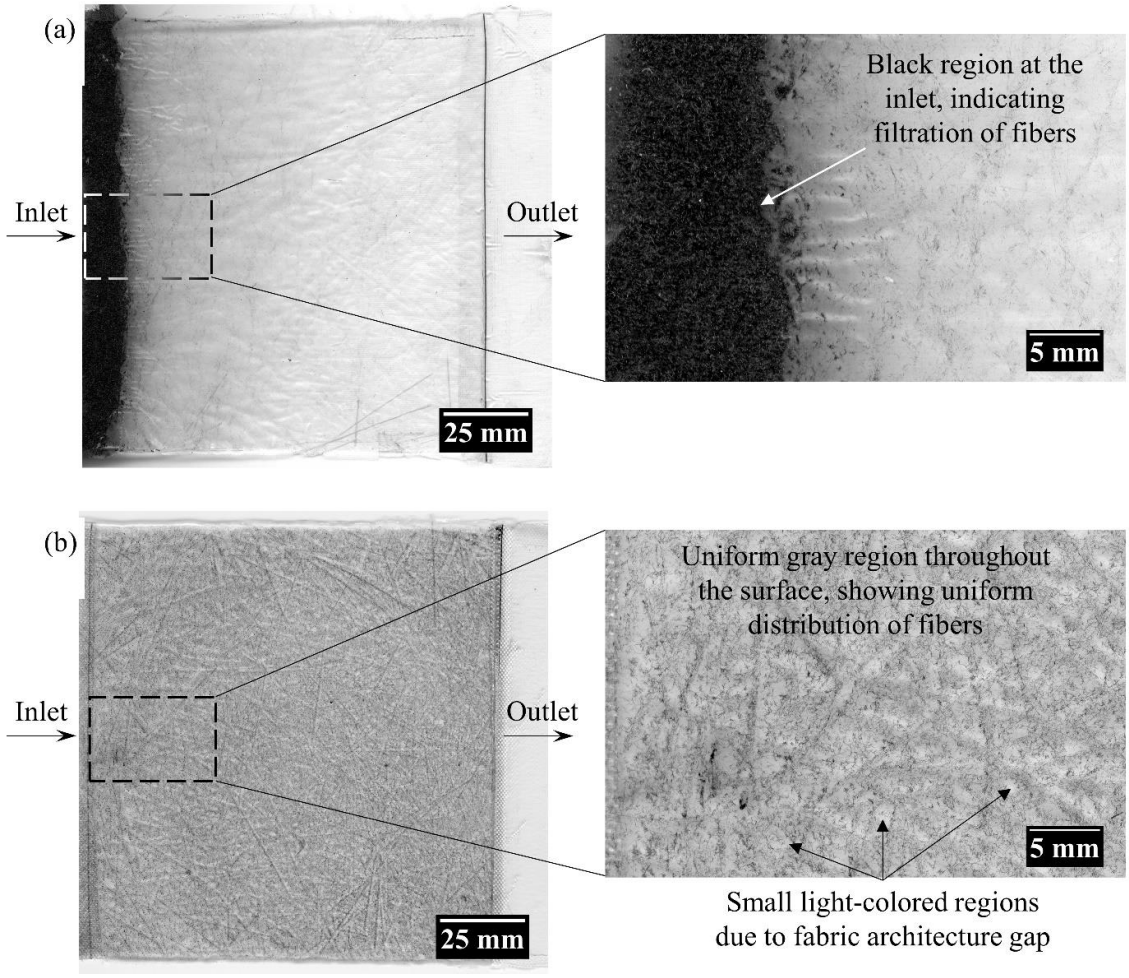

Figure 24. Top surface of a laminate fabricated by: (a) Conventional mixing approach (M-R-1%NiC), illustrating the filtration of NiC fibers from the fibers/resin mixture near the inlet during infusion and (b) Cascaded suspension deposition technique followed by infusion of a neat resin (CD-R-1%NiC), indicating a uniform, well-dispersed distribution of NiC fibers on the surface of a random mat laminate. Right-hand panels are enlarged views of the boxed area in the left panels.

3.3.2. Spatial uniformity of fiber deposition

To identify the spatial uniformity of fiber deposition along the fill and transverse directions, the local gray value of pixels is normalized with respect to 255, which is the gray value of the NiC fiber. Figs. 25(a) and (b) illustrate the fiber occurrence (i.e., normalized gray value) in random mat laminates at various fiber concentrations (i.e. 0.5,

1 and 2% wt. of resin) parallel and transverse to the resin flow direction, respectively. The average gray value of pixels, in the 100 × 100 mm^2 images of CD-R-0.5%NiC, CD-R-1%NiC, and CD-R-2%NiC laminates are 77, 110, and 123, respectively. This increasing trend in the average gray value or fiber occurrence prove that there is more NiC fiber in CD-R-1%NiC than CD-R-0.5%NiC laminate and in CD-R-2%NiC than CD-R-1%NiC laminate. As expected this increase does not linearly correlate with weight fraction of the fibers, which can be due to the overlapping of the fibers in the scanned image. The variation of normalized gray value along or transverse to the resin flow direction represents the changes in fiber volume fraction at the laminate surface. Thus, a lower variation in normalized gray value indicates a better uniformity in the spatial distribution of NiC fibers. Comparison of Figs. 25(a) and (b) clearly indicates the mostly uniform spatial distribution of NiC fibers throughout the laminate surface. In fact, regardless of the fiber concentration, an almost perfectly uniform distribution of fibers can be seen in the transverse direction, evidenced by the horizontal fiber occurrence lines in Fig. 25(b). The fiber occurrence is not as uniform in parallel to the resin flow direction which might be due to slight movement of fibers along the flow (see Fig. 25(a)). It should be noted that the observed uniformity of fiber deposition is independent of the fiber concentration, which is an important benefit of the cascaded deposition method.

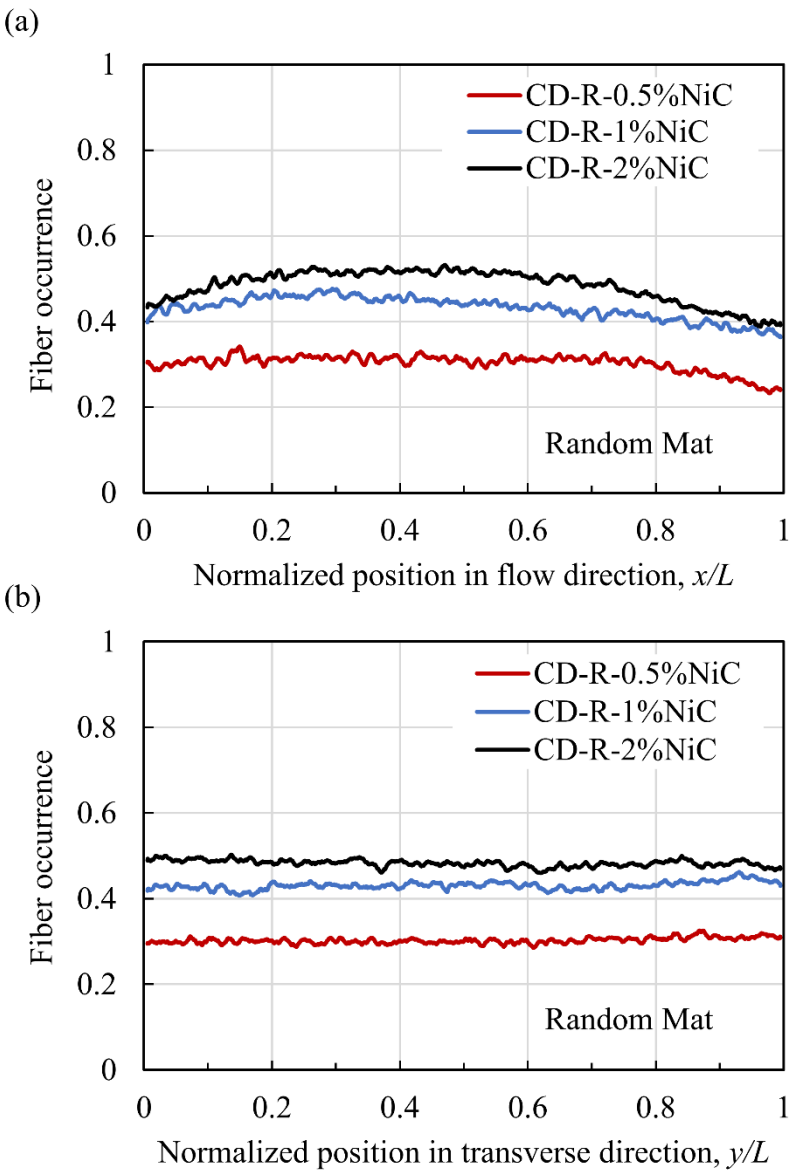

Figure 25. Variation of fiber occurrence (i.e. normalized gray value) indicating the uniformity of fiber distribution in: (a) resin flow direction and (b) transverse direction of random mat laminate at 0.5, 1, and 2% fiber concentration (CD-R-0.5%NiC, CD-R-1%NiC, and CD-R-2%NiC).The local gray value of pixels is normalized with respect to 255, which is the gray value of the NiC fiber.

Figs. 26(a) and (b) presents the fiber occurrence (i.e. normalized gray value) in a plain weave laminate at 1% fiber concentration (CD-P-1%NiC) along the resin flow and in transverse direction, respectively. The average gray value of pixels in the 100 × 100

mm^2 image of CD-P-1%NiC laminate is 68. Similar to the random mat, mostly uniform fiber distribution is observed in both directions for the plain weave. At the same time, variation of the fiber distribution in the transverse direction is slightly less than that in the fill direction. Comparison of the random mat and plain weave fabric indicates that, at the same fiber concentration, the variation of fiber occurrence at a smaller length scale along both directions is higher in plain weave laminates. This can be due to the presence of the gaps between the tows in the plain weave architecture, resulting in local deposition of NiC fibers at the crossings of glass fiber tows. Thus, the fiber volume fraction is more uniform at a smaller length scale on the random mat compared to plain weave laminates.

Overall, it is observed that with cascaded suspension deposition technique, uniform deposition of the micron-sized fibers is achieved throughout the glass fabric-epoxy laminate surface. In addition, this method provides the flexibility of depositing various types of microfibers on different fabric architectures, and thus enables manufacturing of three-phase composites with tailored surface properties. Achieving spatially uniform fiber deposition is particularly significant since fabrication of multi-functional, advanced composites with highly conductive or magnetic surface properties becomes possible.

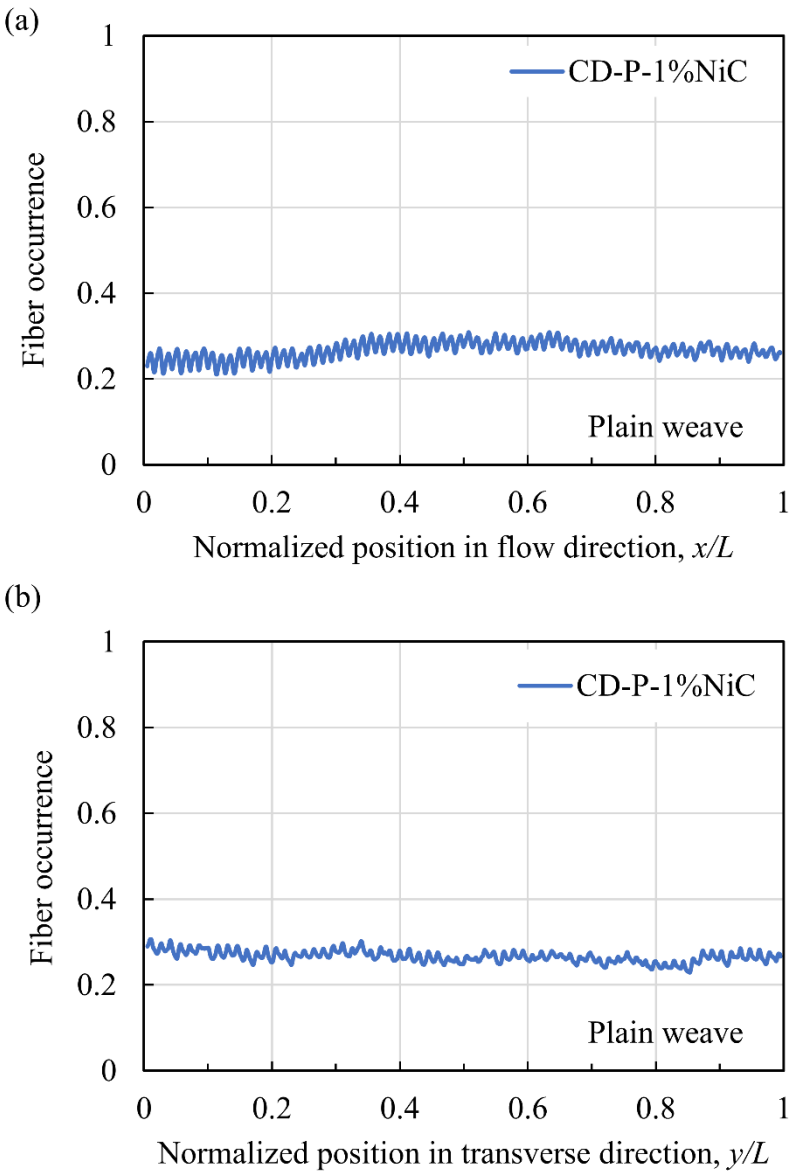

Figure 26. Variation of fiber occurrence (i.e. normalized gray value) indicating the uniformity of fiber distribution in: (a) resin flow direction and (b) transverse direction of plain weave laminate at 1% fiber concentration (CD-P-1%NiC). The local gray value of pixels is normalized with respect to 255, which is the gray value of the NiC fiber.

3.3.3. Degree of dispersion and alignment of fibers on fabric and composite laminate

This section discusses the results of the dispersion and alignment of fibers after deposition and how these two parameters are altered by the resin flow during infusion.

3.3.3.1. Effect of resin flow during infusion on the deposited fiber microstructure

Fig. 27 illustrates the changes in the dispersion and orientation of the deposited fibers due to resin infusion. The images shown in Fig. 27(a) and (b) are captured at the same 2 mm × 2 mm location by a microscope camera before and after the resin infusion. To illustrate the effect of flow-induced changes in fiber dispersion, the Delaunay network is generated, area disorder, AD_{del}, is estimated and the results are presented in Figs. 27(c) and (d). In these cases, AD_{del} is found to be 0.465 before and 0.498 after infusion. A small decrease in degree of dispersion is reflected in the slightly increased AD_{del} value. Thus, considering that the reference area disorder for a perfect dispersion is $AD_{del}(ref.)=0.466$, the proposed cascaded suspension deposition technique resulted in well-dispersed fibers on the random mat fabric surface. Having a slightly higher area disorder of 0.498 after infusion reveals that dispersion is only marginally reduced after flow front passes. However, still, short fibers are well-dispersed on the surface of the random mat laminate. In other words, even though the resin flow through the random mat could be relatively fast [13], it does not cause a considerable transport or clustering of fibers which could have resulted in a significant increase in AD_{del} .These results demonstrate that one can easily fabricate a three-phase composite by cascaded deposition of short fibers followed by VARTM.

Flow-induced alignment of fibers is investigated by comparing normalized frequencies of the orientation angle of fibers on the fabric before and after infusion and their kernel distribution (see Figs. 27(e) and (f), respectively). Fig. 27(e) shows that most of the fibers are orientated in the ranges between -10° to -70° and probability density of the orientation angle of fibers has a small and discernible peak near -30°. This can be explained by the tendency of the fibers to orient along the direction of fabric tows during deposition. Degree of orientation of fibers after infusion (see Fig. 27(f)) shows that the flow induces a slight alignment along the flow direction. However, the random architecture of fabric and entanglement of short fibers with fabric reduce the tendency of the fibers to align perfectly with the flow during infusion, thus mostly maintaining the level of isotropy induced during deposition.

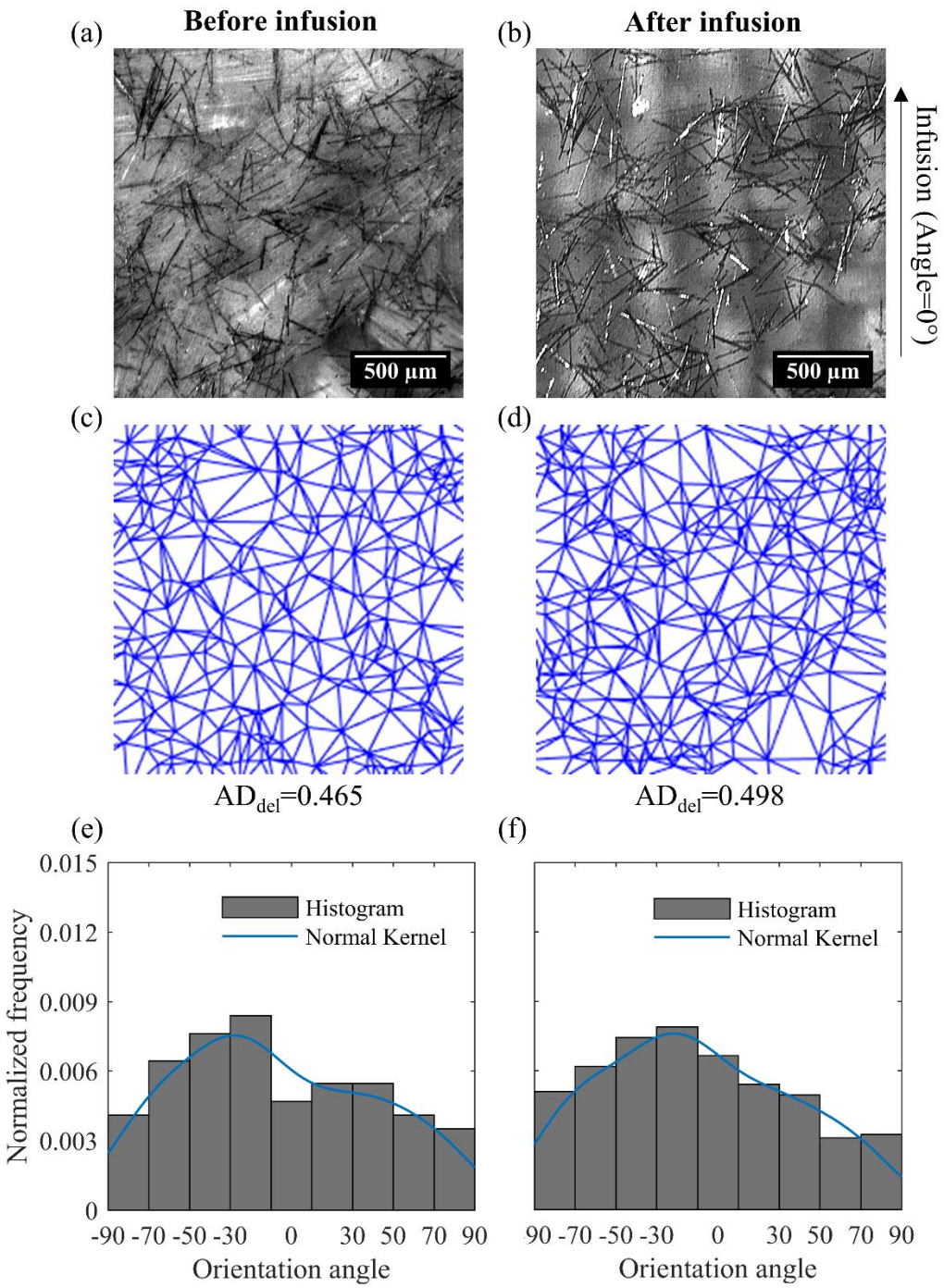

Figure 27. The changes in dispersion and orientation of NiC fibers due to resin infusion in VARTM. (a) and (b) are optical images of the same 2 mm × 2 mm location before and after infusion, respectively. (c) and (d) demonstrate generated Delaunay triangles from fibers position and calculated degree of dispersion before and after infusion, respectively. (e) and (f) show normalized frequencies of the orientation angle of fibers before and after infusion and their kernel distribution.

3.3.3.2. Microstructural changes caused by resin flow at multiple locations

The degree of dispersion of fibers as deposited on the fabric and on the laminate at five different locations are depicted in Fig. 28(a). Similarly, AD_{del} of all cases is normalized with the reference value of AD_{del}(ref.)=0.466. The closer the normalized area disorder is to 1, the better the dispersion. It is seen that the normalized value of AD_{del} for the deposition on random mat is up to 1.05, which illustrates that fibers are well-dispersed on the fabric surface. The laminate dispersion results suggest that during infusion, the normalized AD_{del} may change by 5-16% to 1.08-1.21 at different locations. As a result, the average and 95% confidence interval of area disorder values at multiple locations for random mat increases from 0.476 ± 0.010 to 0.523 ± 0.022 for the laminate. This change in dispersion quality, although not high enough to result in visually identifiable fiber clusters, can still be prevented by controlling the speed of the resin flow. For this purpose, external pressure can be applied by compressed air [17] or by permanent magnets (if fibers are not magnetic) on the VARTM lay-up [14], which may greatly restrict the fiber movement during infusion.

Normalized frequencies of the orientation of a total of approximately 3000 fibers from five different locations on the random mat fabric and laminate surface and their kernel distributions are presented in Figs. 28(b) and (c). The small orientation peaks observed at angles between 30-70° could be explained by the local orientation of fabric tows. The fiber orientation histograms for the laminate reveal that NiC fibers are slightly rotated during infusion and a more random orientation distribution is formed. In fact, wetting of fabric and resin flow overcome the friction of short fibers entanglement with fabric, helping the fibers to slightly rotate. Thus, in a random mat, resin flow can

favor the formation of an isotropic distribution of fibers, thus leading to improved isotropic microstructure in the laminate.

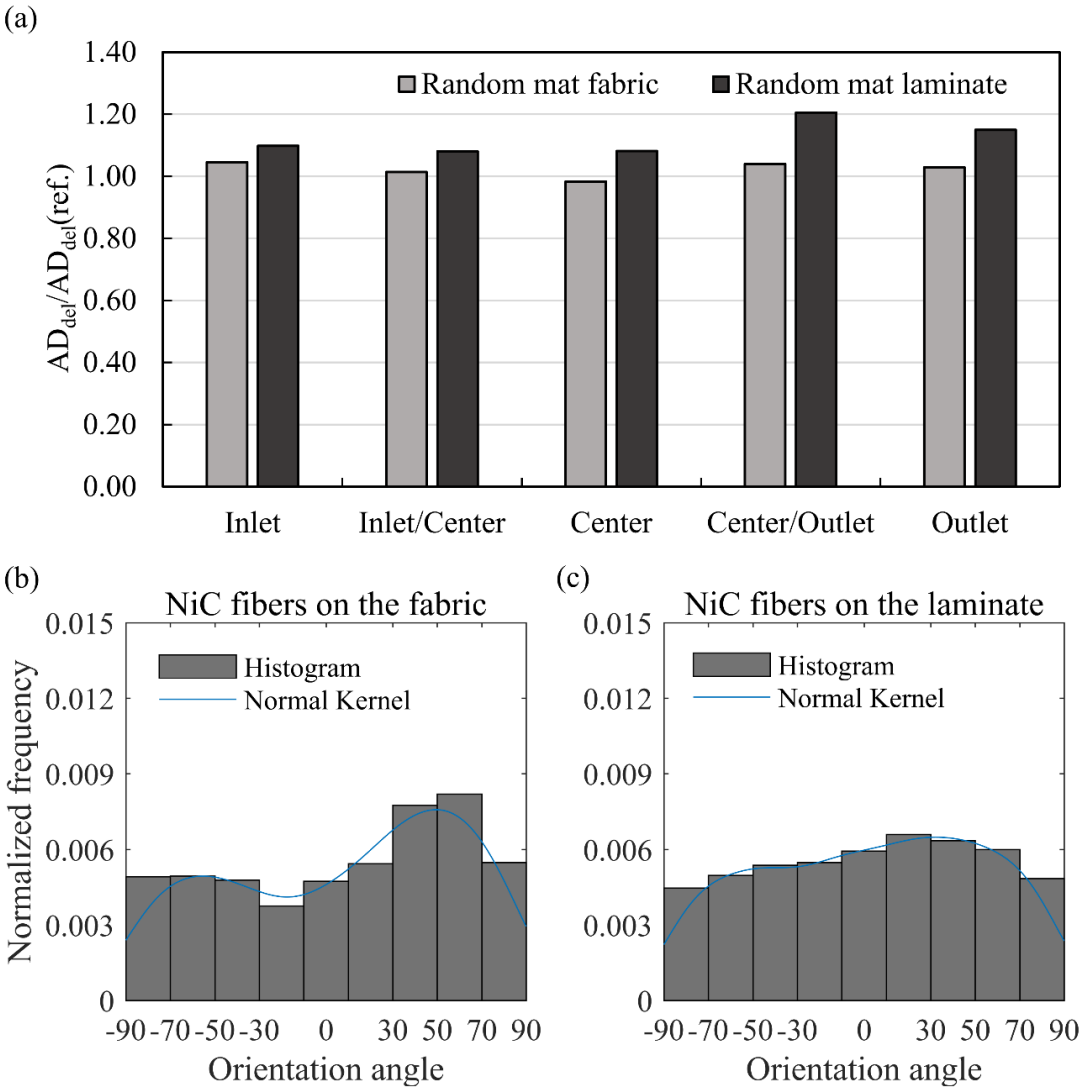

Figure 28. (a) Normalized area disorder of NiC fibers on the random mat fabric and laminate. Normalized frequencies of the orientation of fibers on the random mat: (b) fabric and (c) laminate and their kernel distributions at five locations along the flow direction. Note: A value of normalized area disorder close to 1 corresponds to well-dispersed, randomly-distributed fibers.

3.3.4. Effect of concentrations of fibers on microstructure morphology

To quantify the effect of fiber concentration on the dispersion and alignment, laminates containing fibers at 0.5, 1, and 2% wt. of resin are prepared. The degree of dispersion of the NiC fibers at five equidistant locations on the laminates is depicted in Fig. 29. The vertical axis is the normalized area disorder, where the values close to 1 correspond to good dispersion of the short fibers. As shown in Fig. 29, at each concentration, the normalized area disorder, or in other words degree of dispersion of fibers, are rather similar at all locations. Thus, short NiC fibers at different concentrations can be well dispersed throughout the surface of random mat laminate by the cascaded suspension deposition. Fig. 29 also clearly presents that as the fibers concentration is increased, the value of normalized area disorder decreases, approaching 1 for a well-dispersed distribution at each location. In addition, the average value of area disorder at five locations decreases from $\overline{AD}_{Del}$=0.539 ± 0.009 in CD-R-0.5%NiC to 0.523 ± 0.022 in CD-R-1%NiC, and to 0.473 ± 0.017 in CD-R-2%NiC laminates. Therefore, the NiC fibers are slightly better dispersed in the random mat laminates with increasing the fiber concentration.

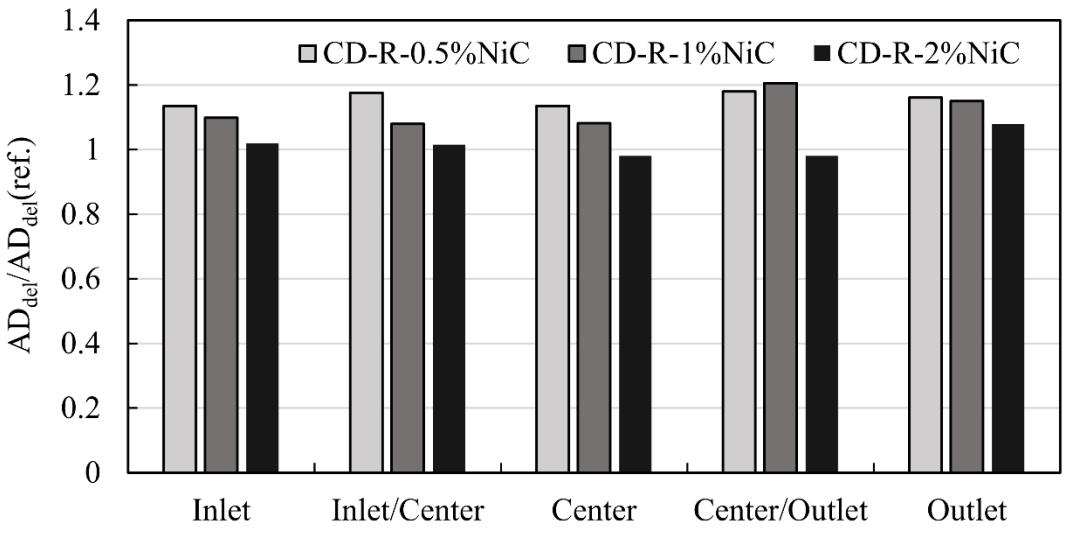

Figure 29. Normalized area disorder of fibers on the random mat laminates at different fibers concentrations (0.5, 1, and 2% wt. of resin) at five locations along the flow direction. A value of normalized area disorder close to 1 corresponds to well-dispersed, randomly-distributed fibers.

Fig. 30 shows the normalized frequencies and kernel distributions of fiber orientations in random mat laminates at different concentrations as a function of orientation angle. In all the laminates, CD-R-0.5%NiC, CD-R-1%NiC, CD-R-2%NiC, NiC fibers are randomly oriented. Given that the1D resin flow direction is at 0°, it can be concluded that the fabrication process does not induce any alignment. In addition, changing the concentrations of fibers does not seem to affect the alignment of NiC fibers. The small variations observed in the alignment of fibers can be due to the local variations in the architecture of random mats.

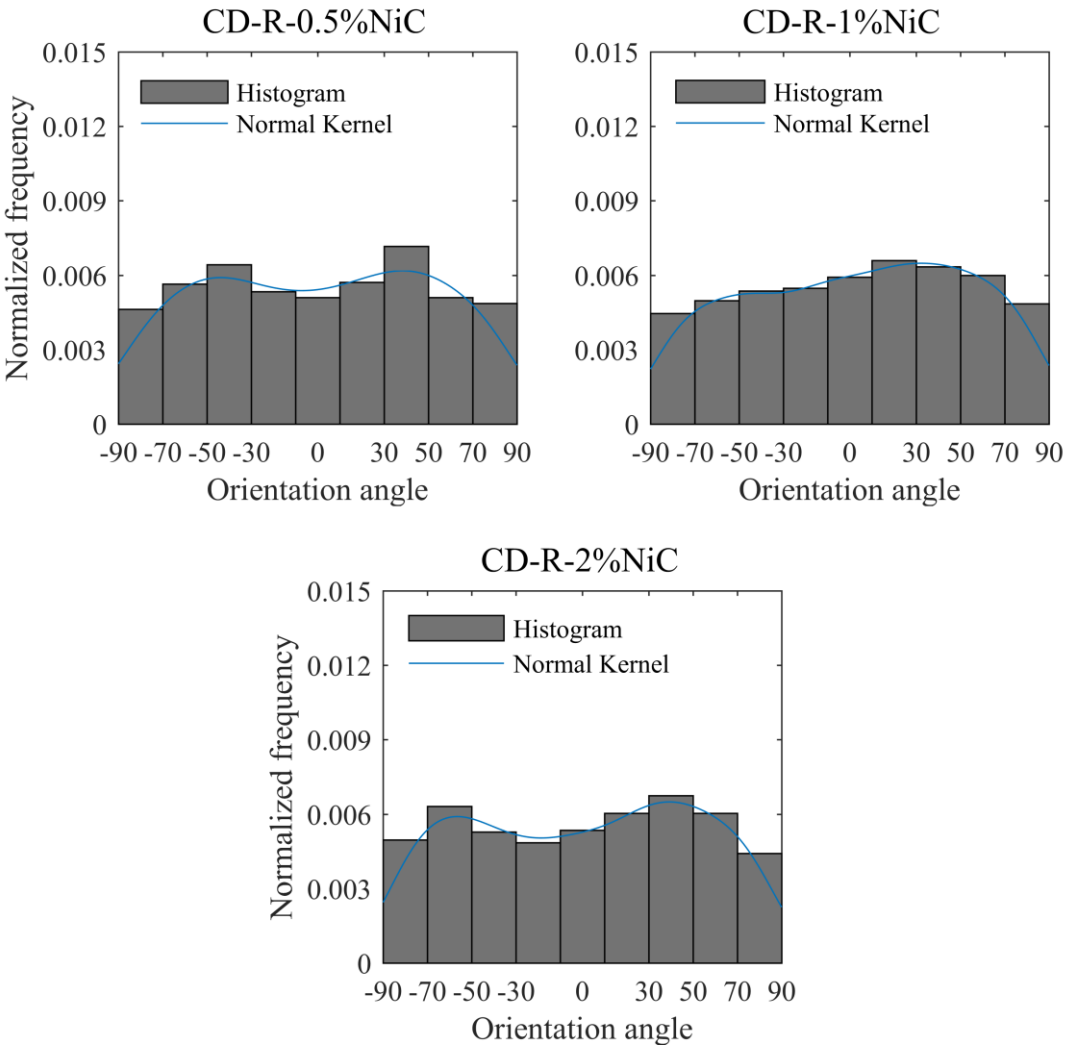

Figure 30. Normalized frequencies and kernel distributions of fibers orientations in random mat laminates at different fibers concentrations (0.5, 1, and 2% wt. of resin) as a function of orientation angle, showing random orientation of fibers.

3.3.5. Effect of fabric architecture on microstructure morphology

To assess the sensitivity of NiC fibers dispersion to fabric architecture, the normalized area disorder of fibers deposited on plain weave fabric is obtained at five locations and compared with those deposited at the same concentration on random mat in Fig. 31(a). As seen in Fig. 31(a), the normalized area disorder of fibers on random mat ($\overline{AD}_{Del}$=0.476 ± 0.010) is lower than that on plain weave fabric ($\overline{AD}_{Del}$=0.504 ±

0.007), suggesting a better dispersion of fibers on the surface of random mat. This could be due to the presence of smaller gaps in the random mat and the random placement of these gaps. Despite achieving a lower degree of dispersion of fibers in plain weave fabric, there is still no agglomeration of NiC fibers. Fig. 31(b) presents the normalized area disorder of fibers on plain weave fabric before and after infusion at five locations along the flow direction. Similar to the random mat, the normalized area disorder of fibers in plain weave laminate ($\overline{AD}_{Del}$=0.525 ± 0.022) is higher than that in plain weave fabric ($\overline{AD}_{Del}$=0.504 ± 0.007), indicating lower degree of dispersion in the laminate than fabric due to resin flow. However, the normalized area disorder of NiC fibers on plain weave laminate reduces from inlet to outlet due to the sharp reduction in resin velocity, indicating a slight improvement in dispersion of NiC fibers along the flow direction. This phenomenon is not observed in random mat laminate because the resin velocity does not change significantly from inlet to outlet in random mat laminates.

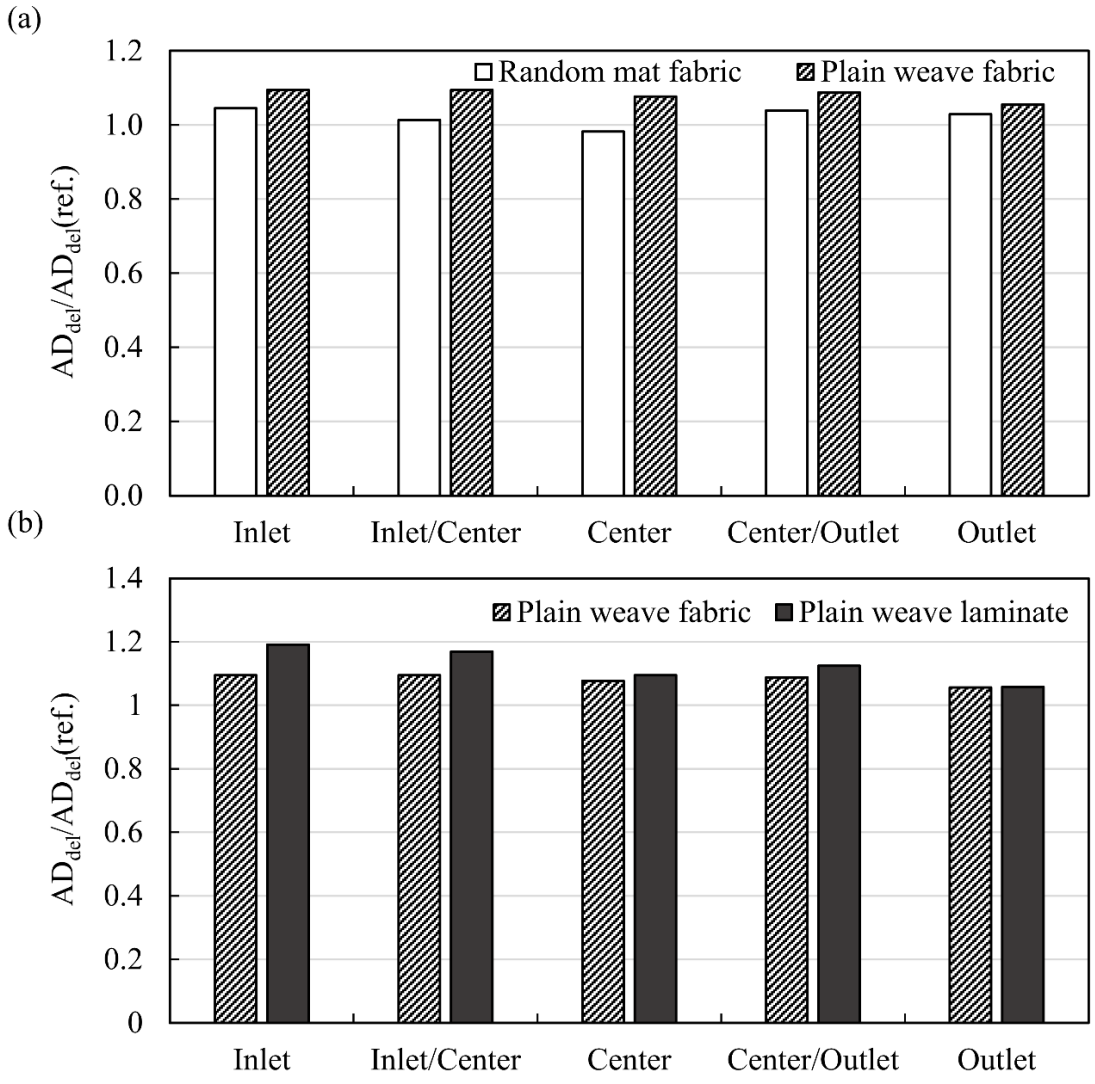

Figure 31. Normalized area disorder of fibers on: (a) plain weave fabric compared to those at similar fibers concentration on random mat fabric and (b) plain weave fabric before and after infusion at five locations along the flow direction. Note: the closer the normalized area disorder is to 1, the higher the degree of dispersion.

Normalized frequencies and kernel distributions of fiber orientation angle for plain weave laminate is shown in Fig. 32. It is seen that the fibers are slightly aligned either towards (0°) or perpendicular (-90° and 90°) to the flow direction. Given that in plain weave fabric the fiber tows are parallel or perpendicular to the flow direction, the flow caused the fibers to marginally align along the warp and weft tows. For this reason,

in plain weave laminate, a slightly higher degree of alignment of fibers in 0°, 90°, and -90° is observed, unlike random mat laminates. Thus, one may benefit from the dependency of NiC fiber orientation on the fabric architecture, and thus may introduce anisotropy to tailor the properties of the composite.

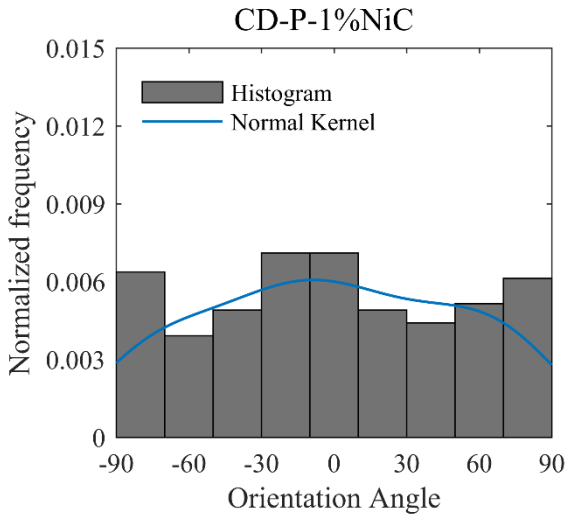

Figure 32. Normalized frequencies and kernel distributions of fiber orientation angle for plain weave laminate, demonstrating fabric architecture-induced orientation of fibers at ≈ 0° and 90° (i.e., along the warp and weft tows of plain weave fabric).

3.4. Concluding remarks

This work introduces the cascaded suspension deposition method to uniformly incorporate short fibers into the molded composite laminates. The effectiveness of the proposed technique to uniformly distribute fibers on the surface of reinforcing fabric and the resulting structural laminates is investigated through a comprehensive analysis of the process-induced microstructure. For this purpose, quantitative assessment of the uniformity of fiber volume fraction, as well as, degree of dispersion and alignment of the fibers are conducted. This chapter also investigates the effects of concentration of

deposited fibers, fabric architecture, and resin flow on the process-induced microstructure.

The results prove that the proposed technique enables fabrication of three-phase composite laminates with uniform fiber volume fraction, as well as good dispersion and isotropic orientation of short fibers (i.e., the third phase). The resin flow in VARTM does not disturb deposition-induced microstructure of the NiC fibers, indicating the compatibility of VARTM with cascaded suspension deposition technique. Thus, composites with uniform microstructure at all concentrations (i.e., 0.5, 1 and 2%) of NiC fibers are fabricated. The results also show that with increasing the concentration of fibers to 2 % wt. of resin, the degree of dispersion of fibers slightly improves. In addition, the fabric architecture is found to influence the microstructure morphology, such that NiC fibers on the plain weave laminate have a slightly lower degree of dispersion and tendency to align at particular directions (i.e. 0° and 90°) compared to random mat laminates. Conclusive results obtained suggest that the proposed technique is capable of depositing short fibers on different fabric substrates at a desired concentration, allowing the fabrication and control of the surface properties of the three-phase composites by VARTM.

Chapter 4. Magnetic Field-Induced Alignment of Short Carbon Fibers in Polymer Composites

In the first part of chapter 4, the alignment of nickel coated carbon (NiC) fibers by a magnetic field during cure of an epoxy resin is explored. Towards this goal, the effects of several parameters such as field strength and fibers length on the microstructure morphology of NiC epoxy composites are investigated. Furthermore, the degree of alignment and the magnetic field strength required for tailoring anisotropy in the composite are identified. The results confirmed that applying magnetic field using a set of permanent magnets is a favorable method for the preparation of aligned NiC fibers polymer composites.

The second part of chapter 4 involves the development of a new magnetic-field assisted composite processing method to align NiC fibers on the surface of three-phase composite laminates. The appropriate level of magnetic field, identified in the first part of chapter 4, is used to induce alignment of NiC fibers without disturbing the uniformity of microstructure in the three-phase (i.e. NiC fibers/glass fabric/epoxy) composites, and thus, controlling their surface anisotropy.

4.1. Alignment of Nickel Coated Carbon Fibers by Magnetic Field during Cure of Polymer Composites

Carbon fibers are widely used as reinforcement in polymer-matrix composites due to their excellent mechanical properties combined with their lightweight. Coating of short carbon fibers with nickel not only preserves the desired specific mechanical properties of both the fiber and the resulting composite but also improves their electrical conductivity and magnetic properties. The short fibers may be randomly dispersed in composites to exhibit isotropic behavior. However, controlling the orientation of the fiber reinforcement can improve the performance of the composite such as electrical conductivity, modulus, and strength in the loading direction. In the first part of chapter 4, the alignment of nickel coated carbon (NiC) fibers by a magnetic field during cure of an epoxy resin is explored. For this purpose, the effects of several parameters such as field strength (10-50 mT) and fibers length (0.1 and 0.25 mm) on the degree of fiber alignment within composites are investigated using scanning confocal microscopy and image analysis techniques. The 0.1 mm long fibers started to align along the direction of magnetic field at around 10 mT. The degree of alignment is enhanced at about 30 mT which enables the NiC fibers to interact easily with each other and build NiC fiber networks. Furthermore, when a higher magnetic field of 50 mT is applied, in addition to the rotation and network formation, pronounced migration of fibers towards the magnetic poles is observed. In addition, under the same magnetic field of 30 mT, longer fibers (0.25 mm) reaches a higher degree of alignment.

4.1.1. Introduction

Thermoset epoxy resins are widely used as coatings for the protection against aggressive environments, adhesives for joining structural components, and matrices for manufacturing fiber reinforced composites [157, 158]. The cured epoxy resins generally exhibit many desirable properties such as good thermal stability, relatively high strength and modulus, and excellent adhesion properties. However, their low fracture toughness and electrical conductivity result in poor resistance to crack propagation and lightning strike, which limit their use, especially for structural applications. Therefore, fillers are often added to epoxy resins to overcome these limitations [159-161]. One of the widely used reinforcing fillers is short carbon fibers due to their excellent mechanical properties combined with their lightweight and relatively low material and processing costs [162-164]. Coating of short carbon fibers with nickel improves the electrical conductivity and magnetic properties of both the fiber and the resulting composite while preserving their specific mechanical properties [149, 165, 166].

The short fibers may be dispersed randomly in liquid thermosetting resins using a combination of sonication and mechanical mixing to exhibit isotropic behavior. However, controlling the orientation of the fiber reinforcement can significantly improve the performance of the composite such as electrical conductivity [77, 167] and mechanical strength [83, 94] in the loading direction. To align fibers, several methods have been developed including applying shear [88], ultrasound field [149], electric field [84], and magnetic field [168, 169]. Applying magnetic field, however, has advantages over other methods because it allows the homogeneous, remote orientation of fibers along a particular direction, and is not sensitive to surface charge. In addition, strong

permanent magnets and electromagnets are currently available which can generate a sufficient magnetic field to effectively align fibers in a polymer matrix [81].

Magnetic alignment can be used for materials that exhibit anisotropic diamagnetic susceptibility such as fibers. Under a static magnetic field, the carbon fiber axis with the largest diamagnetic susceptibility orients parallel to the applied field. There are various factors influencing the alignment of fibers in a resin such as the magnetic field strength, fiber aspect ratio/shape, magnetic properties of the fiber and resin, resin viscosity, and cure rate. Typical diamagnetic particles require extremely high magnetic fields on the order of 1 T for alignment [170]. However, low magnetic field strengths of 1–10 mT can be used to align the micrometer-sized, rod-like or platelet-like nonmagnetic particles coated with superparamagnetic nanoparticles suspended in a fluid [83]. Using a fluid or resin with a higher viscosity increases the time it takes to align particles along the field but does not affect the magnitude of the magnetic field required for alignment. However, if the resin cures too fast, the low magnetic field may not allow fibers to achieve the desired orientation before cure [81].

In the present work, the magnetic alignment of NiC fibers in an epoxy laminate and the resulting material microstructure are explored. The alignment is achieved by placing the mold containing the composite between two permanent magnets at a distance, holding them in place, and thus applying a static magnetic field in the range of 10-50 mT during cure. The confocal microscopic studies are performed to evaluate the effects of field strength and fiber length on the degree of alignment within composite laminates.

4.1.2. Experimental details

4.1.2.1. Materials

Two types of nickel coated carbon (NiC) fibers with different lengths (Conductive Composites Company, LLC) are selected as the reinforcements. The nominal lengths of the fibers are 0.1 and 0.25 mm, and their diameter is 7 μm. Fig. 33 shows SEM images of NiC fibers used in this work, where nickel is 20 wt. % of the coated fiber. As can be seen in Fig. 33(b), some fibers were not coated properly, so they may not align under the low magnetic field. The epoxy resin used in this work is EPIKOTE resin MGS RIMR 135 with EPIKURE curing agent MGS RIMH 137 at a weight ratio of 100:30 (Hexion - currently Momentive). This is a low viscosity resin (310 mPa s at 25 ºC) with a long pot life which allows the necessary time for the fibers to rotate before the resin gels.

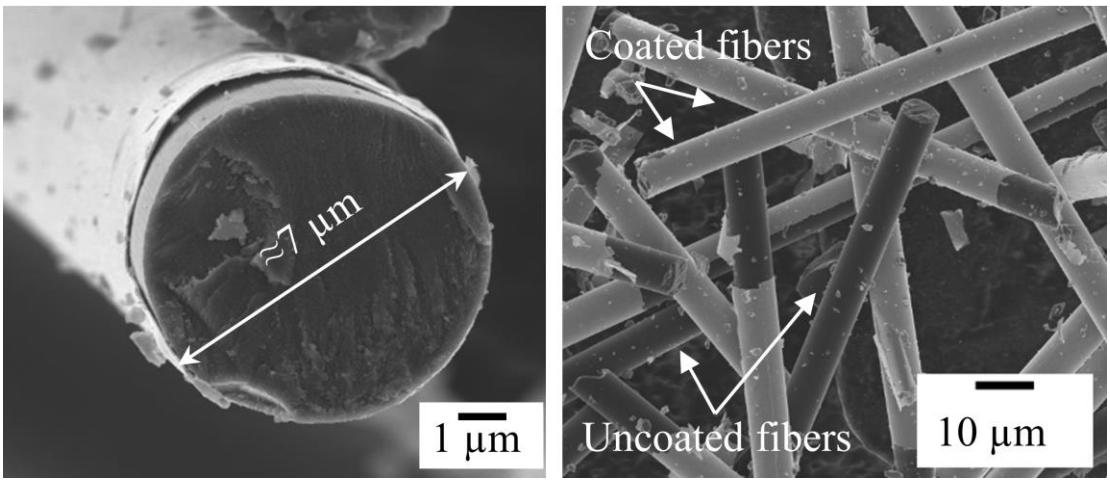

Figure 33. SEM image of (a) a single nickel coated 7-micron diameter AS4D fiber at 7000× and (b) uncoated and coated fibers at 800× magnification.

4.1.2.2. Fabrication of epoxy composites with aligned NiC fibers

NiC fibers are first mixed with epoxy resin by a stirrer at 350 rpm for 5 min, and then the mixture is sonicated for 30 min to help the dispersion of fibers. After that, the

curing agent is added and mixed for 5 min at 350 rpm. The composite is transferred to a silicon mold and placed at a distance between two parallel permanent magnets, as illustrated in Fig. 34. The strength of the magnetic field is measured by a Gaussmeter (Alphalab, model GM1-ST). The curing of epoxy is carried out at room temperature for 24 h, and the magnetic field is applied during the entire curing process. Cured composites are then placed in an oven for post cure at 80 °C for 15 h.

The first part of chapter 4 investigates the effects of field strength and fibers length on the degree of fiber alignment within the composites. To apply different magnetic fields (10-50 mT), block-shaped N52 Neodymium Iron Boron (also referred to as NdFeB) magnets (KJ Magnetics) with dimensions of 2.54 (length) × 2.54 (width) × 1.27 (thickness) cm^3, magnetized through-the-thickness, are used. Recently, these magnets have been used to apply magnetic pressure on the composites, and it was reported that they have a very high surface magnetic field of the order of 0.5 T [171-173]. When these magnets are 60 mm apart, they can generate a magnetic field of approximately 50 mT in the middle. As seen in Fig. 34, an aluminum mold is used to hold the magnets in place, and the field is applied in the horizontal direction. This configuration of magnets generates magnetic field gradient in the horizontal direction; however, within 12 mm at the center of the composite sample, the magnetic field is determined to be almost uniform. To apply a lower field of 30 and 10 mT, the distance between the magnets is increased to 85 and 115 mm by placing spacers. Also, to assess the effect of fiber length on the degree of alignment, 0.1 and 0.25 mm long fibers which have 14 and 36 aspect ratios (α=length/diameter) are employed as the reinforcement. In

all the composite samples, a concentration of 1.0% wt. NiC fibers is used. Also, the thicknesses of the cured samples are measured to be around 1 mm.

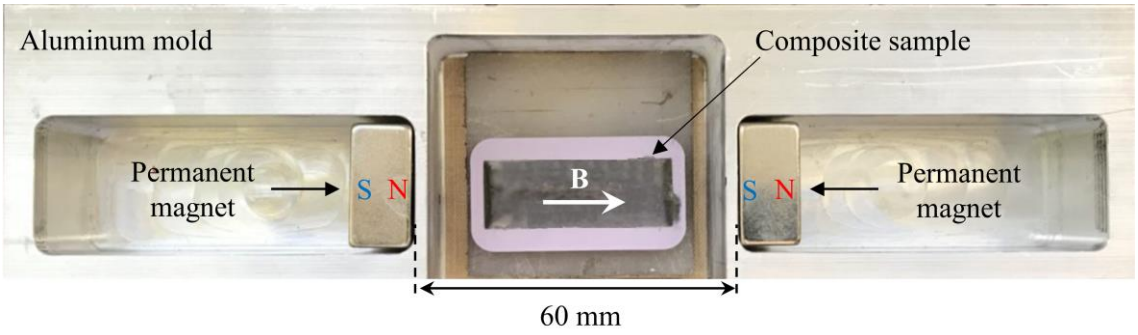

Figure 34. Setup for alignment of NiC fibers during cure of an epoxy laminate, with the sample placed between two 2.54 × 2.54 × 1.27 cm^3, N52 NdFeB, permanent magnets. Magnets are able to generate a 50 mT magnetic field from 60 mm apart.

4.1.2.3. Scanning confocal microscopy

The microstructure of the cured samples is characterized by scanning confocal microscopy. Multiple images are taken covering the whole thickness of the sample using a Leica TCS SP8 confocal microscope. Once all the images are captured, they are then vertically stacked together using ImageJ software.

4.1.2.4. Fiber alignment analysis

The in-plane orientation of each fiber is determined by identifying its major axis with respect to the horizontal axis using ImageJ software, where the horizontal alignment direction corresponds to 0°. A histogram of the angular distribution of fibers is then generated based on the relative frequency of orientation angles and sorted into bins of 10°. Also, a normal distribution is fitted to the histogram of orientation distribution and the mean and standard deviation are estimated.

4.1.3. Results and discussion

Fig. 35 shows confocal microscopic images of the composites containing NiC fibers (α=14) which are cured: (a) without magnetic field, (b) under 10 mT horizontal magnetic field (B=10 mT), (c) B=30 mT, and (d) B=50 mT. All the images are captured from the middle of the composite laminates. Fig. 35(a) shows randomly-oriented fibers in the composite made without magnetic field. However, Fig. 35(b) shows that some of the NiC fibers rotated towards the direction of magnetic field of 10 mT, clearly depicting the formation of a preferred orientation angle. The underlying mechanism is that the magnetic field induces a torque on the fibers and if the torque is large enough to overcome the hydrodynamic drag, the fibers will rotate. Fig. 35(c) shows that the magnetic field of 30 mT caused a higher alignment of NiC fibers and formation of aligned NiC fiber networks. The networks are formed because the fibers experienced positive dipolar interactions in the magnetic field which causes the attraction of NiC fibers in a head-to-tail fashion. As a result, relatively long chains of NiC fibers parallel to the external field are observed in the samples cured under 30 mT. At a higher magnetic field of 50 mT, the fibers migrate towards the magnetic poles. The migration of fibers at this field is due to the increased magnetic field gradient along the horizontal direction. For this reason, a lower number of fiber chains are observed in the middle of the sample (see Fig. 35(d)) and a greater concentration near the edges of the sample which are close to the magnetic poles.

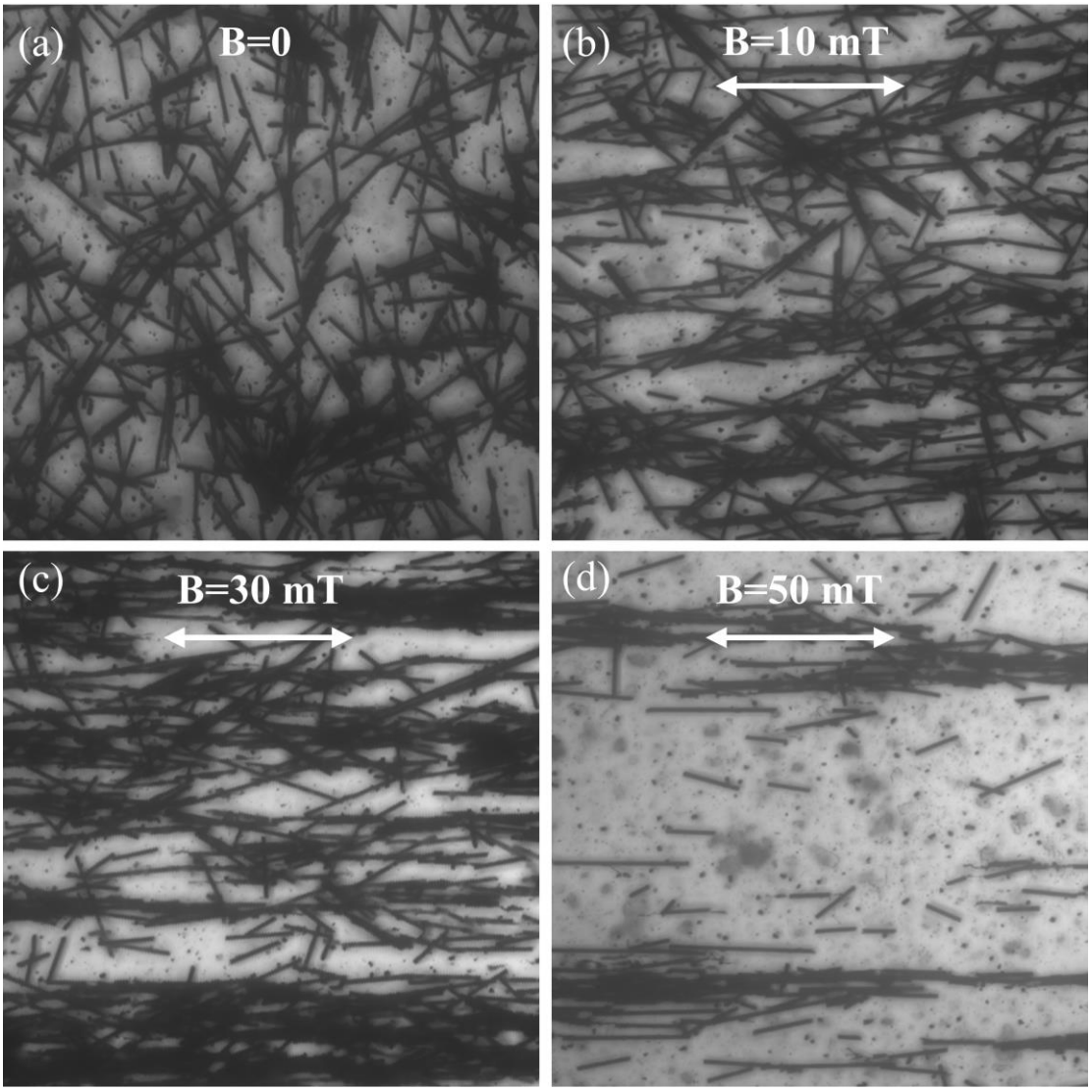

Figure 35. Confocal microscopic images at 10× of NiC fibers with α=14 in the cured composites: (a) without magnetic field and under magnetic field of (b) B=10 mT, (c) B=30 mT, and (d) B=50 mT

A histogram of the orientation angle distribution is shown for the composites cured: (a) without magnetic field, (b) under horizontal magnetic field of B=10 mT, (c) B=30 mT, and (d) B=50 mT in Fig. 36. This quantitative analysis is used to analyze and identify the preferred orientation induced by the magnetic field. The results confirmed that there is no preferential orientation in the samples cured without a magnetic field.

However, in all the samples cured under a magnetic field of 10-50 mT, a peak near the 0° orientation angle is observed. Moreover, with increasing the magnetic field from 10 to 30 mT (see Figs. 36(b) and (c)), the number of fibers aligned with the direction of magnetic field (i.e. 0º) increases. Under 50 mT, the number of aligned fibers is less which is due to migration of fibers.

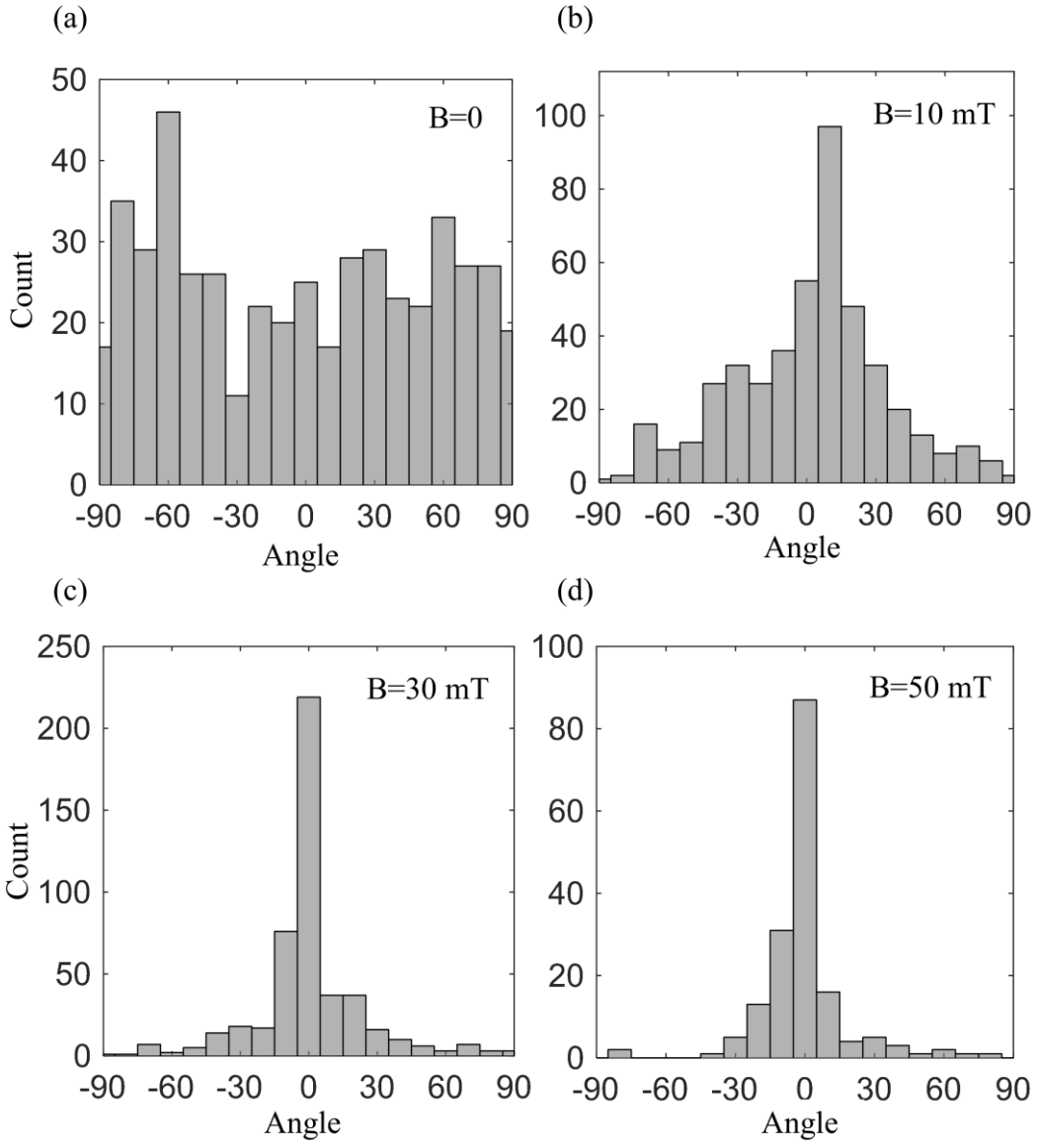

Figure 36. Histogram of orientation angle distribution of NiC fibers with α=14 in the cured composites: (a) without magnetic field, and under magnetic field of (b) B=10 mT, (c) B=30 mT, and (d) B=50 mT.

Fig. 37 shows the probability density functions (PDFs) of the orientation angle of fibers in the samples cured under magnetic field of 10, 30, and 50 mT. Fig. 37 presents that all PDFs have a normal distribution with the same mean (around 0º) but different standard deviations, indicating different levels of alignment along the magnetic field. With increasing the magnetic field from 10 to 30, the standard deviation decreases from 33 to 24º. Thus, the NiC fibers are more aligned with the 30 mT magnetic field than those with 10 mT. Given that the samples made with 50 and 30 mT have almost similar probability densities while the migration of the fibers under 30 mT is less, applying 30 mT could be a better choice for the increased alignment while minimizing the migration of 0.1 mm long NiC fibers.

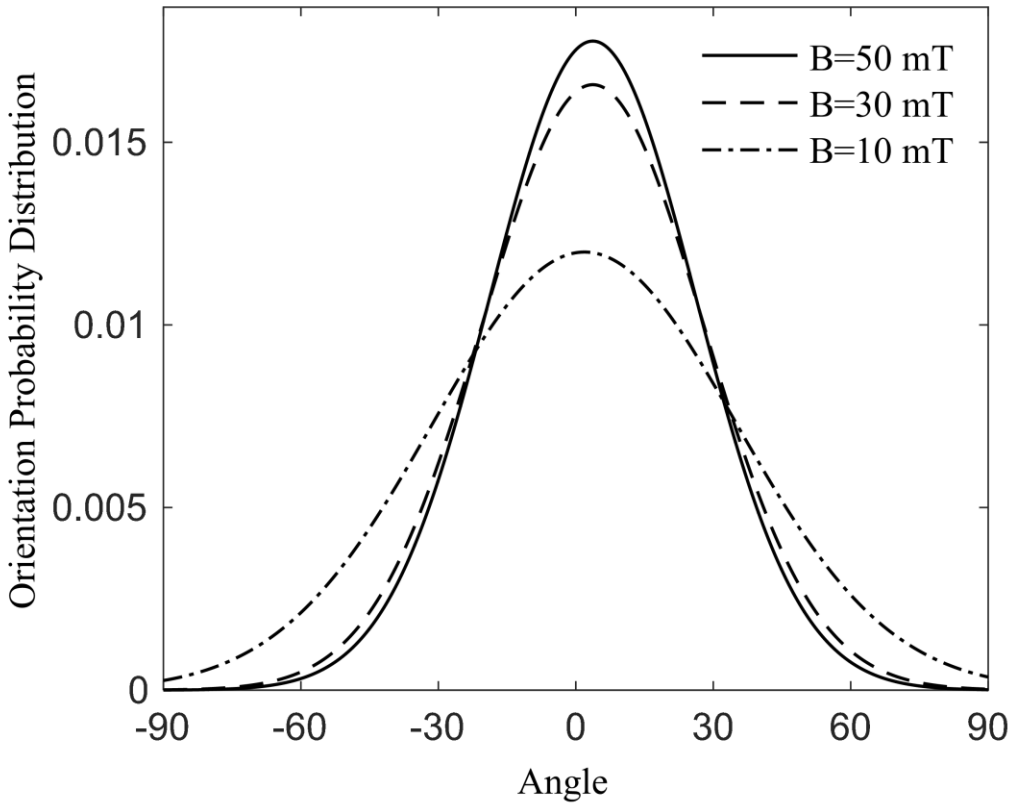

Figure 37. Probability distribution of NiC fibers orientations with α=14 in the cured composites under magnetic field of B=10, 30, and 50 mT.

Figs. 38(a) and (b) present the confocal microscopic images and histogram of orientation distribution of 0.25 mm long NiC fibers (α=36) under 30 mT magnetic field. Similar to the shorter fibers, the NiC fibers aligned with the magnetic field and NiC networks formed. Histogram of orientation distribution shows a peak at 0°. Fig. 38(c) compares the probability distribution of orientation of fibers with different lengths (0.1 mm long with α=14 and 0.25 mm long with α=36) cured under the same magnetic field of 30 mT. The standard deviations of orientation distribution of the fibers with aspect ratios of 14 and 36 are 24° and 12°, respectively. Thus, under the same magnetic field of 30 mT, the alignment of longer fibers (i.e. 0.25 mm long) is considerably higher than

the alignment of 0.1 mm long fibers. The 0.25 mm long fibers could achieve the same degree of alignment as 0.1 mm long fibers under lower magnetic field (<30 mT).

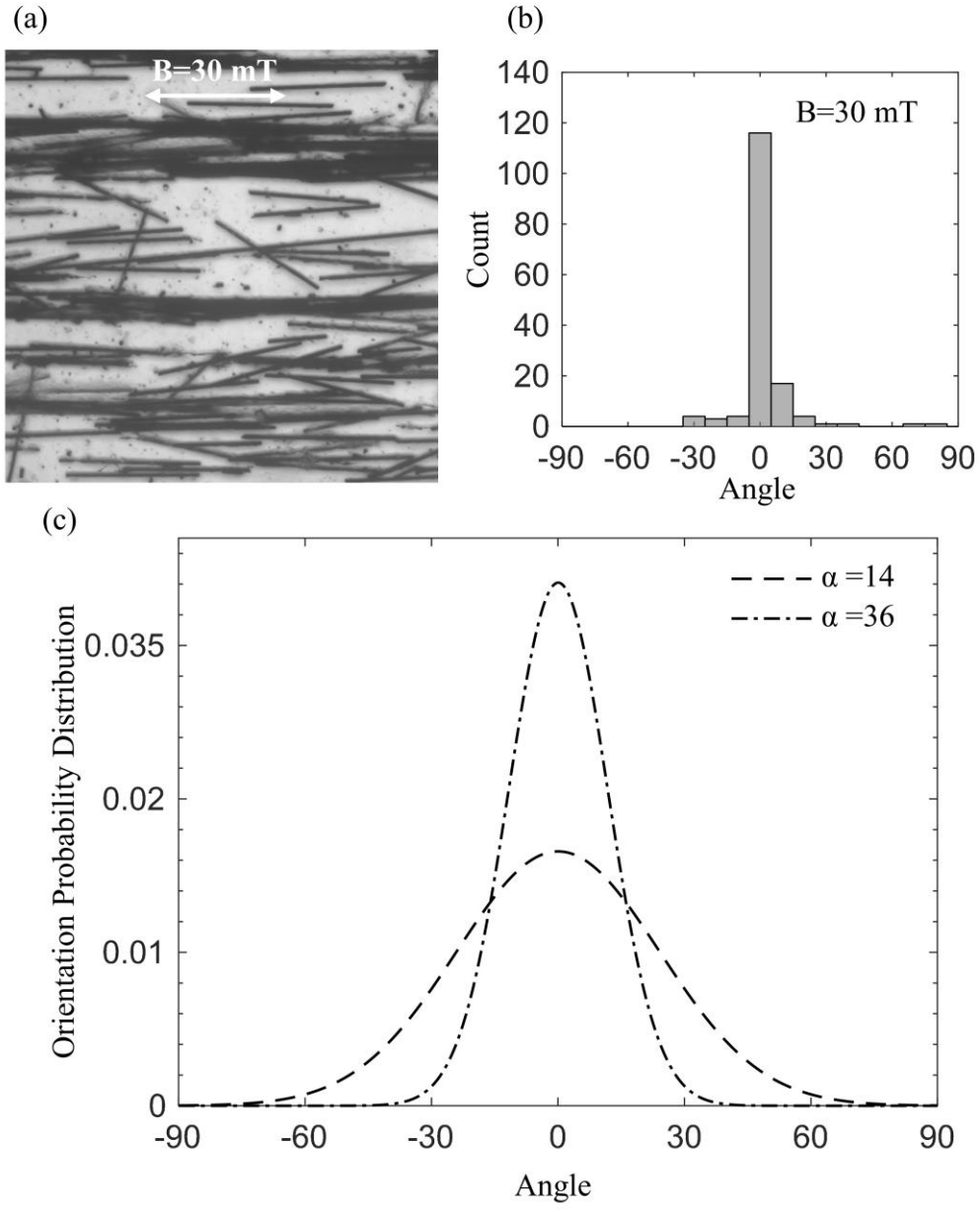

Figure 38. (a) Confocal microscopic images at 10× and (b) histogram of orientation angle distribution of NiC fibers with α=36 in an epoxy resin under B=30 mT. (c) Probability distribution of NiC fiber orientations with α=14 and α=36 under B=30 mT.

4.1.4. Concluding remarks

In the first part of chapter 4, the alignment of nickel coated carbon (NiC) fibers during cure in an epoxy resin under a low magnetic field of 10-50 mT is investigated. Three distinct mechanisms are observed in the magnetic field induced microstructure of the composite: rotation of NiC fibers, network formation, and migration towards the magnetic poles. NiC fibers (0.1 mm long with an aspect ratio of 14) are aligned in a relatively low magnetic field of 10 mT. However, with increasing the magnetic field to 30 mT, the alignment of fibers is improved, and thus highly aligned, fiber chains are formed. At 50 mT, the fibers are observed to migrate towards the magnetic poles. It is also found that under the identical magnetic field, longer NiC fibers, 0.25 mm long with a higher aspect ratio of 36, reach to a higher degree of alignment than 0.1 mm long fibers. Thus, fibers with higher aspect ratios are seen to be more responsive to the magnetic field and can be aligned at a higher degree under a lower magnetic field strength.

4.2. Tailoring Surface Anisotropy in Three-Phase NiC/Glass/Epoxy Laminates by a Magnetic Field

The controlled orientation of conductive fibers in structural laminates is highly desirable for tailoring the anisotropy, and thus improving their functionalities. In the second part of chapter 4, a new magnetic-field assisted fabrication method is proposed to align nickel coated carbon (NiC) fibers on the surface of three-phase composite laminates. Highly dispersed fibers with a uniform spatial volume fraction on the fabric surface are achieved via a recently developed cascaded suspension deposition method. An appropriate level of magnetic field, generated by a set of permanent magnets, is then used to control orientation of NiC fibers without disturbing the uniformity of microstructure in the composite. Different levels of fiber alignment are induced by the presence of magnetic field: (i) on the fabric substrate when the fibers are deposited, (ii) on the deposited fabric after mold filling by vacuum assisted resin transfer molding (VARTM), and (iii) on the fabric substrate during deposition, mold filling, and after mold filling. The effects of fiber aspect ratio and the amount of nickel coating on the process-induced microstructure are investigated. The results show that the proposed method can be successfully used in VARTM to obtain a controlled orientation of fibers while maintaining the uniform fiber volume fraction and good dispersion throughout the surface of laminate. Surface microstructural analysis reveal that the highest alignment of NiC fibers is achieved when the magnetic field is applied throughout the fabrication process.

4.2.1. Introduction

Conductive polymer composites are typically fabricated by the addition of conductive fillers into a polymer matrix which inherently has a low conductivity [174-176]. Currently, metals, carbon-based materials such as carbon fibers, carbon nanotubes, graphene, or a combination of them are widely used as the conductive fillers [63, 64]. To significantly increase the conductivity, the volume fraction of particles within the composite needs to be high (e.g. ~50%), so that the fillers can form conductive networks [68]. However, having a high filler content may lead to deterioration in processability and mechanical properties of the composites due to the aggregation of fillers [72, 177]. To obtain enhanced properties without requiring a high loading of fillers, an effective method is to form interconnected network of fillers by controlling their orientation in the polymer matrix. In this regard, a number of studies have reported much improved thermal and electrical conductivities of composites along the alignment direction compared to those with random distribution of fillers [75-77]. In addition, controlling the orientation of fillers can tailor anisotropy in composites, and thus manipulate their thermo-mechanical properties. For instance, alignment of fillers offers potential applications in electromagnetic interference (EMI) shielding where high conductivity along the desired direction with insulation in other directions is important [178].

Several techniques currently exist for controlling the orientation of short fibers in a solution, including applying magnetic field [81], electric field [84], and shear flow [88]. Among various approaches, magnetic alignment has attracted considerable attention due to several reasons. Being insensitive to the physical and chemical

properties of the resin and not inducing currents in the polymer by accelerating charged particles are examples of the advantages of using magnetic field over the electric field [179, 180]. In addition, compared to the shear flow, the non-contact alignment induced by a magnetic field is easier to implement [181]. Moreover, permanent magnets are easily available, powerful, and inexpensive and can generate high field strength [94]. However, generating a high magnetic field (i.e. in the order of 1 T), required to orient the typical nonmagnetic (diamagnetic) fibers, may be challenging [179]. To overcome this difficulty, fibers can be coated with superparamagnetic nanoparticles, making them responsive to a low magnetic field in the range of 1–10 mT [83]. Accordingly, nickel coated fibers may be utilized because of their excellent magnetic properties and improved electrical and thermal conductivities [182-184]. So far, most of the work in this area has been directed toward controlling the orientation of short fibers in unreinforced polymers, whereas studies on controlling the orientation of fibers in structural laminates are rare.

In recent years, considerable research has been devoted to the development of three-phase multifunctional materials through the addition of reinforcements into traditional composite laminates. The reason is that traditional fiber reinforced polymers (FRP) have high specific strength and modulus but generally exhibit low conductivities [185-188]. However, the multifunctional materials may possess high electrical and thermal conductivities, good magnetic properties, or novel optical responses in addition to excellent specific strength and modulus of FRP composites [189, 190]. A common approach to prepare this type of three-phase composites is the distribution of reinforcements on the fabric surface using one of the deposition methods such as

chemical vapor deposition (CVD) [36, 78, 79], electrophoretic deposition [59, 191, 192], and spray-coating [193]. Then, resin is infused into the deposited fabric using vacuum assisted resin transfer molding (VARTM). For obtaining planar alignment of reinforcements, an available approach is to shear press the vertically grown reinforcement films and then inserting the films between the prepreg plies [80, 194]. However, this approach does not allow precise control of planar orientation of reinforcements in the desired direction. Therefore, a new method which facilitates controlling the orientation of fibers while obtaining good dispersion and uniform spatial distribution of fibers in the three-phase composites is highly desirable.

In chapter 3 of this dissertation, the cascaded suspension deposition method is introduced which enables uniform deposition of short fibers a fibrous fabric surface in an aqueous environment [195]. The deposited fabric was successfully used in VARTM to fabricate a structural laminate with tailored surface microstructure. Also, the quantitative assessment of the microstructure showed fibers were well-dispersed and randomly-oriented throughout the laminate surface. Thus, alignment of fibers in three-phase composites may be possible by integrating one of the methods for inducing alignment of fibers into cascaded deposition method.

In the second part of chapter 4, a new magnetic-field assisted composite processing is presented to tailor the surface anisotropy in composite laminates. Towards this goal, magnetic field generated by permanent magnets is utilized for controlling the orientation of short nickel coated carbon (NiC) fibers on the surface of NiC/glass/epoxy laminates. To achieve good dispersion and uniform distribution of fibers on the fabric surface, our recently developed cascaded suspension deposition is used. The alignment

behavior of NiC fibers is evaluated by applying an appropriate level of magnetic field in three ways: (i) during deposition, (ii) after mold filling in VARTM, and (iii) during deposition, mold filling and after mold filling. The microstructure of fabricated laminates is quantitively characterized to assess their degree of alignment and dispersion and uniformity of fiber volume fraction. To assess the influence of physical properties of fibers on the surface anisotropy of composite, fibers with various aspect ratios and nickel coatings are considered.

4.2.2. Materials and methods

4.2.2.1. Materials

Three-phase composites are fabricated using nickel coated carbon (NiC) fibers, chopped strand, glass fiber mat, and INF-114/ INF-211 epoxy resin. The NiC fibers, produced by the CVD method, are obtained from Conductive Composites Company. The following three types of NiC fibers with different coatings and lengths are selected: NiC1 (20%Ni-0.25mm), NiC2 (40%Ni-0.25mm), and NiC3 (20%Ni-0.1mm). Figs. 39(a) and (b) show the scanning electron micrographs of NiC1 and NiC2 fibers, where nickel is 20 and 40 wt. % of the coated fiber, respectively. The average diameter of fibers is 7 μm and the coating thicknesses are in the order of 50-80 nm and 270-430 nm, respectively for NiC1 and NiC2 fibers. Also, there is no significant variation in the diameter of the fibers. Fig. 39(c) shows that some fibers are bare or not coated properly, thus they may not be aligned under the low magnetic field. Also, the length distribution of NiC1 (20%Ni-0.25mm) and NiC3 (20%Ni-0.1mm) fibers are determined and presented in Fig. 40. The actual average fiber length is measured to be 169.6 ± 61.2 μm and 134.9 ± 69.6 μm, which give the aspect ratio (α=fiber length/fiber diameter) of

α=24 and 19, respectively for NiC1 and NiC3. The density of fibers is measured by a nitrogen pycnometer to be 2.144 ± 0.008 and 2.596 ± 0.004 g/cm^3, respectively for fibers with 20% (i.e. NiC1 and NiC3) and 40% coatings (i.e. NiC2). Randomly oriented, chopped strand glass mat with a planar density of 0.458 kg/m^2 (Fiberglast, part#250) is used as the fabric. The resin system, INF-114/INF-211 (PRO-SET), is chosen for its low viscosity of 0.245 Pa·s at room temperature, which makes it suitable for infusion processes. Moreover, the long resin pot life of 76-94 min allows the time required for the rotation of fibers under the magnetic field before the resin gelation occurs.

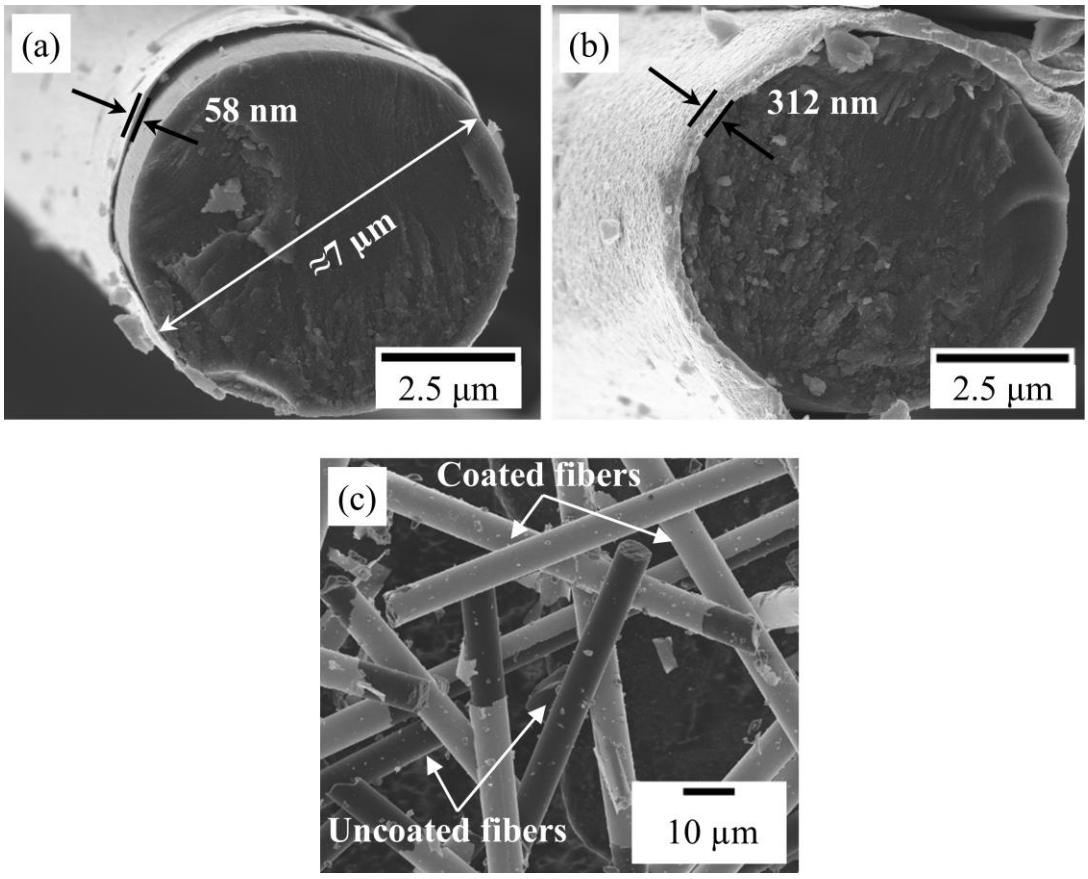

Figure 39. SEM image of: (a) a single carbon fiber with 20% nickel coating, NiC1 (20%Ni-0.25mm), (b) a single carbon fiber with 40% nickel coating, NiC2 (40%Ni-0.25mm), and (c) examples of uncoated and coated fibers.

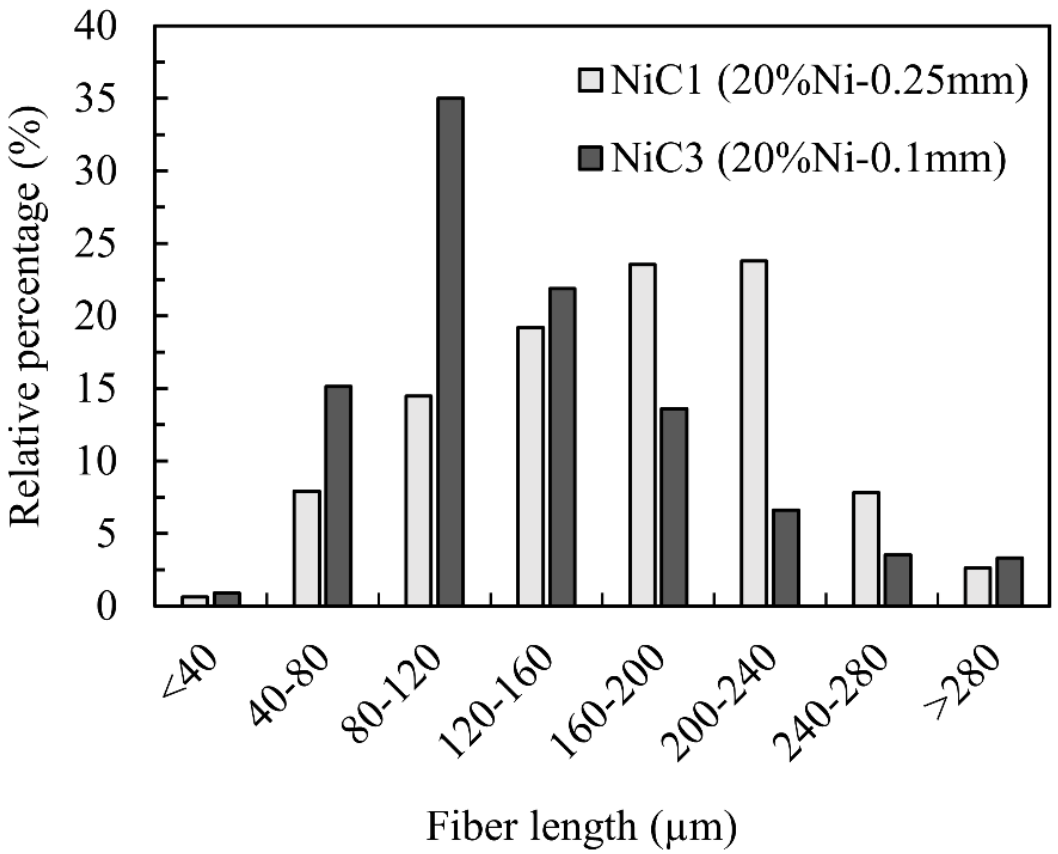

Figure 40. Distributions in fibers length for NiC1 (20%Ni-0.25mm) and NiC3 (20%Ni-0.1mm) fibers. The corresponding mean values are 169.6 ± 61.2 μm for NiC1 and 134.9 ± 69.6 μm for NiC3 fibers.

4.2.2.2. Magnetic field

Twelve N52 Neodymium Iron Boron (NdFeB) magnets, the strongest permanent magnets commercially available, are used to generate magnetic field. For this purpose, N52 NdFeB-2.54 (length) × 2.54 (width) × 5.08 cm^3 (thickness) magnets (KJ Magnetics), magnetized through-the-thickness, with a surface magnetic field of 700 mT are selected. Fig. 41(a) shows the two sets of parallel-positioned magnet assembly which are used for inducing the alignment. Each set includes six magnets placed side by side, with like poles adjacent to each other, and the poles of one set face opposite poles

of the other set. The arrangement of magnets is secured in place by aluminum and wooden holders screwed to the wooden supports, as can be seen in Fig. 41(a). The distance between the two sets of magnets can be varied depending on the required magnetic field for inducing alignment. The appropriate level of magnetic field is selected based on the results in chapter 4.1, demonstrating that a magnetic field of 30 mT induces a preferred orientation and the formation of aligned NiC fiber networks [196]. At a higher magnetic field of 50 mT, pronounced migration of fibers towards the magnetic poles was observed due to the increased magnetic field gradient. Hence, two sets of magnets are spaced 24 cm apart to produce a magnetic field of ≈20-30mT, measured by a Gaussmeter (Alphalab, model GM1-ST), at the center 12.7 × 12.7 cm^2 section of the laminate (dashed boxed in Fig. 41(a)).

Fig. 41(b) shows the 2D map of magnetic field calculated using the FEMM software (Finite Element Method Magnetics). The direction of magnetic flux lines shown by the solid lines in Fig. 41(b), are from north to south (NS) and south to north (SN) poles. It can be seen in Fig. 41(b) that there is almost no change in magnetic flux density in the dashed boxed region, thus making the migration of fibers negligible. Also, in this area, the magnetic flux lines are almost horizontal (along the *x*-direction), near the corner, however, the direction of the lines changes slightly. To avoid the effect of curved magnetic field, the small region near the corners are not considered for the orientation analyses.

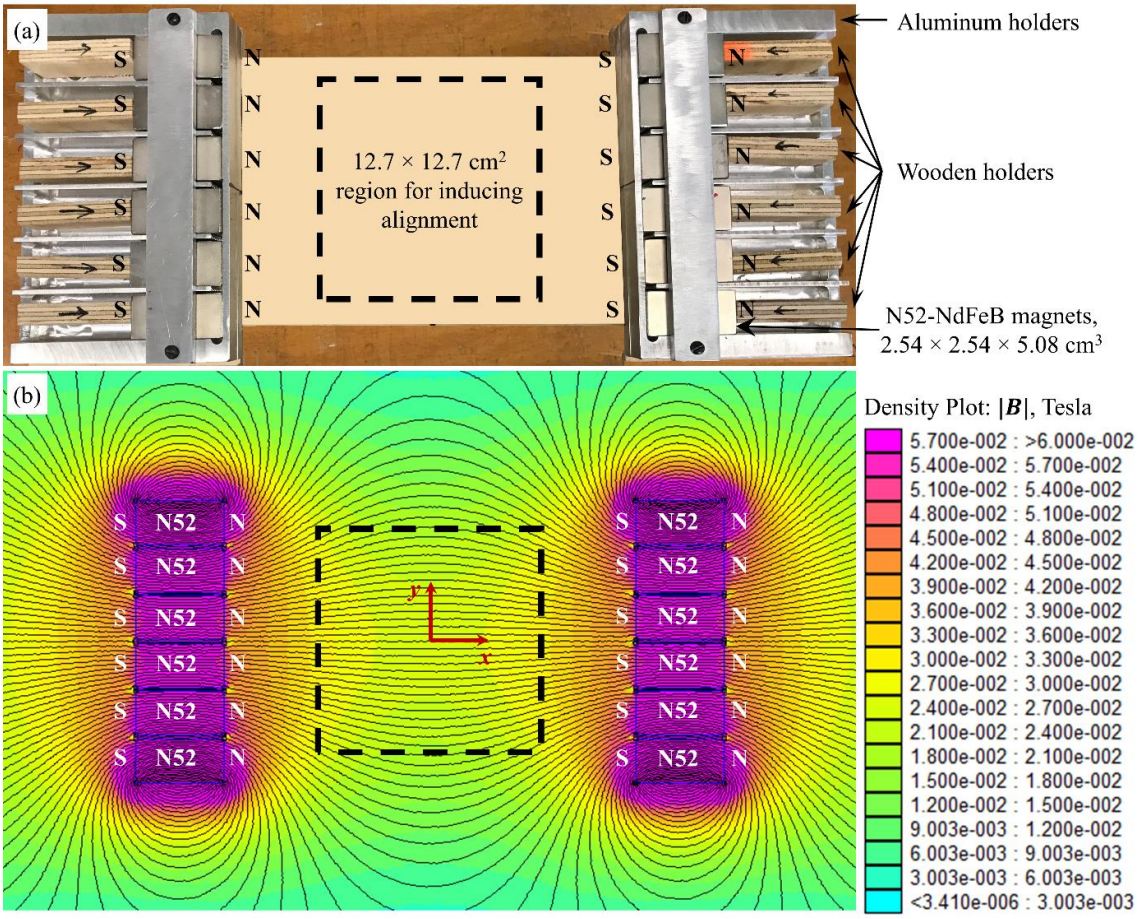

Figure 41. (a) Configuration of twelve N52-NdFeB 2.54 × 2.54 × 5.08 cm³ magnets used to induce alignment in the dashed rectangle region (b) Magnetic flux density distribution generated by the magnets with the same configuration shown in Fig. 3(a). The magnetic flux density generated in the dashed rectangle is between 20-30 mT.

4.2.2.3. Preparation of aligned NiC fibers-deposited fabric

In the second part of chapter 4, to achieve a uniform distribution of short fibers on the fabric surface, cascaded suspension deposition, is adopted (see chapter 3). A comprehensive microstructural analysis demonstrated that after the NiC fibers are deposited on random glass mats, a uniform fiber volume fraction, excellent dispersion, and isotropic orientation of NiC fibers are obtained without the magnetic field. To achieve a desired level of anisotropy on the fabric while maintaining a uniform volume

fraction and well-dispersion of NiC fibers, a new magnetic-field assisted composite processing is developed. The glass mat prepared with this method can then be utilized for the fabrication of laminates with tailored anisotropy. For this purpose, the cascaded suspension deposition is performed in the presence of magnetic field, generated by two sets of parallel-positioned permanent magnets (see Fig. 42). As the fibers are sedimented on the fabric surface during deposition, the entire assembly is placed in an external magnetic field ($\vec{B}$), which tends to align the fibers in the same direction of the magnetic field. Thus, the direction of magnetic field determines the preferential orientation of fibers. However, the degree of alignment of fibers depends on the strength of magnetic field and the physical as well as the magnetic properties of fibers (aspect ratios and nickel coatings).

Fig. 42 depicts the preparation of a glass mat with aligned NiC fibers deposited on its surface. Briefly, two cascaded trays are used: suspension and deposition tray. The suspension tray contains a well-dispersed suspension of fibers in water while the deposition tray contains the fabric immersed in a few-inch deep water bath. The suspension tray has perforations for water/fiber suspension drainage which are covered prior to the deposition stage. The suspension tray is placed at a short distance above the deposition tray, its perforations are uncovered, cascading fibers/water suspension into the deposition tray. At the deposition tray, the fibers are sedimented on the fabric surface under gravity. After the sedimentation is complete, water is slowly drained from the bottom of the deposition tray and the deposited fabric is dried. The fibers prepared with this method are uniformly distributed and randomly oriented on the fabric. However, to achieve alignment of fibers on the fabric in a particular direction, after

sedimentation of fibers on the fabric, the deposition tray is placed in the middle of the magnet assembly, where the magnetic field is applied. Afterward, water is drained, the field is removed, and glass mat with aligned NiC fibers is dried. It should be noted that after the magnetic field is removed, the magnetic field-induced alignment of NiC fibers remains unchanged on the glass mat surface.

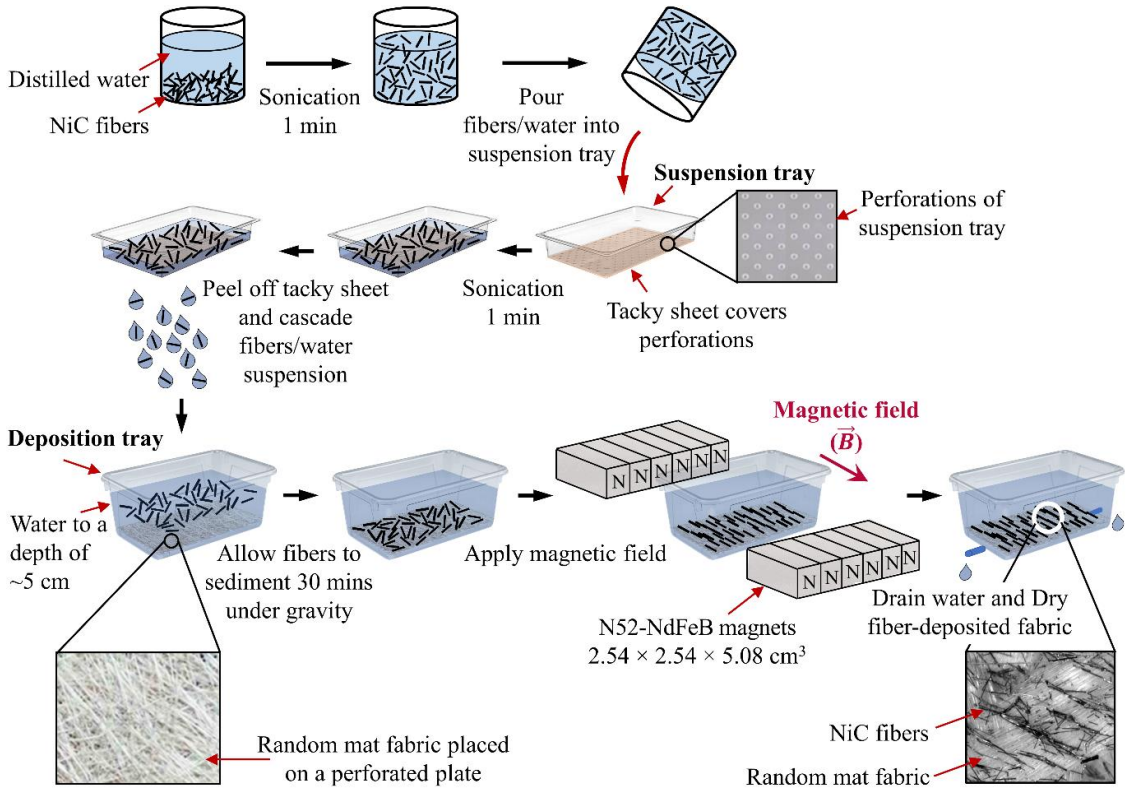

Figure 42. Schematic of the cascaded suspension deposition in the presence of magnetic field to prepare aligned NiC fibers-deposited fabric. After fibers are sedimented on fabric, alignment is induced by applied magnetic field using twelve N52-NdFeB 2.54 × 2.54 × 5.08 cm³ magnets.

4.2.2.4. Fabrication of aligned NiC fibers in three-phase composites

To obtain the desired surface anisotropy, the magnetic field is utilized in three different approaches: (i) only during deposition in cascaded suspension deposition; (ii) only after resin infusion in VARTM, and (iii) throughout the process (i.e. during

deposition and infusion, as well as after infusion). These approaches give the flexibility in fabrication of three-phase composite laminates with unique microstructure morphology. For instance, the first approach may allow fabrication of engineered composite laminates comprised of multiple plies of deposited fabric, where on each ply fibers are aligned in a specified direction. In addition, for large composite laminates, inducing alignment at the desired location may be possible with the second approach by local application of magnetic field after infusion.

Fig. 43 schematically illustrates the application of magnetic field in the fabrication of composite parts by VARTM. Briefly, VARTM lay-up, shown in Fig. 43, consisted of deposited fabric placed on a non-magnetic tool plate, inlet and vacuum lines, a release film, and a vacuum bag to seal the assembly. The resin is infused into the deposited fabric under vacuum. It should be noted that both inlet and outlet tubings are clamped 5 mins after completion of the mold filling in all experiments. In cases with magnetic field in VARTM, as illustrated in Fig. 43, field direction is parallel to the resin flow direction, at an angle of 0°.

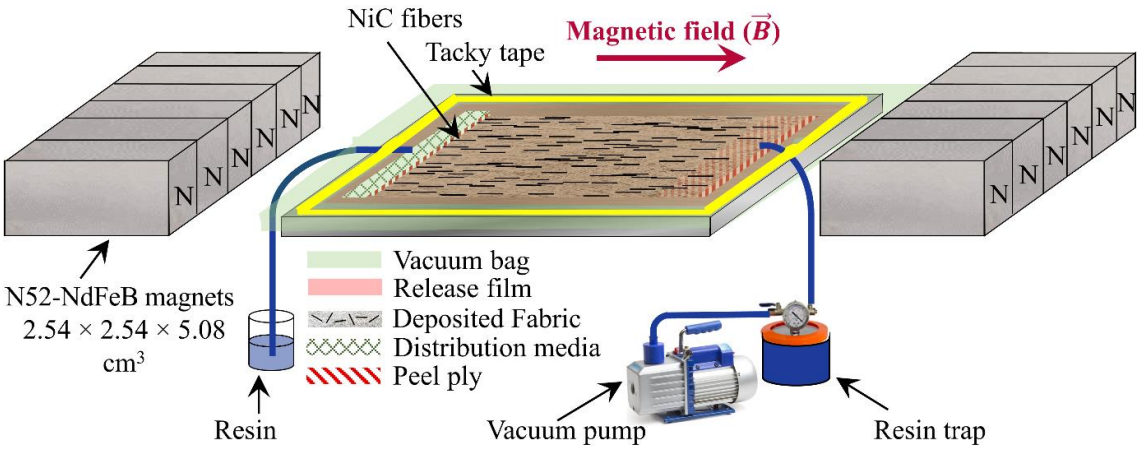

Figure 43. Schematic illustration of applying magnetic field during the fabrication of three-phase composite parts by VARTM. Magnetic field is applied parallel to the resin flow at an angle of 0°.

In this work, three-phase NiC fibers/glass fabric/epoxy laminates (12.7 × 12.7 cm^2) are fabricated under eight scenarios as listed in Table 4. These scenarios are labeled according to: NiC fiber type, deposition process, and fabrication process. For the NiC fiber type, "NiC1", and "NiC2", and "NiC3" stands for "NiC1 (20%Ni-0.25mm)", "NiC2 (40%Ni-0.25mm)", and "NiC3 (20%Ni-0.1mm)". For the deposition process, "D" and "MD" stands for cascaded suspension deposition without and with magnetic field, respectively. Finally, "V" represents the conventional VARTM, "M1V" is for VARTM with magnetic field applied after mold filling, and "M2V" refers to VARTM with magnetic field applied during and after mold filling. In this work, NiC1-D-V, corresponds to using cascaded suspension deposition and conventional VARTM without applying magnetic field. This case is used as a reference to compare the other seven fabrication scenarios. In scenarios NiC1-MD-V, NiC1-D-M1V, and NiC1-MD-M2V, magnetic field is utilized under three different approaches described earlier. In addition, nickel coating and aspect ratio of fibers are two important parameters affecting

the response of fibers to the magnetic field, leading to different degree of anisotropy. Therefore, in addition to NiC1 fibers, the second types of fibers with a thicker coating layer, NiC2, and the third type of fibers with a lower aspect ratio, NiC3, are used in the last four scenarios.

Table 4. Eight scenarios for the fabrication of three-phase NiC fibers/glass fabric/epoxy composite laminates with aligned and random NiC short fibers.

NiC fiber type-deposition process-fabrication process	NiC fiber type	Deposition process	Fabrication process
NiC1-D-V	NiC1 (20% Ni-0.25 mm)	D (Deposition without magnetic field)	V (VARTM without magnetic field)
NiC1-MD-V	NiC1 (20% Ni-0.25 mm)	MD (Deposition with magnetic field)	V (VARTM without magnetic field)
NiC1-D-M1V	NiC1 (20% Ni-0.25 mm)	D (Deposition without magnetic field)	M1V (VARTM with magnetic field applied after mold filling)
NiC1-MD-M2V	NiC1 (20% Ni-0.25 mm)	MD (Deposition with magnetic field)	M2V (VARTM with magnetic field applied during and after mold filling)
NiC2-MD-V	NiC2 (40% Ni-0.25 mm)	MD (Deposition with magnetic field)	V (VARTM without magnetic field)
NiC2-D-M1V	NiC2 (40% Ni-0.25 mm)	D (Deposition without magnetic field)	M1V (VARTM with magnetic field applied after mold filling)
NiC2-MD-M2V	NiC2 (40% Ni-0.25 mm)	MD (Deposition with magnetic field)	M2V (VARTM with magnetic field applied during and after mold filling)
NiC3-MD-M2V	NiC3 (20% Ni-0.1 mm)	MD (Deposition with magnetic field)	M2V (VARTM with magnetic field applied during and after mold filling)

4.2.2.5. Comprehensive analysis of magnetic field-induced microstructure of three-phase laminates

To establish magnetic-field assisted composite processing as a viable method, the microstructure of laminates fabricated with applying magnetic field under different scenarios are compared to the laminate made without magnetic field. Thus, a comprehensive microstructural characterization of composite laminates is carried out by assessing: (i) spatial uniformity of fiber volume fraction, (ii) degree of dispersion, and (iii) preferred orientation and degree of alignment of fibers. Fig. 44 illustrates examples of four different microstructural patterns with different spatial uniformity, degree of dispersion, and alignment. These images schematically demonstrate how the three microstructural parameters can convey distinct yet complementary information about the microstructure. For example, Figs. 44(a) and (b) both illustrate uniform volume fraction and well-dispersion of fibers, with a preferred orientation at 0°. However, unlike a relatively low degree of alignment in Fig. 44(a), Fig. 44(b) demonstrate a higher degree of alignment. Similarly, well-dispersed fibers with a relatively high degree of alignment are exhibited in Figs. 44(b) and (c). However, Fig. 44(b) depicts a uniform fiber volume fraction, unlike a non-uniform fiber volume fraction with a low fiber content region at the middle in Fig. 44(c). Fig. 44(d) is an example of poorly-dispersed, non-uniform volume fraction fibers with a preferred angle at 0°. The quantitative assessment of each one of these microstructural parameters is necessary which are described in detail in subsequent subsections.

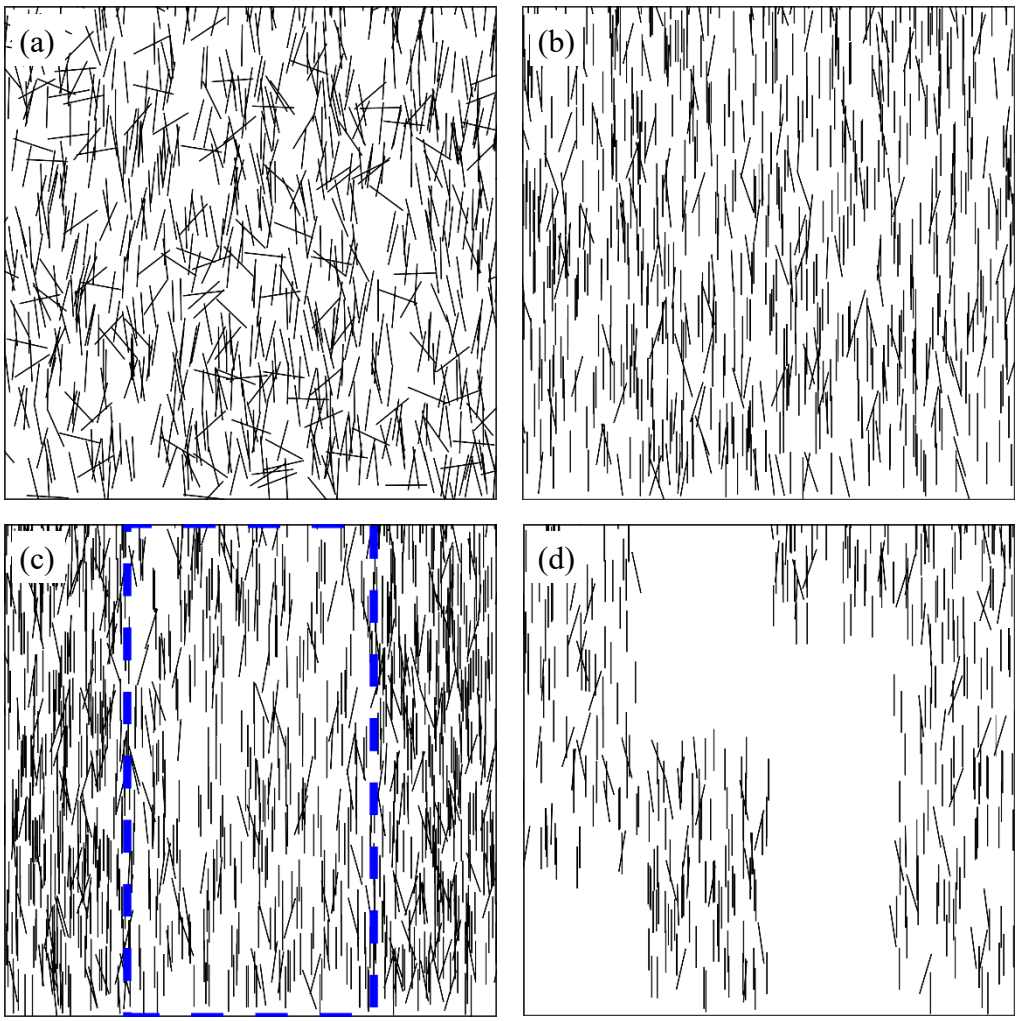

Figure 44. Schematic representation of discontinuous fibers forming different microstructural patterns: (a) uniform fiber volume fraction/well-dispersed/preferred angle at 0° with a relatively low degree of alignment; (b) uniform fiber volume fraction/well-dispersed/preferred angle at 0° with a relatively high degree of alignment; (c) non-uniform fiber volume fraction/well-dispersed/preferred angles at 0°; and (d) non-uniform fiber volume fraction/poorly-dispersed/preferred angles at 0°.

4.2.2.5.1. Spatial uniformity of fiber volume fraction

A homogenous composite microstructure, especially uniform distribution of fibers, is an important parameter to be considered for the composite laminates. To assess the spatial uniformity of fiber volume fraction, a high-resolution optical scanning (Epson Perfection V550) and image processing (ImageJ software) are used. For this

purpose, the entire surface of each composite is scanned at a resolution of 4800 dpi, which results in a pixel size of ~5.3 μm. From each resulting image, a 100 × 100 mm^2 region is extracted and the background light-scatter caused by the surface roughness of the laminate is filtered. The resulting images, such as the one shown in Fig. 45, are binarized and inverted, as shown in Figs. 45(a) and (b), respectively. The inversion makes the pixels corresponding to NiC fibers white (gray value of 255) and those of background black (gray value of 0), helping to identify the location and orientation of NiC fibers better. In this work, the variation of fiber volume fraction is quantified based on the grayscale values of the pixels within the scanned images. Thus, a spatially uniform fiber volume fraction gives rise to images with almost constant grey value throughout the scanned image, whereas images of composites with non-uniform fiber volume fraction contain regions with ‘high’ and ‘low’ grey values. To quantify the variation of fiber volume fraction along parallel (x) and transverse (y) to the resin flow direction, each processed image is divided into 18700 overlapping windows of 100-mm long × 1-mm wide along each direction. This window size is determined based on the size of fibers, measurement accuracy, and the noise levels in the scanned images. The spacing between consecutive windows is 5.3 μm, which is the same as the resolution of the image. The average gray value within each window is used as a representative measure of fiber presence at the center point location (x) of that window. Then, the variation in the gray value is plotted along the x- and y-direction, an indication of uniformity of fiber volume fraction parallel and transverse to the resin flow.

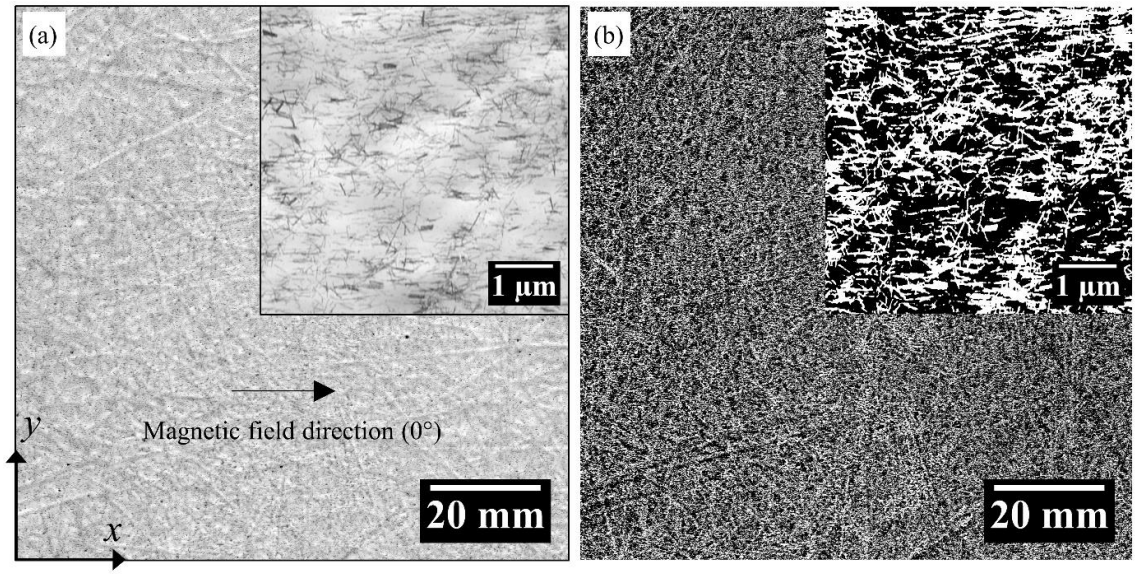

Figure 45. Example of a scanned image of NiC2-MD-M2V laminate: (a) grayscale image after removing light scattering and (b) binarized and inverted image. The ability to identify each NiC fiber deposited on the laminate surface is clearly enhanced by image processing.

4.2.2.5.2. Degree of dispersion of fibers

A good dispersion of short fibers in the composite typically leads to their enhanced thermo-mechanical properties, while a poor dispersion as a result of agglomeration or phase separation leads to a dramatic reduction of these properties. The degree of dispersion of fibers deposited on the glass mat and the fabricated laminates is quantified by measuring the Area Disorder (AD_{del}) value [154]. From the 2 mm × 2 mm optical images of the deposited glass mats and the composite laminates, similar to the one shown in Fig. 46(a), the individual fibers are selected. The coordinates (x, y) of the centroids of all fibers are determined (see Fig. 46(b)). The periodic boundary condition is imposed to all four sides of the image in order to generate a Delaunay network over the whole image, as demonstrated in Fig. 46(c). A Delaunay network of the fibers is constructed with the centroids of fibers at the vertices of the triangles (see Fig. 46(d)).

The AD_{del} provides a measure of order or disorder in a microstructure and is calculated from the mean and standard deviation of the areas of the triangles in a Delaunay network:

$$AD_{del}=1-(1+s_{\Omega}/\overline{\Omega})^{-1} \quad (9)$$

where $\overline{\Omega}$ and s_{Ω} are the average and standard deviation of the areas of the triangles in the Delaunay network, respectively. For calculation of AD_{del}, the Delaunay triangles whose centers fall outside the boundaries of the image, i.e. the solid black rectangle in Fig. 46(d), are not considered. The value of the Area Disorder lies between 0 and 1, and a high Area Disorder value indicates a low degree of dispersion (or poor dispersion) of fibers. For reference of comparison, the position of 300 fibers (the same number of fibers in an actual image) is randomly generated in a 2×2 mm^2 area and the AD_{del}(ref.) is calculated to be 0.466 ± 0.004 with 95% confidence interval. Therefore, having an AD_{del} equal or close to the reference value of 0.466 AD_{del}(ref.), implies a good dispersion of fibers, while the larger values of AD_{del} suggests a clustered distribution.

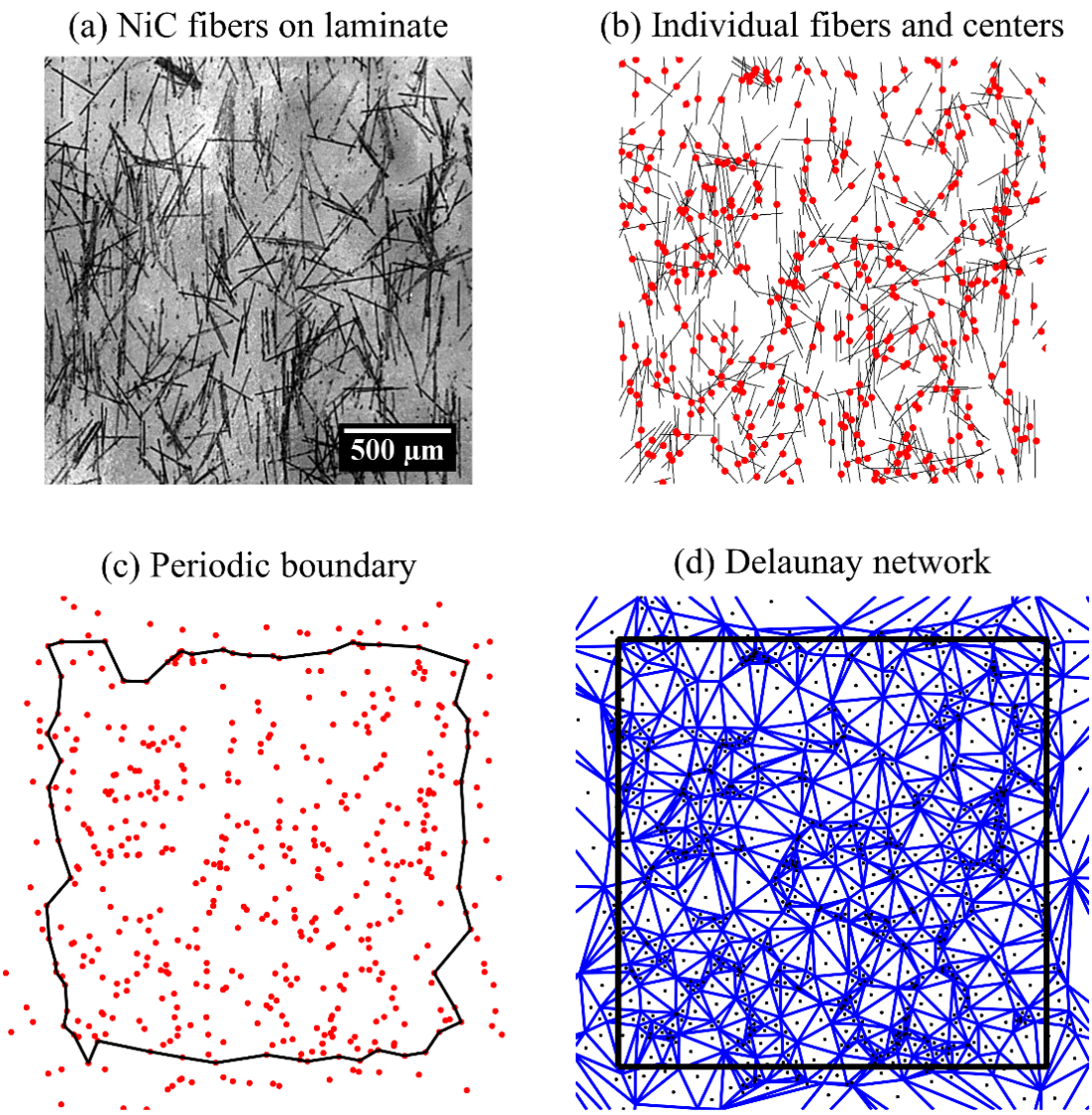

Figure 46. Image processing for quantitative assessment of dispersion: (a) optical image of NiC/glass/epoxy laminate, (b) selection of individual fibers and specifying their centers, (c) applying periodic boundary condition, and (e) construction of Delaunay network, determination of center of triangles, and identifying triangles whose centers lie inside the image (i.e. solid black rectangle), and determination of area disorder, AD_{del}.

4.2.2.5.3. Preferred orientation and degree of alignment

The importance of fibers orientation in final composite properties is emphasized in Refs. [159, 197]. Even a slight anisotropy evidenced by a low degree of alignment of fibers along a particular direction significantly alters the thermal and electrical

conductivities of composites along the alignment direction. Thus, the effect of applying magnetic field during deposition and fabrication of composites on the preferential in-plane orientation as well as degree of alignment of fibers are quantitatively studied. From the 2 mm ×2 mm optical images of the glass mat with deposited NiC fibers and the composite laminates, the angle (θ) between each fiber principal axis and the horizontal axis (magnetic field direction) is measured. A histogram of the frequencies of the orientation angles is calculated, with nine orientation bins evenly spaced from -90° to 90°. The principal fiber orientation direction, referred to as the "preferential orientation" or "preferred angle", can be determined by the peak(s) in the histogram. Also, the probability density function of fibers with respect to orientation angle of fibers is estimated using kernel density estimation (KDE). KDE is a nonparametric density estimation technique applicable to problems where the functional form or mathematical expression of the underlying density distribution is not known. Given a set of *n* data samples, u_i, $1 \leq i \leq n$, the kernel density estimator, $f_h(u)$, is computed as:

$$f_h(u) = \frac{1}{nh}\sum_{i=1}^{n} K\left(\frac{u-u_i}{h}\right) \tag{10}$$

where *h* is the bandwidth which controls the smoothness of the kernel estimator. A large *h* results in an over-smoothed estimator, while a small *h* results in an under-smoothed estimator containing too much noise. Thus, the bandwidth, *h*, is estimated by minimizing the asymptotic mean squared error [155]. *K(u)* is a fiber orientation kernel density function and here the Gaussian kernel is adopted:

$$K(u) = \frac{1}{\sqrt{2\pi}} e^{-\frac{1}{2}u^2} \tag{11}$$

The degree of alignment of fibers under different fabrication scenarios can be compared through their kernel density estimates.

4.2.3. Results and discussion

4.2.3.1. Magnetic field-induced microstructure of fibers-deposited fabric

To determine the effect of magnetic field on the microstructural changes induced during deposition, representative optical images of NiC1 (20% Ni-0.25 mm) fibers deposited on random mat fabric without and with magnetic field are presented in Figs. 47(a) and (b), respectively. In Fig. 47(a), fibers are randomly deposited on the fabric surface without the presence of magnetic field. However, with magnetic field, both alignment of fibers and formation of fibers networks along the magnetic field are clearly visible. To clarify the effect of applying magnetic field during deposition on the degree of dispersion of fibers, the Delaunay network is constructed. The corresponding area disorder, AD_{del}, is obtained and the results are presented in Figs. 47(c) and (d). Without applying magnetic field, the AD_{del} is found to be 0.473. Since the area disorder for a random distribution of fibers is $AD_{del}(ref.)=0.466$, the AD_{del} of 0.473 indicates an excellent dispersion level is achieved with the cascaded suspension deposition technique. With applying magnetic field in deposition, AD_{del} increases slightly to 0.488, suggesting a slightly lower degree of dispersion than that without magnetic field. This slight reduction can be as a result of fibers alignment and network formation in the presence of magnetic field. Figs. 47(e) and (f) show the frequency distribution of orientation angle of fibers deposited on fabric without and with magnetic field, respectively. In Fig. 47(e), fibers are distributed in a random orientation on the fabric surface, indicating that the cascaded suspension deposition does not induce any

preferential alignment. Upon applying magnetic field during the deposition phase, the orientation of NiC fibers indicates strong preferential alignment of fibers along the magnetic field direction, i.e. 0° (Fig. 47(f)). Thus, with applying magnetic field in deposition, fibers can be aligned in a specified angle on the fabric surface while maintaining an excellent dispersion. The aligned fibers-deposited fabric plies can be then used in liquid composite molding processes to make functionally engineered materials.

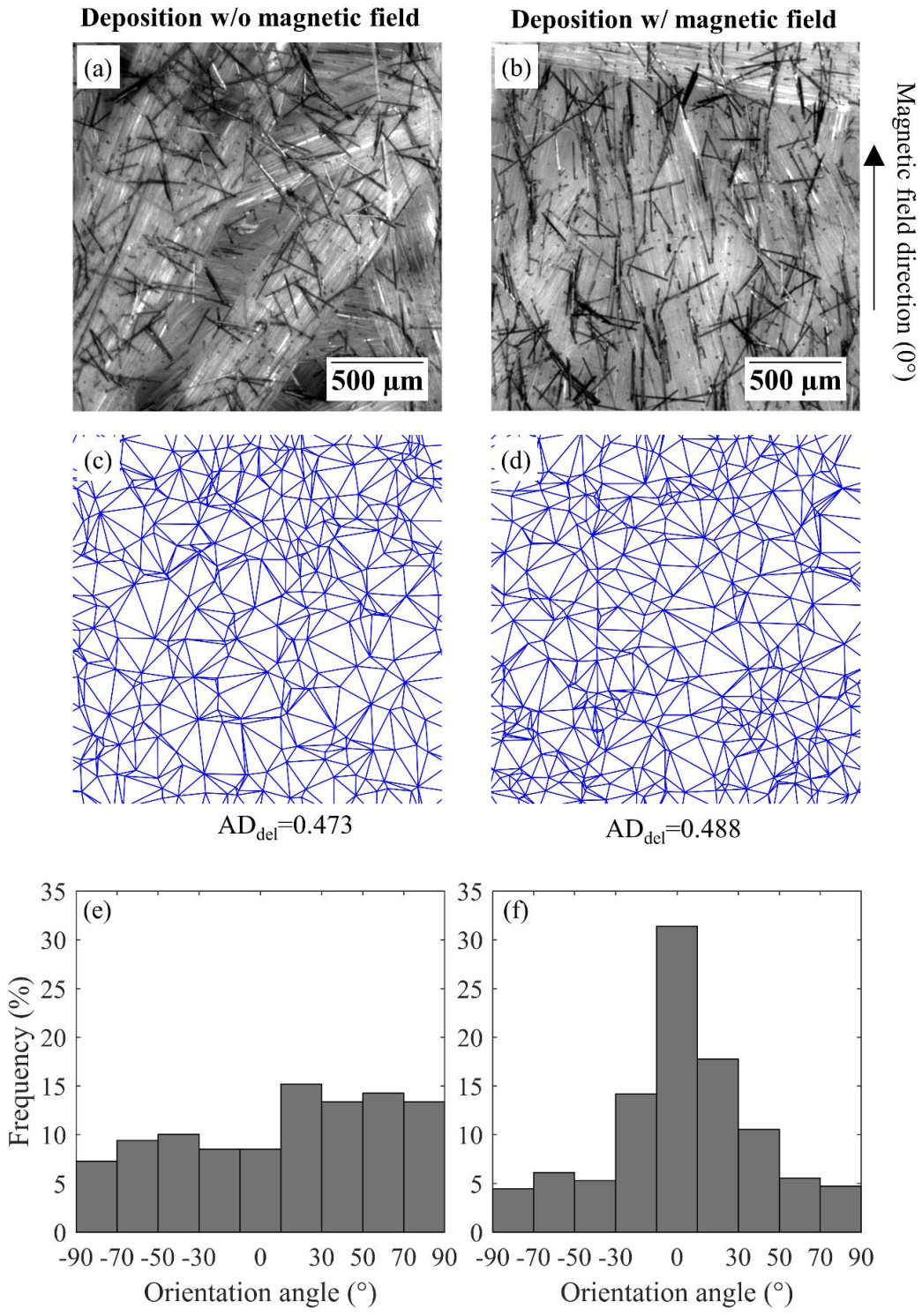

Figure 47. Comparison of optical images from the NiC1 (20% Ni-0.25 mm) fibers deposited on random mat fabric: (a) without and (b) with magnetic field. Construction of generated Delaunay triangles from fibers position: (c) without and (d) with magnetic field. Distribution frequencies of the orientation angle of fibers deposited on fabric: (e) without and (f) with magnetic field.

4.2.3.2. Process-induced microstructure of three-phase composite laminates

4.2.3.2.1. Degree of alignment and dispersion of fibers under magnetic field

To understand the level of anisotropy at the laminate surface, the orientation angle of fibers and their dispersion in the laminates made with and without magnetic fields are compared. Thus, optical images are captured from the laminate surface at five locations (near inlet, between inlet and center, center, between center and outlet, and close to outlet) and the orientation angle of all fibers are determined. Fig. 48 presents the frequency histogram of orientation angle of fibers in the laminates made under different scenarios: (a) NiC1-D-V, without magnetic field, (b) NiC1-MD-V, with magnetic field during deposition, (c) NiC1-D-M1V, with magnetic field after mold filling, and (d) NiC1-MD-M2V, with magnetic field during deposition and during and after mold filling. Fig. 48(a) shows random orientation of fibers in NiC1-D-V, indicating that resin flow does not induce alignment of fibers. However, Figs. 48(b)-(d) present a preferential orientation of fibers that peaks between -10° and 10°, suggesting anisotropy in the surface microstructure of the laminates along the magnetic field direction (0°). The degree of alignment of fibers under different scenarios is compared by their kernel density estimates, as presented in Fig. 48(e). It is found that the highest degree of alignment of fibers is obtained with applying magnetic field throughout the fabrication process, as in scenario NiC1-MD-M2V. Next, the degree of alignment of fibers in NiC1-D-M1V, where magnetic field is applied after mold filling, is slightly higher than that obtained in NiC1-MD-V, where magnetic field is applied during deposition. In the absence of magnetic field, in NiC1-D-V, no alignment is observed, as

expected. In general, a higher degree of alignment is more advantageous since it results in higher properties, such as electrical conductivity, along the alignment direction due to the combined effects of the alignment and formation of conductive networks of fibers [198, 199]. However, the ability to obtain microstructure anisotropy with applying magnetic field only during deposition and then making the composite laminate opens future possibilities for multilayer engineered materials.

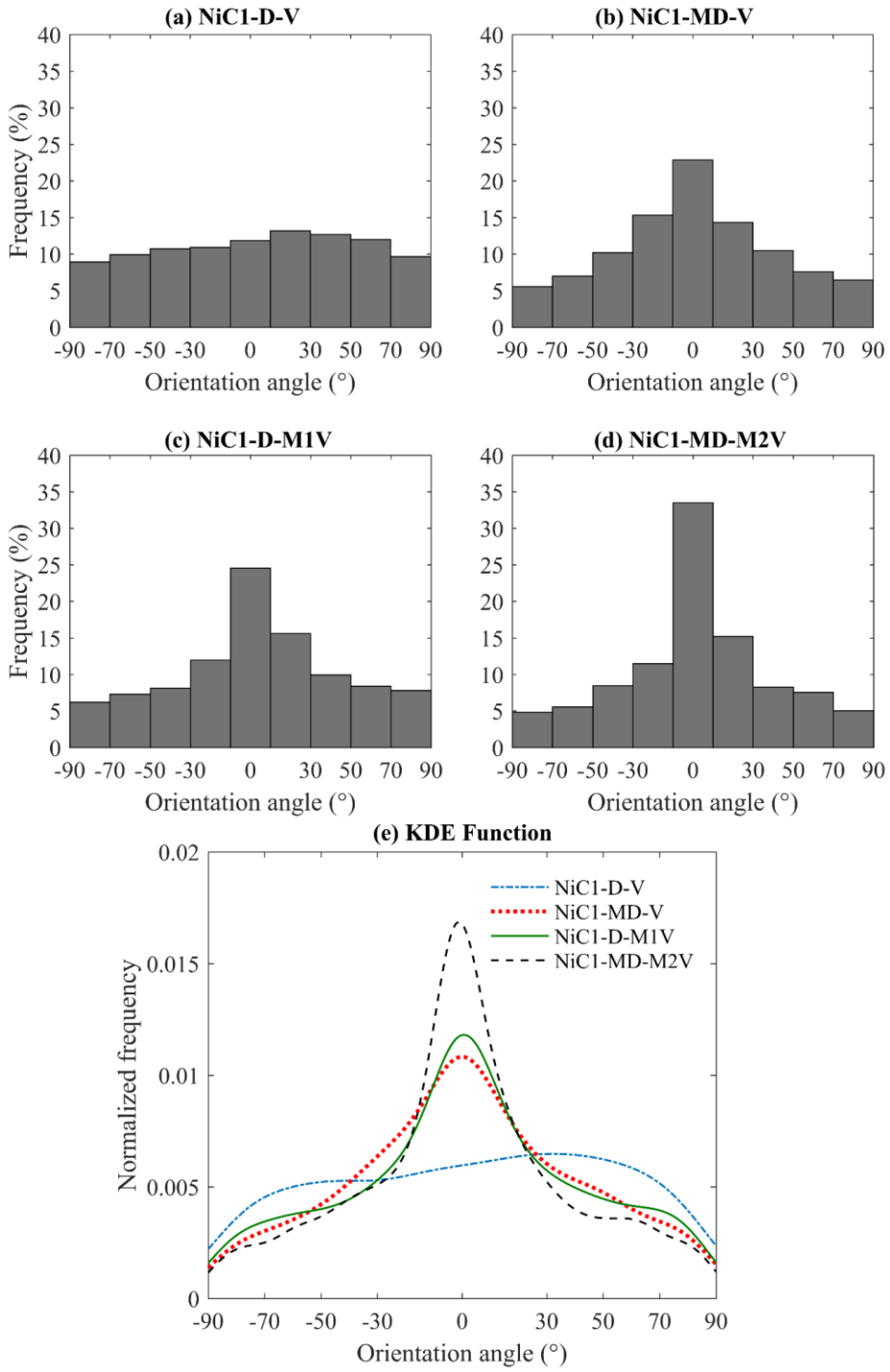

Figure 48. Frequency histogram of orientation angle of NiC1 (20% Ni-0.25 mm) fibers on the laminates made under different scenarios of: (a) NiC1-D-V, without magnetic field, (b) NiC1-MD-V, with magnetic field during deposition, (c) NiC1-D-M1V, with magnetic field after mold filling, (d) NiC1-MD-M2V, with magnetic field during deposition and during and after mold filling, and (e) their kernel density estimates (KDE). Note that magnetic field direction is applied at an angle of 0°.

To evaluate the degree of dispersion of fibers on the laminate, the area disorder AD_{del} of fibers at five locations (near inlet, between inlet and center, center, between center and outlet, and close to outlet) is calculated and then averaged over all locations ($\overline{AD}_{del}$). Fig. 49 depicts the overall normalized area disorder of fibers ($\overline{AD}_{del}/AD_{del}(ref.)$) on the laminates made under different scenarios: (a) NiC1-D-V, without magnetic field, (b) NiC1-MD-V, with magnetic field during deposition, (c) NiC1-D-M1V, with magnetic field after mold filling, and (d) NiC1-MD-M2V, with magnetic field during deposition and during and after mold filling. The closer the normalized area disorder is to 1, the higher the degree of dispersion. Fig. 49 clearly demonstrates that in all scenarios, the normalized area disorder ranges between 1.10-1.15, illustrating that fibers are well-dispersed on the laminate surface with and without magnetic field. Among all scenarios, in NiC1-MD-M2V, applying magnetic field during deposition and during and after mold filling resulted in a slightly better degree of dispersion (i.e. $\overline{AD}_{del}/AD_{del}(ref.) = 1.10$), indicating that the presence of a magnetic field restricted the movements of the fibers during the resin flow. However, in NiC1-D-M1V, applying magnetic field after mold filling resulted in a slightly lower degree of dispersion (i.e. $\overline{AD}_{del}/AD_{del}(ref.) = 1.15$) compared to other scenarios. The reason can be that the position of fibers is disturbed two times after deposition, one due to the resin flow and then as a result of applying magnetic field.

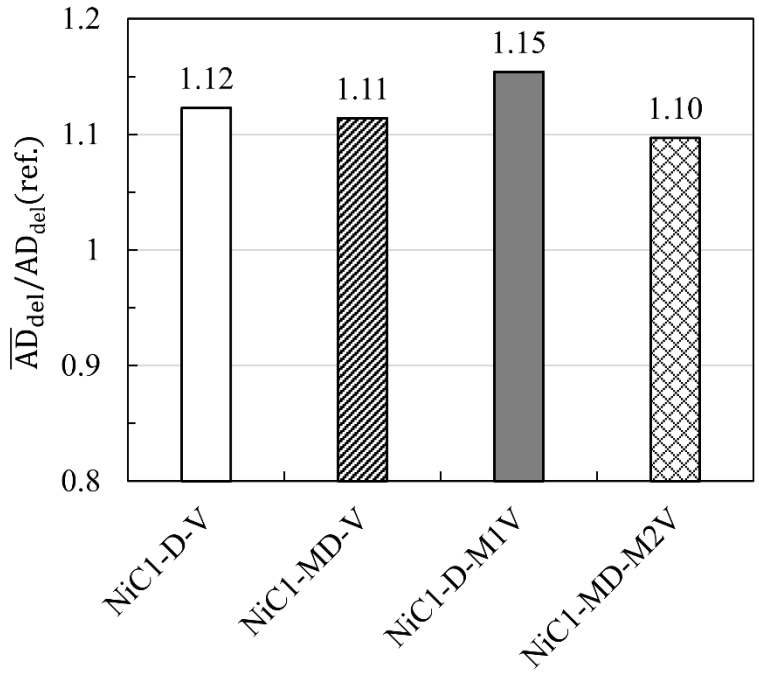

Figure 49. Normalized area disorder of NiC1 (20% Ni-0.25 mm) fibers on the laminates made under different scenarios of: (a) NiC1-D-V, without magnetic field, (b) NiC1-MD-V, with magnetic field during deposition, (c) NiC1-D-M1V, with magnetic field after mold filling, (d) NiC1-MD-M2V, with magnetic field during deposition and during and after mold filling. Note: the closer the normalized area disorder to 1, the higher is the degree of dispersion.

4.2.3.2.2. Spatial uniformity of fibers under magnetic field

To evaluate the spatial uniformity of fiber deposition along the fill and transverse directions, the local gray value of pixels is normalized with respect to gray value of NiC fiber (i.e. 255). Figs. 50(a) and (b) show the fiber occurrence (i.e., normalized gray value) in the laminates fabricated under four different scenarios (NiC1-D-V, NiC1-MD-V, NiC1-D-M1V, and NiC1-MD-M2V) parallel and transverse to the resin flow direction, respectively. The average gray value of pixels, in the 100 × 100 mm^2 images of all of these laminates is measured to be almost the same, within the range of 109-112. This similar value of the average gray value or fiber occurrence

implies that regardless of whether the magnetic field is applied during deposition or fabrication or if it is not applied at all, the final fiber content of the laminate remains the same. Overall, Fig. 50 indicates a uniform spatial distribution of fibers throughout the surface of laminates, regardless of their fabrication process. Comparing Figs. 50(a) and (b), it is seen that the fiber occurrence is more uniform in the transverse direction than fill direction, which might be due to slight movement of fibers during infusion along the flow. However, it is observed that having the magnetic field throughout the fabrication process (i.e. NiC1-MD-M2V), slightly reduces the variation of fiber distribution in the fill direction (Fig. 50(a)). This can be explained by the fact that the magnetic dipolar interaction between the NiC fibers induces the formation of chain-like structures, which may keep the NiC fibers in place, preventing the disruption of the fibers' distribution due to resin flow.

Overall, it is noted that the presence of magnetic field induces surface anisotropy without adversely affecting the almost perfect uniform distribution of fibers. This gives the flexibility of tailoring the surface anisotropy in the composite microstructure, thus manipulating the desired functionality of the entire composite part in a specific direction.

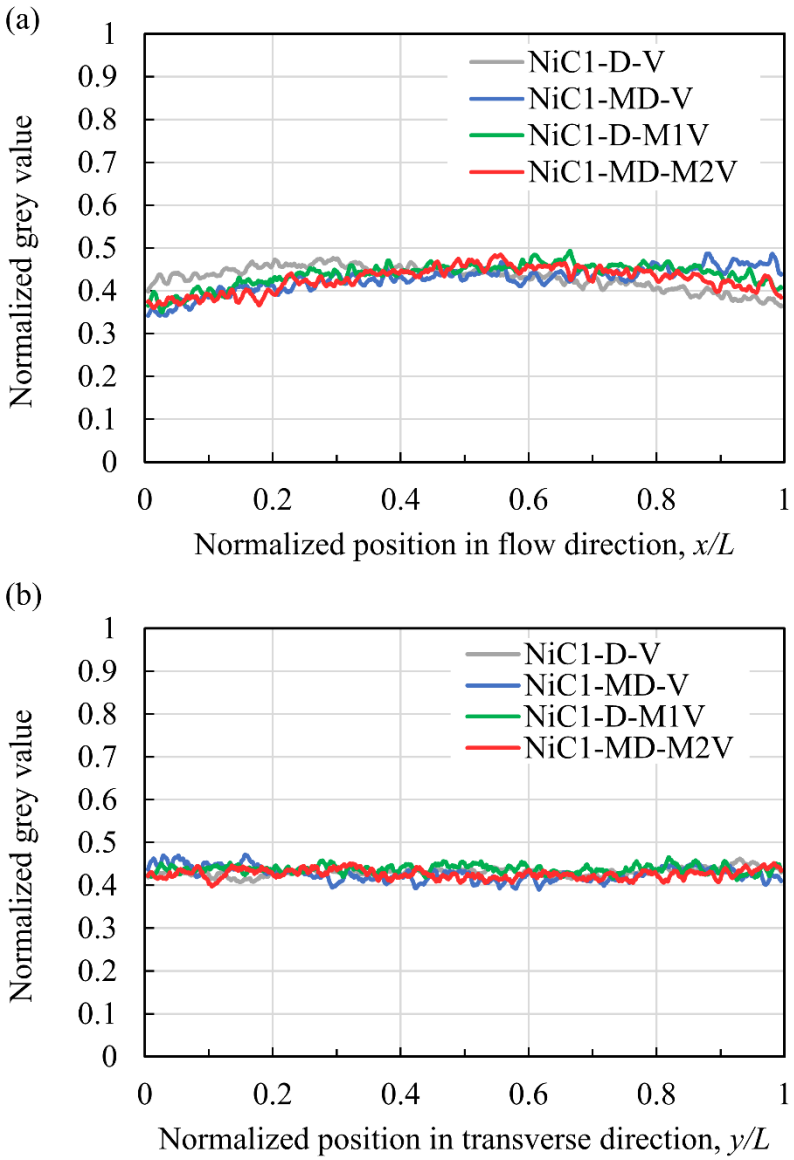

Figure 50. Variation of fiber occurrence (i.e. normalized gray value) indicating the uniformity of fiber distribution in: (a) resin flow direction and (b) transverse direction of random mat laminate for laminates made without magnetic field (NiC1-D-V), with magnetic field during deposition (NiC1-MD-V), with magnetic field after mold filling (NiC1-D-M1V), and with magnetic field during deposition and during and after mold filling (NiC1-MD-M2V). The local gray value of pixels is normalized with respect to 255, which is the gray value of the NiC fiber.

4.2.3.2.3. Degree of alignment and dispersion of fibers at different nickel coatings

Magnetic field-induced alignment of fibers with a thicker nickel coating (NiC2, 40% Ni-0.25 mm) is investigated by comparing the frequency histogram of orientation angle of all fibers in the laminates fabricated under different scenarios: (a) NiC2-MD-V, (b) NiC2-D-M1V, and (c) NiC2-MD-M2V (see Fig. 51). Figs. 51(a)-(c) clearly demonstrate that in all the laminates fabricated in the presence of magnetic field, there is a preferred orientation angle close to 0°, along the magnetic field direction. To compare the degree of alignment of fibers in the laminates made by NiC2 fibers under different scenarios and NiC1 fibers under NiC2-MD-M2V scenario, their kernel density functions are shown in Fig. 51(e). Similar to the laminates made by NiC1 fibers (20% Ni), the highest degree of alignment among the parts made by NiC2 fibers is obtained in NiC2-MD-M2V laminates, where magnetic field is applied throughout the process (see Fig. 51(d)). Fig. 51 (d) also depicts that under the same fabrication scenario, i.e. applying magnetic field throughout the process, MD-M2V, the degree of alignment of NiC2 fibers is higher than that of NiC1 fibers. The reason is that by increasing the nickel coating from 20% in NiC1 to 40% in NiC2, the fibers become more responsive to the magnetic field and thus, the microstructure morphology of laminates shows a higher anisotropy toward the field direction. However, with a lower nickel coating, the resulting composite is lighter. Thus, one can benefit from this lighter weight composite and reach the same level of anisotropy with applying a higher magnetic field.

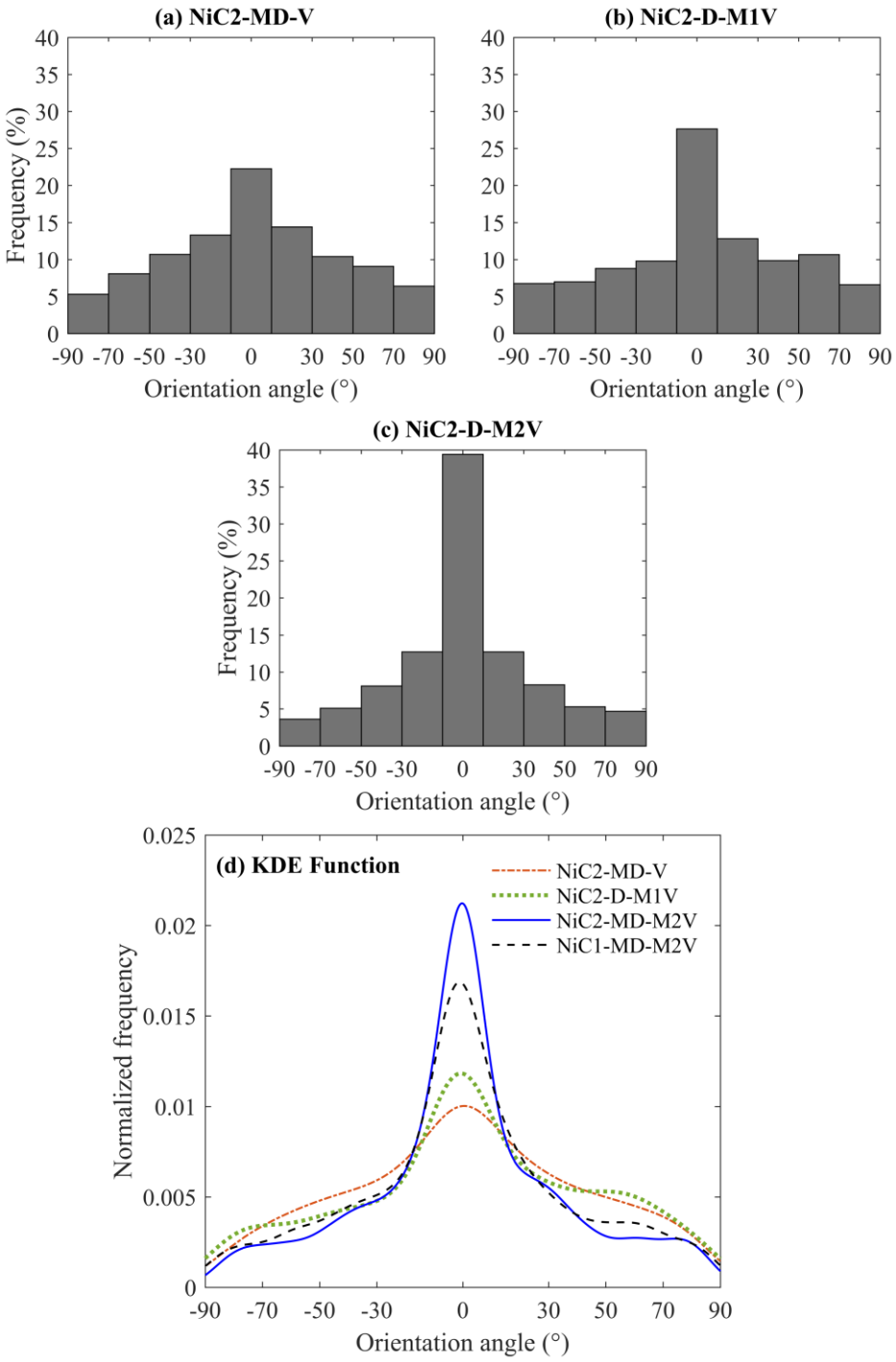

Figure 51. Frequency histogram of orientation angle of NiC2 (40% Ni-0.25 mm) fibers on the laminates made under different scenarios of: (a) NiC2-MD-V, with magnetic field during deposition, (b) NiC2-D-M1V, with magnetic field after mold filling, (c) NiC2-MD-M2V, with magnetic field during deposition and during and after mold filling, and (d) their kernel density estimates (KDE) compared to that of NiC1-MD-M2V, with magnetic field during deposition and during and after mold filling. Note that magnetic field direction is applied at an angle of 0°.

Fig. 52 depicts the degree of dispersion of fibers, i.e. the normalized area disorder of fibers with respect to reference area disorder (i.e. $AD_{del}(ref.)=0.466$), for the laminates made using NiC1 and NiC2 fibers under different fabrication scenarios. As mentioned earlier, the normalized area disorder ($\overline{AD}_{del}/AD_{del}(ref.)$) close to 1 corresponds to the excellent dispersion of the short fibers. The normalized area disorder of 1.10-1.15 obtained for all the laminates indicates that short NiC fibers are well dispersed throughout the surface of laminates, regardless of the amount of nickel coating and when magnetic field is applied. Fig. 52 also clearly presents that when infusion is performed in the presence of magnetic field, the value of normalized area disorder slightly decreases. This may suggest that the presence of a magnetic field not only does not disturb the distribution of fibers, but also counteracts the flow-induced microstructure morphology of laminates.

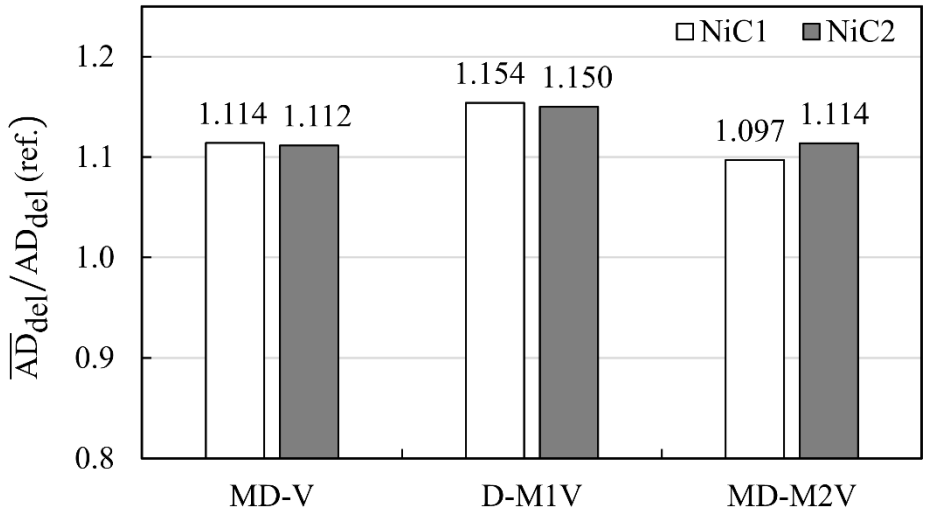

Figure 52. Comparison of normalized area disorder of NiC2 (40% Ni-0.25 mm) and NiC1 (20% Ni-0.25 mm) fibers on the laminates made under different scenarios of: (a) MD-V, with magnetic field during deposition, (b) D-M1V, with magnetic field after mold filling, (c) MD-M2V, with magnetic field during deposition and during and after mold filling. A lower value of normalized area disorder (i.e. values closer to 1) is indicative of well dispersion.

4.2.3.2.4. Degree of alignment and dispersion of fibers at different aspect ratios

To investigate the effect of fibers aspect ratio on degree of alignment and dispersion of fibers, NiC fibers with two different aspect ratios (i.e. α=19 and 24) are used in the fabrication of three-phase laminates under the same level of magnetic field. Fig. 53 presents the optical images of NiC3-MD-M2V and NiC1-MD-M2V laminates, as well as the kernel density estimates of orientation angles and normalized area disorder of NiC3 (20% Ni-0.1 mm) and NiC1 (20% Ni-0.25 mm) fibers. Optical images in Figs. 53(a) and (b) show that there is a considerable difference in the aspect ratio of the fibers. However, under the same magnetic field of ≈20-30mT, both NiC1 and NiC3 fibers are aligned along the direction of magnetic field (0°). In addition, the fibers interact easily with each other and build NiC fiber networks. Fig. 53(c) demonstrates that the degree of alignment of fibers with a higher aspect ratio (NiC1, α=24) is considerably higher than that of NiC3 fibers with an aspect ratio of 14. Thus, fibers with higher aspect ratios are more responsive to the magnetic field and their orientation can be controlled at a higher degree under a lower magnetic field strength. This provides the flexibility for fabrication of large composite parts where generating higher level of magnetic field may be difficult. Fig. 53(d) shows that the degree of dispersion of shorter fibers (i.e. NiC3) is slightly better than longer fibers (i.e. NiC1). This can be explained by the fact that the possibility of making chains and migration of longer fibers, NiC1, under the same level of magnetic field, is slightly higher than that of shorter fibers, thus leading to a marginally lower degree of dispersion.

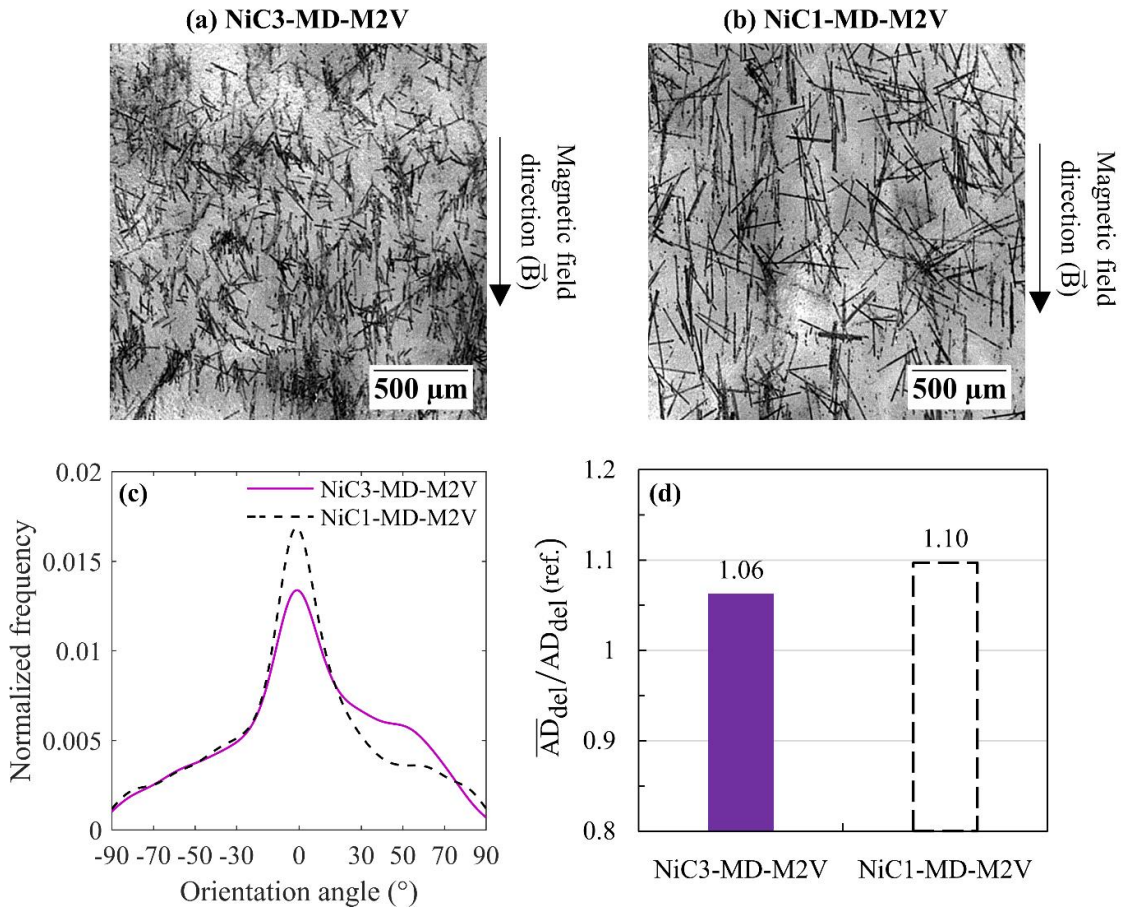

Figure 53. Optical image from the (a) NiC3 (20% Ni-0.1 mm) and (b) NiC1 (20% Ni-0.25 mm) fibers on the laminates made with applying magnetic field throughout the process, MD-M2V, (c) comparison of kernel density estimate of their orientation angle, and (d) comparison of their normalized area disorder.

4.2.3.2.5. Spatial uniformity of distribution of fibers with different nickel coatings and aspect ratios

Fig. 54 demonstrates the variation of fiber occurrence in flow direction for laminates made with NiC1 (20% Ni, 0.25 mm), NiC2 (40% Ni, 0.25 mm), and NiC3 (20% Ni, 0.1 mm) fibers. These laminates are all fabricated in the presence of magnetic field throughout the process (i.e. MD-M2V). Fig. 54 indicates that the fiber distribution along the flow direction is almost uniform for all the laminates. However, the results show that higher amount of coating in NiC2 fibers (i.e. 40%) leads to a slightly more

uniform fiber volume fraction in NiC2-MD-M2V laminate compared to the laminates made by NiC1 and NiC3 fibers with 20% nickel coating. The reason can be that the attraction force between the magnets and the NiC fibers enhances with increasing the thickness of Ni coating which prevents the movement of fibers due to resin flow during infusion.

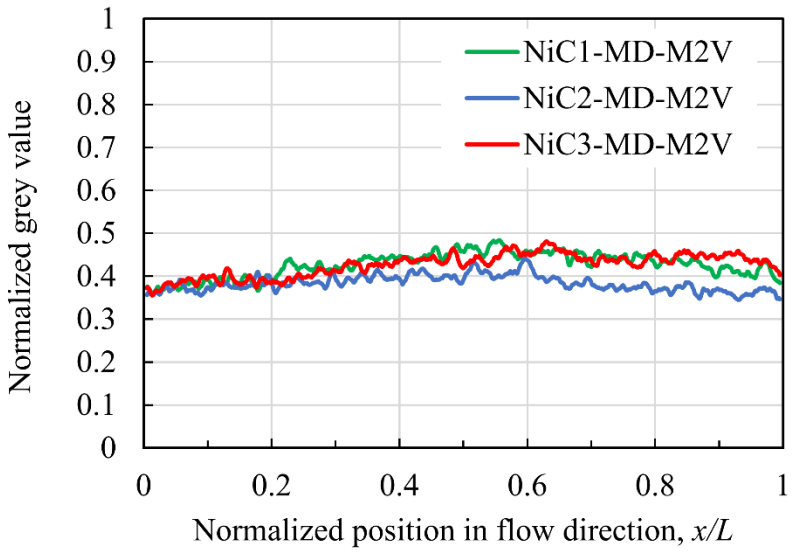

Figure 54. Variation of fiber occurrence (i.e. normalized gray value) indicating the uniformity of fiber distribution in flow direction for laminates made with NiC1 (20% Ni, 0.25 mm), NiC2 (40% Ni, 0.25 mm), and NiC3 (20% Ni, 0.1 mm) fibers in the presence of magnetic field throughout the process. The local gray value of pixels is normalized with respect to 255, which is the gray value of the NiC fiber.

4.2.4. Concluding remarks

In the second part of chapter 4, a novel magnetic-field assisted composite processing is introduced as a viable manufacturing technique for tailoring the surface anisotropy and thus improving the functionalities of structural composites. This process uses a set of permanent magnets to generate the appropriate level of magnetic field for inducing alignment of nickel coated carbon (NiC) fibers on the surface of three-phase laminates. For this purpose, magnetic field is applied: (i) during deposition of fibers on

the fabric surface, (ii) after mold filling in VARTM on fibers-deposited fabric, and (iii) during deposition, mold filling, and after mold filling. The effectiveness of this processing technique is investigated by comparing the microstructure morphology of laminates fabricated in the presence of magnetic field with that made without magnetic field. In addition, the effects of two important physical properties of fibers, fibers aspect ratio and nickel coating, on the microstructural morphology of laminates are studied.

The comprehensive microstructural characterization revealed that this technique enables the fabrication of both fibers-deposited fabric and the three-phase laminate with surface anisotropy while maintaining the uniformity of microstructure and well dispersion of fibers. The results suggested that applying magnetic field throughout the entire process (i.e. deposition mold filling, and after mold filling) results in the highest degree of alignment of NiC fibers. Moreover, having a higher nickel coating is beneficial for obtaining a higher degree of alignment and more uniform fiber distribution. In addition, fibers with higher aspect ratio led to the laminates with higher degree of alignment since they experience higher dipole moment under the same level of magnetic field.

Chapter 5. Conclusions and Recommendations

5.1. Conclusions

The primary objectives of the current dissertation were threefold. First, a novel fabrication method, magnet assisted composite manufacturing (MACM), was introduced as a viable OOA method for fabrication of structural composite laminates. In the MACM technique, a set of high-temperature Neodymium permanent magnets were placed on the vacuum bag to generate sufficiently high magnetic compressive pressure during cure of laminates. The effect of applying magnetic compressive pressure on the prepreg lay-up was investigated to enhance mechanical properties and overall quality of composite laminates. For this purpose, eight-ply, woven carbon/epoxy laminates were fabricated in an oven by MACM and compared with those made in an autoclave using the same thermal cycle. It was shown that with MACM an effective consolidation pressure of 0.29 MPa (42 psi) can be generated which is high enough for fabricating 8-ply laminates with high fiber volume fraction (60%) and low void volume fraction (<3%). Moreover, with applying magnetic compressive pressure at the minimum viscosity of resin, even a lower void volume fraction (<1%) was obtained. Accordingly, a substantial improvement (≈21%) in flexural properties was observed with applying magnets during cure in an oven, matching or exceeding the properties obtained in an autoclave. These results indicate that, in some cases, MACM technique enables manufacturing of structural composite laminates at relatively low cost compared to autoclave curing.

Second, a novel cascaded suspension deposition method was proposed to incorporate well-dispersed short fibers into the molded laminates, which allows

controlling the surface properties of the resulting composite. This technique was successfully implemented to deposit short nickel coated carbon (NiC) fibers on the surface of glass fabric. The resin was then infused into the deposited fabric to manufacture three-phase NiC/glass/epoxy composite laminates. Spatial uniformity of fiber volume fraction, as well as the degree of dispersion and alignment of short fibers were quantitatively assessed both on the deposited fabric surface and on the three-phase laminate surface after fabrication. To demonstrate the flexibility of the proposed method, different fiber concentrations and fabric architectures were considered. A detailed microstructural analysis suggested that the proposed technique is capable of depositing short fibers on the fabric surface with a uniform fiber volume fraction and excellent dispersion with random orientation. This indicates that it is possible to produce structural composites with controlled surface morphology using the proposed cascaded suspension deposition method.

Third, the alignment of NiC fibers in polymer composites under the magnetic field was studied, and the appropriate level of magnetic field to induce anisotropy in the composites was determined. Furthermore, a new magnetic-field assisted composite processing method was developed for controlling the orientation of conductive fibers in structural laminates, thus tailoring the surface anisotropy in the resulting composite. To demonstrate the feasibility of the proposed method, alignment of NiC fibers on the surface of three-phase NiC/glass/epoxy composite laminates was studied. To deposit fibers uniformly on the fabric surface, cascaded suspension deposition method was adopted. Different degrees of alignment were induced in the fibers using an appropriate level of magnetic field in three ways: (i) during deposition, (ii) after mold filling in

VARTM, and (iii) during deposition, mold filling, and after mold filling. The influences of physical properties of fibers (i.e. fibers aspect ratio and nickel coating) were assessed on the microstructure morphology of composites. The results revealed that NiC fibers were aligned with the highest anisotropy toward the magnetic field direction while maintaining the uniform fiber volume fraction and good dispersion throughout the surface of the laminate. Tailoring surface anisotropy in structural laminates by magnetic field-induced alignment may lead to the development of new materials, which will expand the application range of fiber reinforced polymer (FRP) composites.

5.2. Recommendations for future work

The various studies presented in this dissertation are open for further development. One area that can be developed is the MACM manufacturing process. In this dissertation, the MACM process was used to apply sufficiently high consolidation pressure during cure of structural laminates. It would be advantageous, to further develop the process so that it could be utilized in additive manufacturing (AM). One of the problems associated with AM is the bonding between adjacent layers, which significantly affects the mechanical properties of the final part. Thus, applying sufficient magnetic consolidation pressure in AM may help to improve interlayer bonding, thus enhancing the strength of AM parts. Therefore, fabrication of AM parts with improved properties will lead to increased use of the AM process in high performance and other critical applications.

Traditional FRP composites typically possess poor through-the-thickness structural and conductivity properties. Thus, a second area available for future work is the use of magnetic-field assisted composite processing method for improving the

interlaminar shear strength and through-the-thickness conductivity of traditional FRP composites. For this purpose, an appropriate level of the through-the-thickness magnetic field may be used to orient short fibers between the fabric layers in three-phase composites during cure. For obtaining a uniform deposition of short fibers on the fabric surface, cascaded suspension deposition method can be adopted. Moreover, for fabrication of three-phase composites, the resin can be infused into deposited fabric by VARTM. To assess the effectiveness of this method, the microstructure morphology, as well as short beam shear and conductivity properties of the fabricated laminates can be assessed. It is expected that this work could contribute to the development of new materials with enhanced properties, thus expanding the applications of FRP composites.

References

[1] Garg M, Sharma S, Mehta R. Pristine and amino functionalized carbon nanotubes reinforced glass fiber epoxy composites. Composites Part A: Applied Science and Manufacturing, 2015;76:92-101.

[2] Varvani-Farahani A. Composite materials: characterization, fabrication and application-research challenges and directions. Applied Composite Materials, 2010;17(2):63-7.

[3] Alderliesten RC. Critical review on the assessment of fatigue and fracture in composite materials and structures. Engineering Failure Analysis, 2013;35:370-9.

[4] Torres J, Simmons M, Sket F, González C. An analysis of void formation mechanisms in out-of-autoclave prepregs by means of X-ray computed tomography. Composites Part A: Applied Science and Manufacturing, 2019;117:230-42.

[5] Hernández S, Sket F, González C, LLorca J. Optimization of curing cycle in carbon fiber-reinforced laminates: void distribution and mechanical properties. Composites Science and Technology, 2013;85:73-82.

[6] Aleksendrić D, Carlone P, Ćirović V. Optimization of the temperature-time curve for the curing process of thermoset matrix composites. Applied Composite Materials, 2016;23(5):1047-63.

[7] Grunenfelder LK, Dills A, Centea T, Nutt S. Effect of prepreg format on defect control in out-of-autoclave processing, Composites Part A: Applied Science and Manufacturing, 2017;93:88-99.

[8] Simacek P, Advani SG. Desirable features in mold filling simulations for liquid

composite molding processes. Polymer Composites, 2004;25(4):355.

[9] Francucci G, Rodriguez E. Processing of plant fiber composites by liquid molding techniques: An overview. Polymer Composites, 2016;37(3):718-33.

[10] Kim J-I, Hwang Y-T, Choi K-H, Kim H-J, Kim H-S. Prediction of the vacuum assisted resin transfer molding (VARTM) process considering the directional permeability of sheared woven fabric. Composite Structures, 2019;211:236-43.

[11] Kuentzer N, Simacek P, Advani SG, Walsh S. Correlation of void distribution to VARTM manufacturing techniques. Composites Part A: Applied Science and Manufacturing, 2007;38(3):802-13.

[12] Rubino F, Carlone P. A semi-analytical model to predict infusion time and reinforcement thickness in VARTM and SCRIMP processes, Polymers, 2019;11(1):20.

[13] Amirkhosravi M, Pishvar M, Altan MC. Void reduction in VARTM composites by compaction of dry fiber preforms with stationary and moving magnets. Journal of Composite Materials, 2019;53(6):769-82.

[14] Amirkhosravi M, Pishvar M, Altan MC. Fabricating high-quality VARTM laminates by magnetic consolidation: Experiments and process model. Composites Part A: Applied Science and Manufacturing, 2018;114:398-406.

[15] Sun X, Li S, Lee LJ. Mold filling analysis in vacuum-assisted resin transfer molding. Part I: SCRIMP based on a high-permeable medium. Polymer Composites, 1998;19(6):807-17.

[16] Niggemann C, Song YS, Gillespie JW, Heider D. Experimental investigation of the controlled atmospheric pressure resin infusion (CAPRI) process. Journal of

Composite Materials, 2008;42(11):1049-61.

[17] Yalcinkaya MA, Guloglu GE, Pishvar M, Amirkhosravi M, Sozer EM, Altan MC. Pressurized infusion: A new and improved liquid composite molding process. Journal of Manufacturing Science and Engineering, 2019;141(1):011007.

[18] Grunenfelder LK, Nutt SR. Void formation in composite prepregs–effect of dissolved moisture. Composites Science and Technology, 2010;70(16):2304-9.

[19] Schlimbach J, Ogale A. Out-of-autoclave curing process in polymer matrix composites. Manufacturing techniques for polymer matrix composites (PMCs), Elsevier, 2012; pp. 435-80.

[20] Grunenfelder LK, Centea T, Hubert P, Nutt SR. Effect of room-temperature out-time on tow impregnation in an out-of-autoclave prepreg. Composites Part A: Applied Science and Manufacturing, 2013;45:119-26.

[21] Hamill L, Centea T, Nutt SR. Surface porosity during vacuum bag-only prepreg processing: Causes and mitigation strategies. Composites Part A: Applied Science and Manufacturing, 2015;75:1-10.

[22] Marsh G. Quick stepping to fast fluid curing. Reinforced Plastics, 2006;50(7):20-5.

[23] Khan LA, Kausar A, Day RJ. Aerospace composite cured by quickstep and autoclave processing techniques: Evaluation and comparison of reaction progress. Aerospace Science and Technology, 2017;65:100-5.

[24] Agius SL, Magniez KJC, Fox BL. Cure behaviour and void development within rapidly cured out-of-autoclave composites. Composites Part B: Engineering,

2013;47:230-7.

[25] Zhang J, Fox BL. Characterization and analysis of delamination fracture and nanocreep properties in carbon epoxy composites manufactured by different processes. Journal of Composite Materials, 2006;40(14):1287-99.

[26] Khan LA, Kausar A, Hussain ST, Iqbal Z, Day RJ, Syed AS, Khan ZM. Cure characterization of Cycom 977-2A carbon/epoxy composites for quickstep processing. Polymer Engineering & Science, 2014;54(4):887-98.

[27] Khan LA, Nesbitt A, Day RJ. Hygrothermal degradation of 977-2A carbon/epoxy composite laminates cured in autoclave and Quickstep. Composites Part A: Applied Science and Manufacturing, 2010;41(8):942-53.

[28] Muric-Nesic J, Compston P, Stachurski ZH. On the void reduction mechanisms in vibration assisted consolidation of fibre reinforced polymer composites. Composites Part A: Applied Science and Manufacturing, 2011;42(3):320-7.

[29] Lee J-M, Kim B-M, Ko D-C. Development of vacuum-assisted prepreg compression molding for production of automotive roof panels. Composite Structures, 2019;213:144-52.

[30] Choi HS, Ahn KJ, Nam J-D, Chun HJ. Hygroscopic aspects of epoxy/carbon fiber composite laminates in aircraft environments. Composites Part A: Applied Science and Manufacturing, 2001;32(5):709-20.

[31] Strong AB. Fundamentals of composites manufacturing: materials, methods and applications. Society of Manufacturing Engineers, 2008.

[32] Van Den Einde L, Zhao L, Seible F. Use of FRP composites in civil structural applications. Construction and Building Materials, 2003;17(6-7):389-403.

[33] Balakrishnan P, John MJ, Pothen L, Sreekala MS, Thomas S. Natural fibre and polymer matrix composites and their applications in aerospace engineering. Advanced composite materials for aerospace engineering, Elsevier, 2016; pp. 365-83.

[34] Lu K. The future of metals. Science, 2010;328(5976):319-20.

[35] Godara A, Mezzo L, Luizi F, Warrier A, Lomov SV, Van Vuure AW, Gorbatikh L, Moldenaers P, Verpoest I. Influence of carbon nanotube reinforcement on the processing and the mechanical behaviour of carbon fiber/epoxy composites. Carbon, 2009;47(12):2914-23.

[36] Thostenson ET, Li WZ, Wang DZ, Ren ZF, Chou TW. Carbon nanotube/carbon fiber hybrid multiscale composites. Journal of Applied Physics, 2002;91(9):6034-7.

[37] Gojny FH, Wichmann MHG, Fiedler B, Bauhofer W, Schulte K. Influence of nano-modification on the mechanical and electrical properties of conventional fibre-reinforced composites. Composites Part A: Applied Science and Manufacturing, 2005;36(11):1525-35.

[38] Yokozeki T, Iwahori Y, Ishiwata S. Matrix cracking behaviors in carbon fiber/epoxy laminates filled with cup-stacked carbon nanotubes (CSCNTs). Composites Part A: Applied Science and Manufacturing, 2007;38(3):917-24.

[39] Fan Z, Santare MH, Advani SG. Interlaminar shear strength of glass fiber reinforced epoxy composites enhanced with multi-walled carbon nanotubes. Composites Part A: Applied Science and Manufacturing, 2008;39(3):540-54.

[40] Wichmann MHG, Sumfleth J, Gojny FH, Quaresimin M, Fiedler B, Schulte K.

Glass-fibre-reinforced composites with enhanced mechanical and electrical properties–benefits and limitations of a nanoparticle modified matrix. Engineering Fracture Mechanics, 2006;73(16):2346-59.

[41] Shen Z, Bateman S, Wu DY, McMahon P, Dell'Olio M, Gotama J. The effects of carbon nanotubes on mechanical and thermal properties of woven glass fibre reinforced polyamide-6 nanocomposites. Composites Science and Technology, 2009;69(2):239-44.

[42] Zhou Y, Pervin F, Rangari VK, Jeelani S. Fabrication and evaluation of carbon nano fiber filled carbon/epoxy composite. Materials Science and Engineering: A, 2006;426(1-2):221-8.

[43] Kim M, Park Y-B, Okoli OI, Zhang C. Processing, characterization, and modeling of carbon nanotube-reinforced multiscale composites. Composites Science and Technology, 2009;69(3-4):335-42.

[44] Thostenson ET, Ren Z, Chou T-W. Advances in the science and technology of carbon nanotubes and their composites: a review. Composites Science and Technology, 2001;61(13):1899-912.

[45] Rachmadini Y, Tan VBC, Tay TE. Enhancement of mechanical properties of composites through incorporation of CNT in VARTM-A review. Journal of Reinforced Plastics and Composites, 2010;29(18):2782-807.

[46] Sager RJ, Klein PJ, Lagoudas DC, Zhang Q, Liu J, Dai L, Baur JW. Effect of carbon nanotubes on the interfacial shear strength of T650 carbon fiber in an epoxy matrix. Composites Science and Technology, 2009;69(7-8):898-904.

[47] Qian H, Bismarck A, Greenhalgh ES, Shaffer MSP. Carbon nanotube grafted

carbon fibres: a study of wetting and fibre fragmentation. Composites Part A: Applied Science and Manufacturing, 2010;41(9):1107-14.

[48] Bekyarova E, Thostenson ET, Yu A, Kim H, Gao J, Tang J, Hahn HT, Chou T-W, Itkis ME, Haddon RC. Multiscale carbon nanotube-carbon fiber reinforcement for advanced epoxy composites. Langmuir, 2007;23(7):3970-4.

[49] Zhang J, Zhuang R, Liu J, Mäder E, Heinrich G, Gao S. Functional interphases with multi-walled carbon nanotubes in glass fibre/epoxy composites. Carbon, 2010;48(8):2273-81.

[50] Zhu J, Imam A, Crane R, Lozano K, Khabashesku VN, Barrera EV. Processing a glass fiber reinforced vinyl ester composite with nanotube enhancement of interlaminar shear strength. Composites Science and Technology, 2007;67(7-8):1509-17.

[51] Davis DC, Wilkerson JW, Zhu J, Ayewah DOO. Improvements in mechanical properties of a carbon fiber epoxy composite using nanotube science and technology. Composite Structures, 2010;92(11):2653-62.

[52] Thakre PR, Lagoudas DC, Riddick JC, Gates TS, Frankland S-JV, Ratcliffe JG, Ratcliffe JG, Zhu J, Barrera EV. Investigation of the effect of single wall carbon nanotubes on interlaminar fracture toughness of woven carbon fiber-epoxy composites. Journal of Composite Materials, 2011;45(10):1091-107.

[53] Shan FL, Gu YZ, Li M, Liu YN, Zhang ZH. Effect of deposited carbon nanotubes on interlaminar properties of carbon fiber-reinforced epoxy composites using a developed spraying processing. Polymer Composites, 2013;34(1):41-50.

[54] Li M, Gu Y, Liu Y, Li Y, Zhang Z. Interfacial improvement of carbon fiber/epoxy composites using a simple process for depositing commercially functionalized carbon nanotubes on the fibers. Carbon, 2013;52:109-21.

[55] Wang Y, Xu Z, Chen L, Jiao Y, Wu X. Multi-scale hybrid composites-based carbon nanotubes. Polymer Composites, 2011;32(2):159-67.

[56] He D, Fan B, Zhao H, Lu X, Yang M, Liu Y, et al. Design of electrically conductive structural composites by modulating aligned CVD-grown carbon nanotube length on glass fibers. ACS Applied Materials & Interfaces, 2017;9(3):2948-58.

[57] Boccaccini AR, Cho J, Roether JA, Thomas BJC, Minay EJ, Shaffer MSP. Electrophoretic deposition of carbon nanotubes, Carbon, 2006;44(15):3149-60.

[58] Wu DC, Shen L, Low JE, Wong SY, Li X, Tjiu WC, Liu Y, He CB. Multi-walled carbon nanotube/polyimide composite film fabricated through electrophoretic deposition. Polymer, 2010;51(10):2155-60.

[59] Rodriguez AJ, Guzman ME, Lim C-S, Minaie B. Synthesis of multiscale reinforcement fabric by electrophoretic deposition of amine-functionalized carbon nanofibers onto carbon fiber layers. Carbon, 2010;48(11):3256-9.

[60] Molaei A, Yari M, Afshar MR. Modification of electrophoretic deposition of chitosan–bioactive glass–hydroxyapatite nanocomposite coatings for orthopedic applications by changing voltage and deposition time. Ceramics International, 2015;41(10):14537-44.

[61] Xiao C, Tan Y, Wang X, Gao L, Wang L, Qi Z. Study on interfacial and mechanical improvement of carbon fiber/epoxy composites by depositing multi-

walled carbon nanotubes on fibers. Chemical Physics Letters, 2018;703:8-16.

[62] Dong L, Hou F, Li Y, Wang L, Gao H, Tang Y. Preparation of continuous carbon nanotube networks in carbon fiber/epoxy composite. Composites Part A: Applied Science and Manufacturing, 2014;56:248-55.

[63] Feng A, Wu G, Pan C, Wang Y. The behavior of acid treating carbon fiber and the mechanical properties and thermal conductivity of phenolic resin matrix composites. Journal of Nanoscience and Nanotechnology, 2017;17(6):3786-91.

[64] Eksik O, Bartolucci SF, Gupta T, Fard H, Borca-Tasciuc T, Koratkar N. A novel approach to enhance the thermal conductivity of epoxy nanocomposites using graphene core–shell additives. Carbon, 2016;101:239-44.

[65] Mamunya YP, Davydenko VV, Pissis P, Lebedev EV. Electrical and thermal conductivity of polymers filled with metal powders. European Polymer Journal, 2002;38(9):1887-97.

[66] Han Z, Fina A. Thermal conductivity of carbon nanotubes and their polymer nanocomposites: A review. Progress in Polymer Science, 2011;36(7):914-44.

[67] Xia T, Zeng D, Li Z, Young RJ, Vallés C, Kinloch IA. Electrically conductive GNP/epoxy composites for out-of-autoclave thermoset curing through Joule heating. Composites Science and Technology, 2018;164:304-12.

[68] Shahil KMF, Balandin AA. Thermal properties of graphene and multilayer graphene: Applications in thermal interface materials. Solid State Communications, 2012;152(15):1331-40.

[69] Feng C, Ni H, Chen J, Yang W. Facile method to fabricate highly thermally conductive graphite/PP composite with network structures. ACS Applied

Materials & Interfaces, 2016;8(30):19732-8.

[70] Li C, Thostenson ET, Chou T-W. Effect of nanotube waviness on the electrical conductivity of carbon nanotube-based composites. Composites Science and Technology, 2008;68(6):1445-52.

[71] Kim K, Ju H, Kim J. Vertical particle alignment of boron nitride and silicon carbide binary filler system for thermal conductivity enhancement. Composites Science and Technology, 2016;123:99-105.

[72] Potts JR, Dreyer DR, Bielawski CW, Ruoff RS. Graphene-based polymer nanocomposites. Polymer, 2011;52(1):5-25.

[73] Sekitani T, Noguchi Y, Hata K, Fukushima T, Aida T, Someya T. A rubberlike stretchable active matrix using elastic conductors. Science, 2008;321(5895):1468-72.

[74] Rangari VK, Yousuf M, Jeelani S, Pulikkathara MX, Khabashesku VN. Alignment of carbon nanotubes and reinforcing effects in nylon-6 polymer composite fibers. Nanotechnology, 2008;19(24):245703.

[75] Khan SU, Pothnis JR, Kim J-K. Effects of carbon nanotube alignment on electrical and mechanical properties of epoxy nanocomposites. Composites Part A: Applied Science and Manufacturing, 2013;49:26-34.

[76] Zeng X, Yao Y, Gong Z, Wang F, Sun R, Xu J, Wong C-P. Ice-templated assembly strategy to construct 3D boron nitride nanosheet networks in polymer composites for thermal conductivity improvement. Small, 2015;11(46):6205-13.

[77] Prolongo SG, Meliton BG, Rosario GD, Ureña A. New alignment procedure of magnetite-CNT hybrid nanofillers on epoxy bulk resin with permanent magnets.

Composites Part B: Engineering, 2013;46:166-72.

[78] Wicks SS, Wang W, Williams MR, Wardle BL. Multi-scale interlaminar fracture mechanisms in woven composite laminates reinforced with aligned carbon nanotubes. Composites Science and Technology, 2014;100:128-35.

[79] Yamamoto N, de Villoria RG, Wardle BL. Electrical and thermal property enhancement of fiber-reinforced polymer laminate composites through controlled implementation of multi-walled carbon nanotubes. Composites Science and Technology, 2012;72(16):2009-15.

[80] Stahl JJ, Bogdanovich AE, Bradford PD. Carbon nanotube shear-pressed sheet interleaves for Mode I interlaminar fracture toughness enhancement. Composites Part A: Applied Science and Manufacturing, 2016;80:127-37.

[81] Ciambella J, Stanier DC, Rahatekar SS. Magnetic alignment of short carbon fibres in curing composites. Composites Part B: Engineering, 2017;109:129-37.

[82] Spencer MP, Gao D, Yamamoto N. Tunable one-dimensional assembly of magnetic nanoparticles using oscillating magnetic fields at low frequencies for polymer nanocomposite fabrication. Journal of Magnetism and Magnetic Materials, 2018;468:200-8.

[83] Erb RM, Libanori R, Rothfuchs N, Studart AR. Composites reinforced in three dimensions by using low magnetic fields. Science, 2012;335(6065):199-204.

[84] Rose KA, Meier JA, Dougherty GM, Santiago JG. Rotational electrophoresis of striped metallic microrods. Physical Review E, 2007;75:011503.

[85] Liu Y, Lv H, Lan X, Leng J, Du S. Review of electro-active shape-memory polymer composite. Composites Science and Technology, 2009;69(13):2064-8.

[86] Oliva-Avilés AI, Avilés F, Sosa V, Oliva AI, Gamboa F. Dynamics of carbon nanotube alignment by electric fields. Nanotechnology, 2012;23:465710.

[87] Shi J, Ahmed D, Mao X, Lin S-CS, Lawit A, Huang TJ. Acoustic tweezers: patterning cells and microparticles using standing surface acoustic waves (SSAW). Lab on a Chip, 2009;9:2890-5.

[88] Martin JJ, Riederer MS, Krebs MD, Erb RM. Understanding and overcoming shear alignment of fibers during extrusion. Soft Matter, 2015;11:400-5.

[89] Li X, Cai J, Shi Y, Yue Y, Zhang D. Remarkable conductive anisotropy of metallic microcoil/PDMS composites made by electric field induced alignment. ACS Applied Materials & Interfaces, 2017;9(2):1593-601.

[90] Wu S, Ladani RB, Zhang J, Kinloch AJ, Zhao Z, Ma J, Zhang X, Mouritz AP, Ghorbani K, Wang CH. Epoxy nanocomposites containing magnetite-carbon nanofibers aligned using a weak magnetic field. Polymer, 2015;68:25-34.

[91] Rokhlenko Y, Majewski PW, Larson SR, Gopalan P, Yager KG, Osuji CO. Implications of grain size variation in magnetic field alignment of block copolymer blends. ACS Macro Letters, 2017;6(4):404-9.

[92] Camponeschi E, Vance R, Al-Haik M, Garmestani H, Tannenbaum R. Properties of carbon nanotube-polymer composites aligned in a magnetic field. Carbon, 2007;45(10):2037-46.

[93] Haibat J, Ceneviva S, Spencer MP, Kwok F, Trivedi S, Mohney SE, Yamamoto N. Preliminary demonstration of energy-efficient fabrication of aligned CNT-polymer nanocomposites using magnetic fields. Composites Science and Technology, 2017;152:27-35.

[94] Stanier DC, Ciambella J, Rahatekar SS. Fabrication and characterisation of short fibre reinforced elastomer composites for bending and twisting magnetic actuation. Composites Part A: Applied Science and Manufacturing, 2016;91:168-76.

[95] Singh M, Ohji T, Asthana R. Green and sustainable manufacturing of advanced material. Elsevier, 2015.

[96] Thomas S, Bongiovanni C, Nutt SR. In situ estimation of through-thickness resin flow using ultrasound. Composites Science and Technology, 2008;68(15):3093-8.

[97] Ma Y, Centea T, Nutt SR. Defect reduction strategies for the manufacture of contoured laminates using vacuum BAG-only prepregs. Polymer Composites, 2017;38(9):2016-25.

[98] Abraham D, Matthews S, McIlhagger R. A comparison of physical properties of glass fibre epoxy composites produced by wet lay-up with autoclave consolidation and resin transfer moulding. Composites Part A: Applied Science and Manufacturing, 1998;29(7):795-801.

[99] Stringer LG. Optimization of the wet lay-up/vacuum bag process for the fabrication of carbon fibre epoxy composites with high fibre fraction and low void content. Composites, 1989;20(5):441-52.

[100] Thomas MM, Joseph B, Kardos JL. Experimental characterization of autoclave-cured glass-epoxy composite laminates: Cure cycle effects upon thickness, void content, and related phenomena. Polymer Composites, 1997;18(3):283-99.

[101] De Almeida SFM, Neto ZdSN. Effect of void content on the strength of

composite laminates. Composite Structures, 1994;28(2):139-48.

[102] Jeong H. Effects of voids on the mechanical strength and ultrasonic attenuation of laminated composites. Journal of Composite Materials, 1997;31(3):276-92.

[103] Hagstrand P-O, Bonjour F, Månson J-AE. The influence of void content on the structural flexural performance of unidirectional glass fibre reinforced polypropylene composites. Composites Part A: Applied Science and Manufacturing, 2005;36(5):705-14.

[104] Varna J, Joffe R, Berglund LA, Lundström TS. Effect of voids on failure mechanisms in RTM laminates. Composites Science and Technology, 1995;53(2):241-9.

[105] Tang J-M, Lee WI, Springer GS. Effects of cure pressure on resin flow, voids, and mechanical properties. Journal of Composite Materials, 1987;21(5):421-40.

[106] Boey FYC, Lye SW. Void reduction in autoclave processing of thermoset composites: Part 1: High pressure effects on void reduction. Composites, 1992;23(4):261-5.

[107] Olivier P, Cottu JP, Ferret B. Effects of cure cycle pressure and voids on some mechanical properties of carbon/epoxy laminates. Composites, 1995;26(7):509-15.

[108] Hancox NL. The effects of flaws and voids on the shear properties of CFRP. Journal of Materials Science, 1977;12(5):884-92.

[109] Bowles KJ, Frimpong S. Void effects on the interlaminar shear strength of unidirectional graphite-fiber-reinforced composites. Journal of Composite Materials, 1992;26(10):1487-509.

[110] Sussmann M, Amirkhosravi M, Pishvar M, Altan MC. Fabrication of high quality, large wet lay-up/vacuum bag laminates by sliding a magnetic tool. Polymers, 2018;10(9):992.

[111] Ricotta M, Quaresimin M, Talreja R. Mode I strain energy release rate in composite laminates in the presence of voids. Composites Science and Technology, 2008;68(13):2616-23.

[112] Zhandarov S, Mäder E. Characterization of fiber/matrix interface strength: applicability of different tests, approaches and parameters. Composites Science and Technology, 2005;65(1):149-60.

[113] Campbell FC. Manufacturing technology for aerospace structural materials. Elsevier, 2006.

[114] Anderson JP, Altan MC. Formation of voids in composite laminates: coupled effect of moisture content and processing pressure. Polymer Composites, 2015;36(2):376-84.

[115] Rosato DV, Rosato DV. Reinforced plastics handbook. Elsevier, 2004.

[116] Tavares SS, Michaud V, Månson J-AE. Through thickness air permeability of prepregs during cure. Composites Part A: Applied Science and Manufacturing, 2009;40(10):1587-96.

[117] Centea T, Grunenfelder LK, Nutt SR. A review of out-of-autoclave prepregs–Material properties, process phenomena, and manufacturing considerations. Composites Part A: Applied Science and Manufacturing, 2015;70:132-54.

[118] Advani SG, Hsiao K-T. Manufacturing techniques for polymer matrix composites (PMCs). Elsevier, 2012.

[119] Agius SL, Magniez KJC, Fox BL. Fracture behaviour of a rapidly cured polyethersulfone toughened carbon fibre/epoxy composite. Composite Structures, 2010;92(9):2119-27.

[120] Zhang J, Fox BL. Manufacturing influence on the delamination fracture behavior of the T800H/3900-2 carbon fiber reinforced polymer composites. Materials and Manufacturing Processes, 2007;22(6):768-72.

[121] Davies LW, Day RJ, Bond D, Nesbitt A, Ellis JE, Gardon E. Effect of cure cycle heat transfer rates on the physical and mechanical properties of an epoxy matrix composite. Composites Science and Technology, 2007;67(9):1892-9.

[122] Khan LA, Mahmood AH, Ahmed S, Day RJ. Effect of double vacuum bagging (DVB) in quickstep processing on the properties of 977-2A carbon/epoxy composites. Polymer Composites, 2013;34(6):942-52.

[123] Walczyk D, Kuppers J. Thermal press curing of advanced thermoset composite laminate parts. Composites Part A: Applied Science and Manufacturing, 2012;43(4):635-46.

[124] Ziegenbein JM, Colton JS. Magnetic-clamping structures for the consolidation of composite laminates. Polymer Composites, 2012;33(6):951-60.

[125] Pallapa M, Yeow JTW. A review of the hybrid techniques for the fabrication of hard magnetic microactuators based on bonded magnetic powders. Smart Materials and Structures, 2014;24(2):025007.

[126] Schuring I, Vogel R, Rzadki W. Demagnetization-protected permanent magnet ship propulsion system. Google Patents, 2001.

[127] Guo S, Li D, Zhang X, Xiang J. Buckling and post-buckling of a composite C-

section with cutout and flange reinforcement. Composites Part B: Engineering, 2014;60:119-24.

[128] Yokozeki T, Aoki Y, Ogasawara T. Experimental characterization of strength and damage resistance properties of thin-ply carbon fiber/toughened epoxy laminates. Composite Structures, 2008;82(3):382-9.

[129] Yang T, Zhang J, Mouritz AP, Wang CH. Healing of carbon fibre–epoxy composite T-joints using mendable polymer fibre stitching. Composites Part B: Engineering, 2013;45(1):1499-507.

[130] Liu L, Zhang B-M, Wang D-F, Wu Z-J. Effects of cure cycles on void content and mechanical properties of composite laminates. Composite Structures, 2006;73(3):303-9.

[131] Narayanan RR, Brahmam KV, Soni J, Sudher P. Determination of Exact Pressure Application Point for Autoclave Curing of PAN based Carbon/Polyimide Composites. Journal of Polymer Materials, 2010;27(1):79-86.

[132] Howe CA, Paton RJ, Goodwin AA. A comparison between voids in RTM and prepreg carbon/epoxy laminates. Proceedings of Eleventh International Conference on Composite Materials (ICCM-11). Gold Coast, Queensland, Australia, 1997, pp. 46-54.

[133] Staffan T. Void formation and transport in manufacturing of polymer composites (PhD dissertation). Luleå University of Technology, 1996.

[134] Huang H, Talreja R. Effects of void geometry on elastic properties of unidirectional fiber reinforced composites. Composites Science and Technology, 2005;65(13):1964-81.

[135] Goshkoderia A, Rudykh S. Stability of magnetoactive composites with periodic microstructures undergoing finite strains in the presence of a magnetic field. Composites Part B: Engineering, 2017;128:19-29.

[136] Du C, Li M, Cao M, Feng S, Guo H, Li B. Enhanced thermal and mechanical properties of polyvinlydene fluoride composites with magnetic oriented carbon nanotube. Carbon, 2018;126:197-207.

[137] Singh RP, Onck PR. Magnetic field induced deformation and buckling of slender bodies. International Journal of Solids and Structures, 2018;143:29-58.

[138] Oh Y, Islam MF. Preformed nanoporous carbon nanotube scaffold-based multifunctional polymer composites. ACS Nano, 2015;9(4):4103-10.

[139] Böger L, Sumfleth J, Hedemann H, Schulte K. Improvement of fatigue life by incorporation of nanoparticles in glass fibre reinforced epoxy. Composites Part A: Applied Science and Manufacturing, 2010;41(10):1419-24.

[140] Akcora P, Liu H, Kumar SK, Moll J, Li Y, Benicewicz BC, Schadler LS, Acehan D, Panagiotopoulos AZ, Pryamitsyn V, Ganesan V, Ilavsky J, Thiyagarajan P, Colby RH, Douglas JF. Anisotropic self-assembly of spherical polymer-grafted nanoparticles. Nature Materials, 2009;8(4):354.

[141] Manchado MAL, Valentini L, Biagiotti J, Kenny JM. Thermal and mechanical properties of single-walled carbon nanotubes–polypropylene composites prepared by melt processing. Carbon, 2005;43(7):1499-505.

[142] Boustany K, Arnold RL. Short fibers rubber composites: The comparative properties of treated and discontinuous cellulose fibers. Journal of Elastomers & Plastics, 1976;8(2):160-76.

[143] Yalcinkaya MA, Sozer EM, Altan MC. Fabrication of high quality composite laminates by pressurized and heated-VARTM. Composites Part A: Applied Science and Manufacturing, 2017;102:336-46.

[144] Choi JH, Dharan CKH. Mold fill time and void reduction in resin transfer molding achieved by articulated tooling. Journal of Composite Materials, 2002;36(19):2267-85.

[145] Cox HW, Mentzer CC. Injection molding: the effect of fill time on properties. Polymer Engineering & Science, 1986;26(7):488-98.

[146] Rahmanian S, Thean KS, Suraya AR, Shazed MA, Mohd Salleh MA, Yusoff HM. Carbon and glass hierarchical fibers: influence of carbon nanotubes on tensile, flexural and impact properties of short fiber reinforced composites. Materials & Design, 2013;43:10-6.

[147] Lacerda RG, Teh AS, Yang MH, Teo KBK, Rupesinghe NL, Dalal SH, Koziol KKK, Amaratunga GAJ, Milne WI. Growth of high-quality single-wall carbon nanotubes without amorphous carbon formation. Applied Physics Letters, 2004;84(2):269-71.

[148] Besra L, Liu M. A review on fundamentals and applications of electrophoretic deposition (EPD). Progress in Materials Science, 2007;52(1):1-61.

[149] Greenhall J, Raeymaekers B. 3D Printing macroscale engineered materials using ultrasound directed self-assembly and stereolithography. Advanced Materials Technologies, 2017;2(9):1700122.

[150] Ahmad MS, Zihilif AM, Martuscelli E, Ragosta G, Scafora E. The electrical conductivity of polypropylene and nickel-coated carbon fiber composite.

Polymer Composites, 1992;13(1):53-7.

[151] Kashiwagi T, Du F, Winey KI, Groth KM, Shields JR, Bellayer SP, Kim H, Douglas JF. Flammability properties of polymer nanocomposites with single-walled carbon nanotubes: Effects of nanotube dispersion and concentration. Polymer, 2005;46(2):471-81.

[152] Morcom M, Atkinson K, Simon GP. The effect of carbon nanotube properties on the degree of dispersion and reinforcement of high density polyethylene. Polymer, 2010;51(15):3540-50.

[153] Paul DR, Robeson LM. Polymer nanotechnology: nanocomposites. Polymer, 2008;49(15):3187-204.

[154] Bray DJ, Gilmour SG, Guild FJ, Hsieh TH, Masania K, Taylor AC. Quantifying nanoparticle dispersion: application of the Delaunay network for objective analysis of sample micrographs. Journal of Materials Science, 2011;46(19):6437-52.

[155] Bowman AW, Azzalini A. Applied smoothing techniques for data analysis: The kernel approach with s-plus illustrations. Oxford Science Publications, 1997.

[156] Sadeghian R, Gangireddy S, Minaie B, Hsiao K-T. Manufacturing carbon nanofibers toughened polyester/glass fiber composites using vacuum assisted resin transfer molding for enhancing the mode-I delamination resistance. Composites Part A: Applied Science and Manufacturing, 2006;37(10):1787-95.

[157] Kinloch AJ. Adhesives in engineering. Proceedings of the Institution of Mechanical Engineers, Part G: Journal of Aerospace Engineering, 1997;211(5):307-35.

[158] Jin H, Miller GM, Sottos NR, White SR. Fracture and fatigue response of a self-healing epoxy adhesive. Polymer, 2011;52(7):1628-34.

[159] Ladani RB, Wu S, Kinloch AJ, Ghorbani K, Zhang J, Mouritz AP, Wang CH. Improving the toughness and electrical conductivity of epoxy nanocomposites by using aligned carbon nanofibres. Composites Science and Technology, 2015;117:146-58.

[160] Ravindran AR, Ladani RB, Wu S, Kinloch AJ, Wang CH, Mouritz AP. The electric field alignment of short carbon fibres to enhance the toughness of epoxy composites. Composites Part A: Applied Science and Manufacturing, 2018;106:11-23.

[161] Bauhofer W, Kovacs JZ. A review and analysis of electrical percolation in carbon nanotube polymer composites. Composites Science and Technology, 2009;69(10):1486-98.

[162] Zhang G, Karger-Kocsis J, Zou J. Synergetic effect of carbon nanofibers and short carbon fibers on the mechanical and fracture properties of epoxy resin. Carbon, 2010;48(15):4289-300.

[163] Dong W, Liu H-C, Park S-J, Jin F-L. Fracture toughness improvement of epoxy resins with short carbon fibers. Journal of Industrial and Engineering Chemistry, 2014;20(4):1220-2.

[164] Cholake ST, Moran G, Joe B, Bai Y, Raman RKS, Zhao XL, Bandyopadhyay S. Improved Mode I fracture resistance of CFRP composites by reinforcing epoxy matrix with recycled short milled carbon fibre. Construction and Building Materials, 2016;111:399-407.

[165] Hansen GC. Physical and mechanical properties of nickel coated carbon fibers and their fabricated composites. SAMPE Journal, 2017;53(2):20-7.

[166] Bell J, Hansen G. Properties of Nickel Coated Carbon and Kevlar Fibres Produced by Decomposition of Nickel Carbonyl. Proceedings of 23rd International SAMPE Technical Conference. New York, 1991, pp. 1183-93.

[167] Martin CA, Sandler JKW, Windle AH, Schwarz M-K, Bauhofer W, Schulte K, Shaffer MSP. Electric field-induced aligned multi-wall carbon nanotube networks in epoxy composites. Polymer, 2005;46(3):877-86.

[168] Fujiwara M, Oki E, Hamada M, Tanimoto Y, Mukouda I, Shimomura Y. Magnetic orientation and magnetic properties of a single carbon nanotube. The Journal of Physical Chemistry A, 2001;105(18):4383-6.

[169] Hao C, Li X, Wang G. Magnetic alignment of nickel-coated carbon fibers. Materials Research Bulletin, 2011;46(11):2090-3.

[170] Van der Beek D, Petukhov AV, Davidson P, Ferré J, Jamet JP, Wensink HH, Vroege GJ, Bras W, Lekkerkerker HNW. Magnetic-field-induced orientational order in the isotropic phase of hard colloidal platelets. Physical Review E, 2006;73:041402.

[171] Amirkhosravi M, Pishvar M, Altan MC. Improving laminate quality in wet lay-up/vacuum bag processes by magnet assisted composite manufacturing (MACM). Composites Part A: Applied Science and Manufacturing, 2017;98:227-37.

[172] Pishvar M, Amirkhosravi M, Altan MC. Magnet assisted composite manufacturing: A novel fabrication technique for high-quality composite

laminates. Polymer Composites, 2019;40(1):159-69.

[173] Pishvar M, Amirkhosravi M, Altan MC. Magnet assisted composite manufacturing: A flexible new technique for achieving high consolidation pressure in vacuum bag/lay-up processes. Journal of Visualized Experiments, 2018;(115): e57254.

[174] Lin Y, Huang X, Chen J, Jiang P. Epoxy thermoset resins with high pristine thermal conductivity. High Voltage, 2017;2(3):139-46.

[175] Deng H, Lin L, Ji M, Zhang S, Yang M, Fu Q. Progress on the morphological control of conductive network in conductive polymer composites and the use as electroactive multifunctional materials. Progress in Polymer Science, 2014;39(4):627-55.

[176] Wang N, Xu Z, Zhan P, Dai K, Zheng G, Liu C, Shen C. A tunable strain sensor based on a carbon nanotubes/electrospun polyamide 6 conductive nanofibrous network embedded into poly (vinyl alcohol) with self-diagnosis capabilities. Journal of Materials Chemistry C, 2017;5(18):4408-18.

[177] Zhan C, Yu G, Lu Y, Wang L, Wujcik E, Wei S. Conductive polymer nanocomposites: a critical review of modern advanced devices. Journal of Materials Chemistry C, 2017;5(7):1569-85.

[178] Arjmand M, Apperley T, Okoniewski M, Sundararaj U. Comparative study of electromagnetic interference shielding properties of injection molded versus compression molded multi-walled carbon nanotube/polystyrene composites. Carbon, 2012;50(14):5126-34.

[179] Rikken RSM, Nolte RJM, Maan JC, van Hest JCM, Wilson DA, Christianen

PCM. Manipulation of micro-and nanostructure motion with magnetic fields. Soft Matter, 2014;10(9):1295-308.

[180] Ren L, Zhou X, Liu Q, Liang Y, Song Z, Zhang B, Li B. 3D magnetic printing of bio-inspired composites with tunable mechanical properties. Journal of Materials Science, 2018;53(20):14274-86.

[181] Xu Y, Yuan J, Fang B, Drechsler M, Müllner M, Bolisetty S, Ballauff M, Müller AHE. Hybrids of Magnetic Nanoparticles with Double-Hydrophilic Core/Shell Cylindrical Polymer Brushes and Their Alignment in a Magnetic Field. Advanced Functional Materials, 2010;20(23):4182-9.

[182] Yang J, Yang Y, Duan H, Zhao G, Liu Y. Light-weight epoxy/nickel coated carbon fibers conductive foams for electromagnetic interference shielding. Journal of Materials Science: Materials in Electronics, 2017;28(8):5925-30.

[183] Wang R, Yang H, Wang J, Li F. The electromagnetic interference shielding of silicone rubber filled with nickel coated carbon fiber. Polymer Testing, 2014;38:53-6.

[184] Hussain FA, Zihlif AM. Electrical properties of nickel-coated carbon-fiber/nylon 66 composite. Journal of Thermoplastic Composite Materials, 1993;6(2):120-9.

[185] Ashby MF. Materials selection in mechanical design. MRS Bulletin, 2005;30(12):994-97.

[186] Louis M, Joshi SP, Brockmann W. An experimental investigation of through-thickness electrical resistivity of CFRP laminates. Composites Science and Technology, 2001;61(6):911-9.

[187] Gaier JR, YoderVandenberg Y, Berkebile S, Stueben H, Balagadde F. The

electrical and thermal conductivity of woven pristine and intercalated graphite fiber–polymer composites. Carbon, 2003;41(12):2187-93.

[188] Pilling MW, Yates B, Black MA, Tattersall P. The thermal conductivity of carbon fibre-reinforced composites. Journal of Materials Science, 1979;14(6):1326-38.

[189] Park K-Y, Lee S-E, Kim C-G, Han J-H. Application of MWNT-added glass fabric/epoxy composites to electromagnetic wave shielding enclosures. Composite Structures, 2007;81(3):401-6.

[190] Lee S-E, Kang J-H, Kim C-G. Fabrication and design of multi-layered radar absorbing structures of MWNT-filled glass/epoxy plain-weave composites. Composite Structures, 2006;76(4):397-405.

[191] An Q, Rider AN, Thostenson ET. Electrophoretic deposition of carbon nanotubes onto carbon-fiber fabric for production of carbon/epoxy composites with improved mechanical properties. Carbon, 2012;50(11):4130-43.

[192] An Q, Rider AN, Thostenson ET. Hierarchical composite structures prepared by electrophoretic deposition of carbon nanotubes onto glass fibers. ACS Applied Materials & Interfaces, 2013;5(6):2022-32.

[193] Liao L, Wang X, Fang P, Liew KM, Pan C. Interface enhancement of glass fiber reinforced vinyl ester composites with flame-synthesized carbon nanotubes and its enhancing mechanism. ACS Applied Materials & Interfaces, 2011;3(2):534-8.

[194] Bhanushali H, Bradford PD. Woven glass fiber composites with aligned carbon nanotube sheet interlayers. Journal of Nanomaterials, 2016;2016: Article ID 9705257, 9 pages.

[195] Pishvar M, Amirkhosravi M, Yalcinkaya MA, Altan MC. Fabrication of three-phase NiC/glass/epoxy composites with controlled surface microstructure using a cascaded suspension deposition Method. Submitted to Polymer Composites. 2019.

[196] Pishvar M, Amirkhosravi M, Altan MC. Alignment of nickel coated carbon fibers by magnetic field during cure of polymer composites. Proceedings of the American Society for Composites-Thirty-third Technical Conference. Seattle WA, 2018.

[197] Mecklenburg M, Mizushima D, Ohtake N, Bauhofer W, Fiedler B, Schulte K. On the manufacturing and electrical and mechanical properties of ultra-high wt.% fraction aligned MWCNT and randomly oriented CNT epoxy composites. Carbon, 2015;91:275-90.

[198] Li C, Thostenson ET, Chou T-W. Dominant role of tunneling resistance in the electrical conductivity of carbon nanotube–based composites. Applied Physics Letters, 2007;91(22):223114.

[199] Kazemi Y, Ramezani Kakroodi A, Wang S, Ameli A, Filleter T, Pötschke P, Park CB. Conductive network formation and destruction in polypropylene/carbon nanotube composites via crystal control using supercritical carbon dioxide. Polymer, 2017;129:179-88.